High Repetition Rate Fiber Lasers

by

Jian Chen

B.S., Electrical Engineering, Peking University, China (1996)
M.S., Optical Science and Engineering, CREOL, University of Central Florida (1998)

Submitted to the Department of Electrical Engineering and Computer Science
in partial fulfillment of the requirements for the degree of

Doctor of Philosophy in Electrical Engineering

at the

MASSACHUSETTS INSTITUTE OF TECHNOLOGY

September 2009

Author . . . . . .
Department of Electrical Engineering and Computer Science
August 26, 2009

Certified by. . . . . .
Franz. X. Kärtner
Professor of Electrical Engineering and Computer Science
Thesis Supervisor

Accepted by . . . . . .
Terry P. Orlando
Chairman, Department Committee on Graduate Students

High Repetition Rate Fiber Lasers

by
Jian Chen

Submitted to the Department of Electrical Engineering and Computer Science
On August 28, 2009, in partial fulfillment of the requirements for the degree of

Doctor of Philosophy in Electrical Engineering

Abstract

This thesis reports work in high repetition rate femtosecond fiber lasers. Driven by the applications including optical arbitrary waveform generation, high speed optical sampling, frequency metrology, and timing and frequency distribution via fiber links, low noise fiber laser sources operating at multi-gigahertz repetition rates are developed systematically. A 200 MHz fundamentally mode-locked soliton laser and a 200 MHz fundamentally mode-locked similariton laser are first developed. Intra-cavity soliton formation is recognized as the optimum route towards achieving high fundamental repetition rates compact lasers, under the limitation of realistically available pump power. A 3 GHz fundamentally mode-locked femtosecond fiber laser is developed and verifies the soliton formation theory. Techniques in external cavity repetition rate multiplications are also discussed. A theoretical model that relates the repetition rate of the soliton laser and its other physical measurable parameters is developed to guide further high repetition rate laser development.

Thesis Supervisor: Franz X. Kärtner
Title: Professor of Electrical Engineering and Computer Science

In grateful dedication to my father, Professor Huansheng Chen, and my mother, Professor Zhifen Wu.

献给我的父亲陈焕生教授，和我的母亲吴芝芬教授

ACKNOWLEDGEMENT

First, I would like to thank my advisor Professor Franz Kärtner for the opportunity to work in his laboratory. I have learned from Franz not only technical skills but also his passion in science as well as his rigorous approach in research, which I will benefit for the rest of my career. I thank him for his kindness and patience throughout my graduate school years. I also would like to thank Prof. Ippen my co-advisor, I thank him for his advice and his kindness every time I approached his office to interrupt his work. It has been an honor to work for two pioneers in the field of ultrafast optics.

I also would like to thank Prof. Ömer Ilday, who mentored me into the field of ultrafast optics and wish him the best in his research career. I thank late Prof. Jin Au Kong, whom I have greatest respect. I was not aware of the joyfulness in scientific classes until I took his EM classes. I thank Prof. Rajeev Ram for his generosity to be in my thesis committee, and his time evaluating this thesis work.

Words cannot express my emotion when it comes to acknowledging my patents Zhifen and Huansheng, they offer me paramount of selfless love I only wish I could attempt to return. In exchange to my potential success in the remote new world, they had to cope with loneliness on the other side of the ocean for decades. I thank my wife Betty for her love and support during these years. I thank my sister Yuan, who comes to my help at any moment of notice, under any circumstances.

I thank my officemates Dr. Jonathan Birge, Andrew Benedick, Dr. Amir Nejadmalayeri for numerous inspiring discussions. Dr. Guoqing Chang, Marcus Dahlem, Dr. Jason Sickler, and Dr. Peter Fendel have shared with me great common interests in fiber laser technologies as well as other technologies and business development opportunities. I look forward to continued collaboration with you. I also wish Dave Chao, Jonathan Morse, Michelle Sander, Hyunil Byun, Anatoly Khilo, Aleem Siddiqui successful and happy PhD years. I wish Dr. Edilson, Falcao-Filho, Dr. Milos Popovic, and Dr. Jeffrey Moses the best of luck embarking on their future

academic careers. I gratefully thank Dorothy Fleischer and Donna Gale for their fantastic help to all of us.

Table of Content:

List of Figures

List of Tables

Chapter 1.

Introduction to Ultrafast Fiber Lasers

1.1. Background

The field of ultrafast optics is one of the most exciting fields in science and engineering today. Technologies in this field have played major factors in various applications in our everyday lives, including LASIK surgeries, micro-machining, optical coherence tomography, GPS systems, frequency metrologies, and quantum communications. They will continue to shape our lives and the future of mankind.

The unique characteristics of ultrafast optics are two-fold. In the time domain, unlike their continuous wave (cw) counterparts, ultrafast phenomena involve optical pulses with durations in the range of picoseconds (10^{-12} second) and femtoseconds (10^{-15} second). At this level of pulse duration, pulse trains with moderate average optical power and repetition rates can produce extremely high peak power and hence extremely high electro-magnetic field magnitude, both of which can be exploited in applications that are not possible with cw optical fields. In the frequency domain, the spectra of ultrafast pulses usually contain millions of spectral comb lines with equal spacing. The ability to provide stable sets of millions of comb lines simultaneously greatly helps the field of spectroscopy and frequency metrology.

Ultrafast lasers are the workhorse of ultrafast optics. They are the sources and hence the starting points of all ultrafast systems. As one type of ultrafast lasers, ultrafast fiber lasers has been playing a significant role in the development of ultrafast applications due to their compact

footprint, inexpensive components, ease of operation, and prolonged lifetime compared to their bulk solid state counterparts due to rapid technology development in telecommunication field. However, ultrafast fiber lasers also have their drawbacks such as the amount of pulse energies available directly from the fiber laser cavities, the pulse duration achievable directly from the fiber lasers, and difficulties in scaling up the fundamental repetition rates. These disadvantages have been major roadblocks preventing the use of fiber lasers in general ultrafast applications compared to their solid state counterparts, despite the fact that fiber lasers usually cost much less than the solid state lasers.

Considerable research activities have been carried out to improve the performance of fiber lasers, especially on their limitations in pulse duration, pulse energy, and fundamental repetition rate.

Although there is still work to be done to improve the pulse duration directly out of fiber lasers, in terms of comparing to that of the Ti: Sapphire lasers, significant progress has been reported in achieving the shortest pulse durations in fiber lasers. Pulse trains with duration of 36 femtosecond (fs) and 28 fs generated from Ytterbium doped fiber lasers (YDFL) [1, 2] have been reported.

In regards to scaling up the pulse energy achievable directly from the fiber laser cavity, substantial breakthroughs also took place. Similariton lasers [3] and ANDi lasers [4] have been developed to routinely generate pulse trains with pulse energies around 10 nJ to 20 nJ [4, 5], making fiber lasers comparable and even surpassing that of Ti: Sapphire lasers in pulse energies.

Unfortunately, prior to this thesis research, there had been less significant progress in scaling up the fundamental repetition rate of the fiber lasers. The fundamental repetition rates of the fiber lasers generally were limited to less than 100 MHz, while Ti: Sapphire lasers routinely generate pulse trains with fundamental repetition rates of several gigahertz [6-8], and with recent records reaching 5~ 10 GHz [9, 10].

Because of the tremendous potential advantage of fiber lasers, fiber based ultrafast sources are in high demand in numerous applications including Optical Arbitrary Waveform Generation (OAWG), optical high speed sampling, frequency metrology, and optical timing and frequency

synchronization via optical links. All of these applications require high repetition rate fiber laser sources that provide pulse trains with repetition rates in the multi-gigahertz range. While keeping their advantages including femtosecond pulse duration, compact footprints, low noise, and low-cost, fiber lasers with multi-gigahertz of repetition rates are highly desired.

This thesis reports the experimental and theoretical results in scaling up the repetition rates of the ultrafast fiber lasers.

1.2. Introduction to Ultrafast Fiber Lasers

Depending on the mode-locking mechanism and pulse dynamics, ultrafast fiber lasers can be categorized in the several ways:

Based on whether or not the mode-locking is induced by an electronic modulator, the ultrafast fibers can be categorized into actively mode-locked lasers and passively mode-locked lasers. Actively mode-locked fiber lasers use electro-optical modulators or acousto-optic modulators to produce periodical perturbations inside of the laser cavities. If the perturbations are strong enough and are synchronized with multipliers of the fundamental repetition rates of the laser cavities, electronically induced mode-locking can be achieved. Passively mode-locked lasers do not use any electronic modulation inside of their cavities. Saturable absorbers, either artificial or non-artificial, are used to induce mode-locking.

Within the category of passive mode-locking, fiber lasers can also be categorized based on their mode-locking mechanisms. The most widely seen mode-locking mechanism in passive mode-locking is the Polarization Additive Pulse Mode-locking (P-APM) or otherwise known as Nonlinear Polarization Evolution (NPE) mode-locking. Another widely used mode-locking approach is to use Saturable Bragg Reflectors (SBR) to initiate and maintain mode-locking.

Independent from active-passive categorization criteria, fiber lasers can also be categorized into three general types: soliton lasers, stretched pulse lasers, and similariton lasers, depending on the intra-cavity pulse dynamics. Details of these types of mode-locked lasers are discussed in the following sections 1.3 to 1.5.

1.3. Active Mode-locked Fiber Lasers

Active mode-locking involves the periodic modulation of the resonator losses or the round trip phase changes. Usually acousto-optic modulators, electro-optic modulators, or semiconductor electro-absorption modulators can be used to modulate the intra-cavity loss and induce mode-locking [11-17].

The principle of active mode locking by modulating the resonator losses is easy to understand. A pulse with the "correct" timing can pass the modulator at times where the losses are at a minimum as shown in Figure 1.1. Note that the wings of the pulse experience a little attenuation, which effectively leads to slight pulse shortening in each round trip, this pulse shortening effect is balanced by other effects in the cavity such as gain narrowing effects. As the pulse duration relative to the pulse period is typically much smaller, the pulse-shortening effect of the modulator is reduced rapidly with shorter pulses.

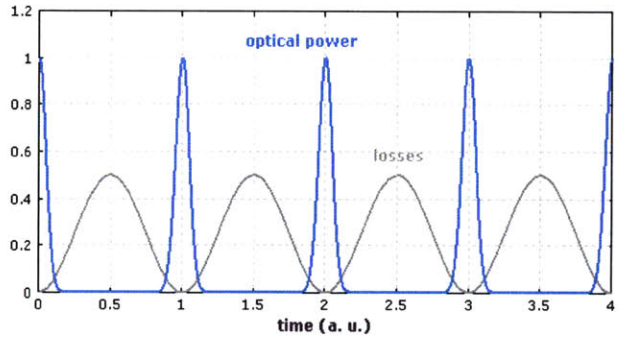

Figure 1.1: Temporal evolution of optical power and losses in an actively mode-locked laser.

In simple cases, the pulse duration achieved in the steady state can be calculated with the Kuizenga–Siegman theory [18]. For the fastest modulation speed, usually in the GHz range, the pulse duration is typically in the picosecond range and is only weakly dependent on parameters such as the strength of the modulation. This weak dependence arises from the fact that the pulse-shortening effect of the modulator becomes less effective for shorter pulse durations, while the

modulation frequency is kept the same, whereas other effects which lengthen the pulse including dispersion and gain narrowing become more effective.

Less obviously, active mode locking can also be achieved with a periodic phase modulation. This technique is called FM mode-locking or phase-modulation mode-locking. Some FM mode-locked lasers exhibit instabilities such as random hopping between two operation modes. The pulses pass the modulator at times where either a minimum or a maximum of the phase delay is reached. The bi-stability can be removed by dispersion and nonlinear effects.

For stable operation, the round-trip time of the resonator must fairly precisely match the period of the modulator signal (or some integer multiple of it), so that a circulating pulse can always pass the modulator at a time with minimum losses. If the frequency mismatch between the laser resonator and the drive signal is beyond the frequency pulling range which is generally small but non-zero, unstable or even to chaotic behavior may occur.

Synchronization between the modulator driver and the laser can be achieved either by highly stable laser setup, or by means of a feedback circuit which automatically adjusts either the modulation frequency or the length of the laser resonator. A frequently used technique is regenerative mode locking [19]. In this scheme, the modulator signal is not generated by a free-running electronic oscillator, but rather is derived from the detected intensity modulation of the pulse train itself. Such schemes are particularly important for achieving tunable pulse repetition rates, and are often applied to mode-locked fiber lasers.

Actively mode-locked fiber lasers can have very high repetition rates, through harmonic mode-locking. Due to geometric constraints while incorporating typically electro-optical modulators, it is difficult to reach high repetition rates by making the laser cavity short. Harmonic mode-locking becomes the natural approach, where multiple pulses circulate in the laser cavity to make up the high repetition rate and the modulator frequency is an integer multiple of the fundamental repetition rate.

Compared to passive mode-locking, active mode-locking typically generates much longer pulses, usually in the picoseconds range. In order to reach durations in the 100 fs range, pulse trains coming out of the actively mode-locked lasers usually have to undergo nonlinear

compressions. This nonlinear process induces significant phase fluctuations to the pulse itself. Depending on the amount of the nonlinear compression needed and the exact method of the nonlinear compression, additional phase noise maybe introduced in the process which may not be desirable in the low noise applications and/or may destroy the comb structure of the spectrum.

In addition to the drawback of having picosecond pulse duration and the noise degradation due to the nonlinear pulse compression, special care needs to be taken to ensure low noise performance of the electronics. Although electronic components exhibit excellent noise characteristics such as timing jitter and relative intensity noise at low frequency range below mega-hertz range, their noise characteristics at high frequency above mega-hertz are inferior compared to the free running ultrafast optical oscillators. In general, actively mode-locked lasers hence have worse noise properties than passive mode-locked lasers if both lasers are using similar electronics locking loops to reduce the thermal and mechanical noise, at low frequencies.

Lastly, the footprints of actively mode-locked fiber lasers are usually large due to their cumbersome electronics detection, filtering, locking loop, and electro-optical modulation. This does not make active mode-locking an ideal candidate for compact applications.

1.4. Passively Mode-locked Fiber Lasers

Passively mode-locked lasers do not need any assistance from a modulator to achieve mode-locking, hence the drawbacks of noise degradation and cumbersome footprints introduced by the modulators are eliminated. This potentially makes them good candidates for low noise and compact applications.

Saturable absorbers used in passively mode-locked lasers can be categorized into two types: artificial saturable absorbers or real saturable absorbers. Artificial saturable absorbers include Nonlinear Optical Loop Mirror (NOLM) and P-APM; real saturable absorbers include semiconductor quantum well Saturable Bragg Reflectors (SBR) and Carbon Nanotubes (CNT) saturable absorbers. Sections 1.4.1 to section 1.4.3 summaries in more detail these types of saturable absorbers.

1.4.1. Nonlinear Optical Loop Mirror Mode-locking

The figure-of-eight lasers [20-24] utilize NOLMs as their locking mechanism as shown in

Figure 1.2. For a figure-of-eight laser, generally the laser cavity is composed with two fiber loops. As shown in

Figure 1.2, in the left loop (isolator loop), the fiber loop has the output port of the laser as well as the isolator to ensure single direction propagation. In the right loop (gain loop), there is a piece of gain fiber located asymmetrically in the loop. When the laser light passes through the 50% coupler from the isolator loop into the gain loop, it will be split into equally two parts by the 50% coupler, one travels clockwise, the other one travels counter-clockwise inside of the gain loop. They will meet again at the 50% coupler once finishing a roundtrip inside of the gain loop.

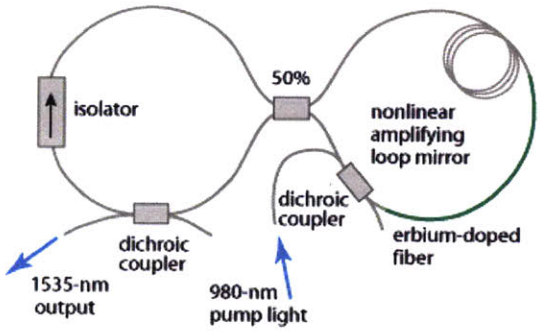

Figure 1.2: Figure-of-eight laser setup

Inside of the gain loop, for cw operation, there is no significant phase difference between the light waves along these two directions; hence the coupler essentially split the incoming light waves in half from each incoming port. Since there is an isolator in the isolator loop, the optical energy from one of the output port of the coupler will be lost in the isolator. In another word, cw operation experiences a 50% loss in the isolator loop due to the isolator.

However, for pulsed operation, since the gain fiber is located asymmetrically in the gain loop, the two pulses experience different nonlinear phase shifts depending on the peak power of the pulses. When they meet up at the 50% coupler again after a roundtrip inside of the gain loop from each direction, the coupling ratio into each of the ports in the isolator loop depends on the phase difference the pulses pick up from their roundtrips in the gain loop. Compared to cw operation, pulse operation will pick up more phase difference, so that by interference, pulsed operation will send more energy to the port that is along the isolator direction at the 50% coupler. Hence this type of the fiber laser cavity favors pulsed operation over cw operation.

Since a NOLM is an artificial saturable absorber, lasers implemented with NOLMs routinely generate pulse trains with durations in the range of 100 femtoseconds. Pulse trains purely generated from NOLMs should have low timing jitter as well as low intensity noise.

One of the significant drawbacks with NOLM lasers is their lack of self-starting. Most of the reported NOLM fiber lasers fail to initiate pulsation without the extra help of SBRs or moving mirrors. This makes fiber lasers with NOLM an unattractive option for practical applications.

1.4.2. Polarization Additive Pulse Mode-locking

The P-APM mode-locking mechanism was first developed at MIT and series of improvements were implemented based on the initial research [25-32]. The principle of P-APM is well explained in reference [32]. As shown in Figure 1.3, assuming the laser starts with cw operation and a small perturbation in the cavity causes a small pulse emerging from the cw background. When this small pulse goes through the fiber portion of the cavity, the fiber section acts as a Kerr medium as well as a birefringent medium, which means that the state of the polarization of the small pulse changes along the time axis depending on its instantaneous power. In another word, the state of the polarization of the peak of the pulse differs from that of the sides of the pulse after the fiber section. If a polarizer is placed after the fiber section and is aligned with the state of the polarization at the peak of the small pulse, the pulsation will be enhanced after each roundtrip. In steady state after thousands of roundtrips with gain and loss dynamics, only pulsed operation can survive in the cavity.

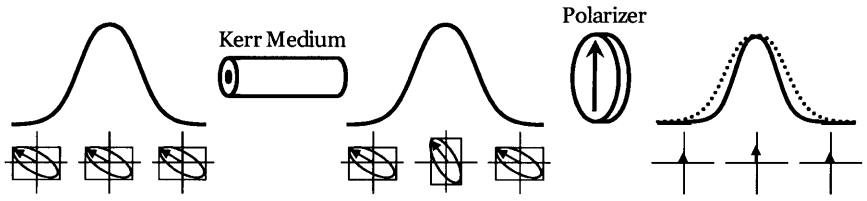

Figure 1.3: P-APM mode-locking principle

Compared to NOLMs, P-APM mode-locked lasers routinely generate self-starting pulse trains in practice. Since the P-APM mechanism is an instantaneous artificial saturable absorption action, which means it reacts to the pulse instantaneously in the time domain, this mode-locking mechanism is able to generate pulse trains with durations only limited by other laser dynamics. Pulse duration in the range of 28 fs has been reported in P-APM lasers [1, 2]. In reality the pulse durations indeed are limited by the gain bandwidth of the gain medium or Kelly sidebands [33] if the fiber laser is running at the soliton regime.

One of the practical drawbacks of the P-APM laser is the graduate shift of the state of polarization of the pulses inside of the fiber laser cavity, due to temperature drift and slow relief of the mechanical stress of the fibers. This effect hinders the long term reliability of the mode-locking action. Periodically the P-AMP laser will fall out of mode-locking due to this problem. This problem has been a major roadblock preventing the commercialization of P-AMP based fiber lasers.

1.4.3. Saturable Bragg Reflector Mode-locking

In general, an SBR [34-37] contains a semiconductor Bragg reflector and a single quantum well absorber layer near the surface as shown in Figure 1.4. The materials of the Bragg reflector have larger bandgap energy, so that essentially no absorption occurs in that region. A thicker absorber layer can be used to obtain a large modulation depth. A suitable passivation layer on the top surface can increase the device lifetime.

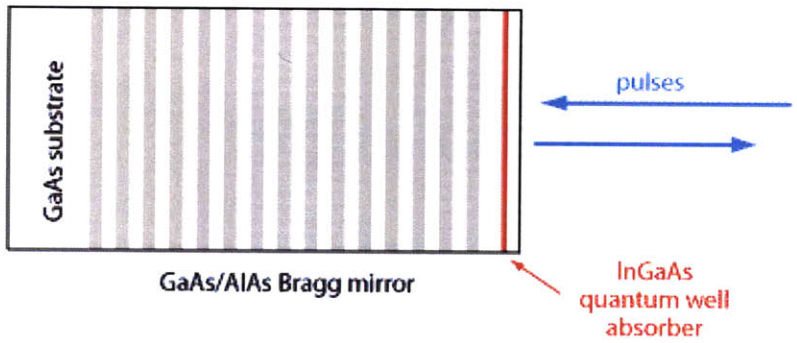

Figure 1.4: Structure of a typical SBR. On a As substrate, a GaAs/AlGaAs Bragg mirror is grown. Within the top layers, there is an InGaAs quantum well absorber layer.

The penetration of the optical field into a SBR can be calculated using multilayer mirror design software. The optical intensity in the region where the saturable material is placed decides the modulation depth and the saturation fluence. The structure of the Bragg reflector decides the bandwidth and the chromatic dispersion of the SBR. More exotic types of SBRs were also developed including quantum dots embedded in glass [38, 39] or carbon nanotubes [40, 41].

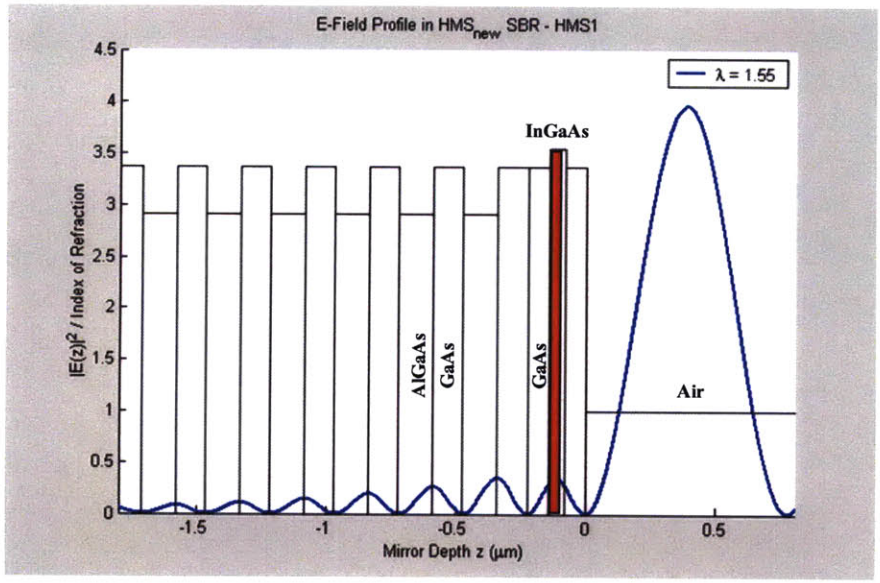

Figure 1.5: Example of refractive index profile and optical intensity distribution within a SBR.

The Fresnel reflection at the semiconductor-air interface together with the Bragg reflection of the SBR leads to a cavity resonance effect which may or may not be desirable in different applications. In some cases, SBRs are designed to be anti-resonant for the operation wavelength. Such SBRs usually exhibit a relatively broad wavelength range with a more or less constant degree of saturable absorption and with small chromatic dispersion. In other cases, resonant designs are used which induces higher modulation depth and lower saturation fluence, in the case of a smaller range of operation wavelengths.

By varying the material composition and certain design parameters, the macroscopic parameters of SBR such as the operation wavelength, modulation depth, saturation fluence, and recovery time can be tailored for operation in very different regimes.

The saturable absorber action is generated by the inter-band transitions in the quantum well layer. When the photons are absorbed by the quantum well layer, the quantum well absorbs the photons energy and the electrons are brought from the valence band to the conduction band. The thermalization relaxation within the conduction and valence band happens fairly quickly in the range of 50~100 fs. However the carrier recombination time is usually in the range of tens or hundreds of picoseconds. In practice, crystal defects are usually exploited to decrease the carriers recombination time.

Very similar to the laser gain dynamics, for low optical intensities, the degree of electronic excitation is small and the absorption is unsaturated. At high optical intensities, electrons can accumulate in the conduction band, so that initial states for the absorbing transition are depleted while final states are occupied known as Pauli blocking, resulting reduced absorption. This effect is demonstrated in Figure 1.6, where it shows the change of the reflectivity of the SBR when receiving a short pulse. After the short pulse leaves the SBR, the absorption recovers due to intra-band thermal relaxation as well as carrier recombination.

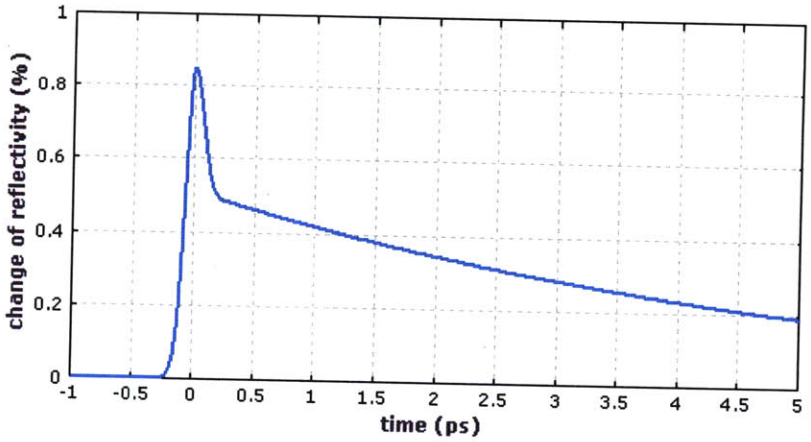

Figure 1.6: Example of reflectivity change of a semiconductor saturable absorber, hit by a short pulse at $t = 0$.

Several important characteristics and definitions for SBRs are listed below, these concepts play a critical role in passive mode-locking dynamics:

1. Modulation Depth: It is defined as the maximum nonlinear change in reflectivity for a pulse which depends on the thickness of the absorber, material composition, optical wavelength, and the amount of optical field penetrated into the absorber structure.
2. Saturation Fluence: It is defined as the fluence of an incident pulse required for significant absorption saturation, which depends on the absorber material, wavelength, and the field penetration into the absorber structure.
3. Recovery Time: it is defined as the exponential time constant of absorption recovery after a saturating pulse. It is normally between a few hundreds of femtoseconds and hundreds of picoseconds. The recovery time is strongly influenced by the defect density in the absorber, and possibly in nearby structures.
4. Un-saturable Losses: it is the loss of the SBR when the SBR is fully saturated. Generally un-saturable losses are unwanted, since they only lead to device heating while not contributing to the pulse shaping.
5. Linear Loss: it is the loss of the SBR when the pulse energy and peak power is minimal which is equal to un-saturable loss plus the modulation depth.

InGaAs quantum-well-based SBRs are typical examples of SBRs, where the indium content is adjusted to achieve an appropriate value of the bandgap energy. The mirror structure is based on GaAs and AlAs, grown on a gallium arsenide wafer. The lattice mismatch of InGaAs on GaAs and AlAs causes significant compressive strain in the absorber layer. Particularly for high indium contents, this can cause the formation of defects. The effect of defects may be helpful, as it reduces the recovery time and may thus allow for shorter pulses and better pulse stability in a mode-locked laser. The defect concentration is therefore often increased by low-temperature growth of the absorber layer. However, if the growth temperature is too low and/or the indium content is too high, non-saturable losses can become too high. The recovery time may also be reduced by bombardment with fast ions after growth known as ion implantation. Partial annealing of defects at some elevated temperature can help to find a better compromise between non-saturable losses and recovery time.

At longer wavelengths such as the bands around 1.3 or 1.5 μm, InGaAs quantum wells can also be used, but they have a very high built-in strain. Therefore, GaInNAs (dilute nitride) absorbers have been developed [42-45], which allow for very low non-saturable losses. It is also possible to use indium phosphide-based absorbers in devices grown on InP wafers [46-48]. Various types of Bragg mirrors are used in the 1.5-μm region, partially depending on the type of absorber layer.

Although most SBRs exhibit only moderate amounts of chromatic dispersion for reflected light, dispersion of any sign can be engineered into a SBR via the multilayer structure [36]. Such dispersive SBRs may then serve the purpose of dispersion compensation in a laser cavity in addition to the function of a passive mode locker.

SBRs are widely used in passive mode locking of fiber lasers. They work with a wide range of laser parameters and usually allow for reliable self-starting mode locking if their device and operation parameters are well chosen. In addition, unlike the P-APM mode-locking method, the state of the polarization does not contribute to the mode-locking action. This means that the gradual shift of the state of polarization, due to temperature drift and slow relief of the mechanical stress of the fibers, do not hinder the long term stability of the mode-locking. This provides a real advantage in industrial and commercial applications.

The disadvantage of SBRs can be long recovery time. The state-of-the-art shortest recovery time for SBRs is around 1~2 picoseconds compared to artificial saturable absorbers which is almost instantaneous. Additional pulse dynamics need to be engineered in SBR based fiber lasers to obtain shorter pulses.

Furthermore, SBRs can only tolerate a certain amount of heat load and therefore incident optical power. Thermal and optical damage issues become important not only at high average power levels, but also for operation with very high pulse repetition rates. In general, high repetition rates lasers demand gain medium with small footprints, high doping concentration, and large amount of pump power. To maintain small footprints, especially in fiber lasers cavity configurations, SBRs are desired to be in physical contact with the gain fibers. As a result, the large amount of heat generated in the short pieces of gain fiber may contribute to thermal damages in addition to that from the average signal power.

1.5. Summary of Ultrafast Fiber Lasers

Based on our discussion in the previous sections, a brief summary of the advantages and drawbacks of each type of ultrafast fiber lasers are listed in

Table 1-1. This comparison is generic, not taking into consideration several extreme cases. For example, generally active mode-locking gives sub-par timing jitter performance. However, under the condition that great care has been taken to lock the system to a thermally and mechanically stable Fabry-Perot (FP) cavity, actively mode-locked lasers can also produce pulse trains with excellent timing jitter performance [49]. Nevertheless, this is at the cost of expensive locking electronics as well as larger footprints, making it non-ideal for integrated approaches.

Another disclaimer regards the self-starting property of the NOLM fiber lasers. Even though several experiments have been reported with self-starting performance [50-52], most of the reported NOLM fiber lasers have a lower self-starting probability than SBR lasers and P-AMP lasers do, making the NOLM approach a less attractive one.

		Pros	Cons
Active mode-locking		Self-starting Expensive with electronics	Pulse duration in picosecond range Sub-bar noise performance Large footprints
Passive mode-locking	NOLM	Femtosecond pulse duration Excellent noise performance Compactness	None self-starting
	P-APM	Femtosecond pulse duration Excellent noise performance Self-starting Compactness	Polarization drift induced instability
	SBR	Self-starting Compactness Excellent noise performance	Heat handling issues Pulse duration in picosecond range

Table 1-1: Comparison between variety of ultrafast fiber lasers

Chapter 2.

En Route to High Repetition Rates

2.1. Motivating Applications

Ultrafast laser sources are the workhorses for all ultrafast application. They are the first step of the applications and one of the fundamental limitations of the entire application. As we discussed in Chapter 1, more and more applications demand ultrashort fiber lasers to produce low jitter pulse trains with durations in the 100 fs range and repetition rates in the GHz range. These applications include femtosecond laser frequency comb generation for frequency metrology, optical arbitrary waveform generation, timing and frequency distribution via optical fiber links, and high speed optical sampling. [53-55]

In all these applications, the four criteria of operating wavelength at 1550 nm, high repetition rates, femtosecond pulse duration, and low timing jitter need to be satisfied simultaneously. The following sections 2.2 and 2.3 discuss two of these applications in detail, Optical Arbitrary Waveform Generation (AOWG) and Photonic Analog-to-Digital Convertion (Photonic ADC).

2.2. Optical Arbitrary Waveform Generation

It has been a researcher's dream to have complete pulse-to-pulse waveform control in the pulse trains, known as Optical Arbitrary Waveform Generation. With applications such as remote chemical identification and ultra-high resolution imaging in mind, researchers are developing the OAWG systems in the visible and near-infrared wavelength regions with 10-40 GHz pulse-to-pulse reconfiguration of the waveform.

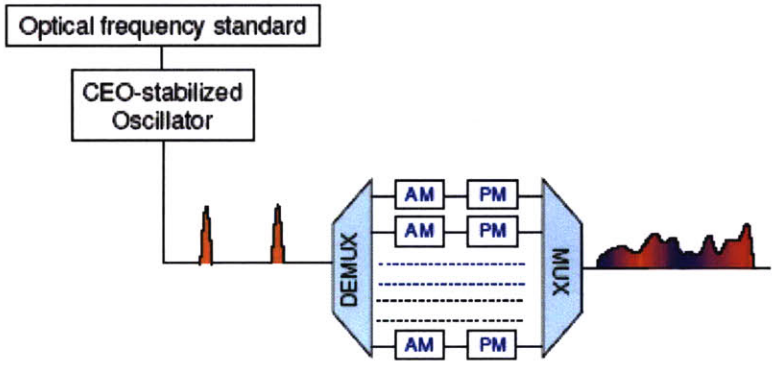

Figure 2.1: An OAWG system consists of an oscillator stabilized using an optical frequency standard to produce the frequency comb; a demultiplexer to separate the comb lines; a bank of modulators to control the amplitude and phase of each comb line, and a multiplexer

The principle of the OAWG is straight forward as shown in Figure 2.1. Starting from a regular pulse train where each pulse in the pulse train has the same shape and characteristics. This pulse train goes through a de-multiplexer (DEMUX) where each of the comb lines will be separated and sent to a bank of modulators. These modulators will modulate each of the comb lines both in amplitudes and in phase domain. After the modulation bank, the modulated comb lines are combined together at the output of the system by a multiplexer (MUX). This can be understood as constructing the optical time-domain waveform in the frequency domain using the relationship expressed by the Fourier Transform pairs. In an OAWG system, the frequency components that construct the final waveform are individually adjusted in amplitude and phase

to create the desired time-domain waveform. Generally, the optical bandwidth is ranging up to 1 THz encompassing ~100 channels, fully flexible in amplitude (0-100%) modulation and phase (0-2π) modulation control.

Even though there has been significant progress in the field of OAWG [56-61], there are still significant limitations. One of the major limitations is the footprint of the reported systems where bulk free space grating pairs are used for de-multiplexing and multiplexing in addition to the phase and amplitude modulators. For practical applications, a more compact footprint is desired.

Various integrated approaches have been developed to solve this problem, such as a novel technique developed at University of California at Davis using integrated photonics to implement the MUX and DEMUX as well as the phase and amplitude modulation in a single chip has opened up the possibility to realize a fully integrated OAWG. However, in order to adapt to this integrated approach, stringent requirements are imposed on the laser sources of the system. The smallest comb line separation needs to be around 10 GHz to avoid crosstalk produced at the photonic integrated MUX and DEMUX. This would require the mode-locked laser source to have 10 GHz repetition rate.

Another reason for high repetition rates is the number of the channels manageable within a single MUX and DEMUX chip. At the optical bandwidth of 1 THz, 100 channels are required if the separation of each channel is 10 GHz. As the result, a mode-locked laser source with repetition rate at 10 GHz is highly desired.

In addition to the requirement of the high repetition rate at 10 GHz, there are other requirements to the laser source. First of all, the carrier-envelope-offset frequency (f_{ceo}) as well as the repetition rate have to be stabilized. Generally either 1f-2f or 2f-3f detection is needed to stabilize the f_{ceo} and repetition rate of the pulse train. In either case, the pulse train is sent to a piece of nonlinear fiber and additional spectra are generated for 1f-2f or 2f-3f detection and locking. Pulse trains with durations in the picosecond range suffer so much distortion in this nonlinear process that additional unwanted phase noise maybe added to the system. As the result, pulse train with duration of 100~200 femtosecond are highly desired from the laser source.

Furthermore, in order to control the pulse to pulse waveform, low noise operation is of utmost importance in the laser source requirement. This low noise operation includes timing jitter and intensity noise of the pulse train. This also put another constraint on the noise performance of the laser source.

Adding all of the requirements together, a mode-locked laser source at 1550 nm to utilize the low cost and high reliability nature of well-developed commercial grade components from the telecomm industry; producing low timing jitter and low intensity noise pulse train, with ~100 femtosecond pulse duration, and at a multi-gigahertz repetition rate is desired.

2.3. Photonic Analog to Digital Conversion

Digital signal processing has revolutionized modern communication and laser LADAR systems over the last decades. As the first step of the digital communications, analog-to-digital conversion (ADC) is the backbone of these systems. However, wide band applications cannot benefit from today's digital signal processing systems due to the inadequate bandwidth of their ADCs [62]. Real-time capture of ultrafast electrical signals is a challenging task and requires wide-band ADCs.

The performance of electronic ADCs is limited by a variety of factors including timing jitter of the sampling clock, settling time of the sample-and-hold circuit, comparator ambiguity, and mismatches between the transistor thresholds and passive component values. All these factors become more severe at higher sampling frequencies imposing a limitation in sampling rates. Approaches utilizing time-interleaved ADC architectures [63, 64] can further improve the performance, however mismatches between the digitizers limit the dynamic range and hence the resolution of the system [63, 64]. Readers are encouraged to refer to [65] for a more detailed discussion on the limits of the electronic ADCs.

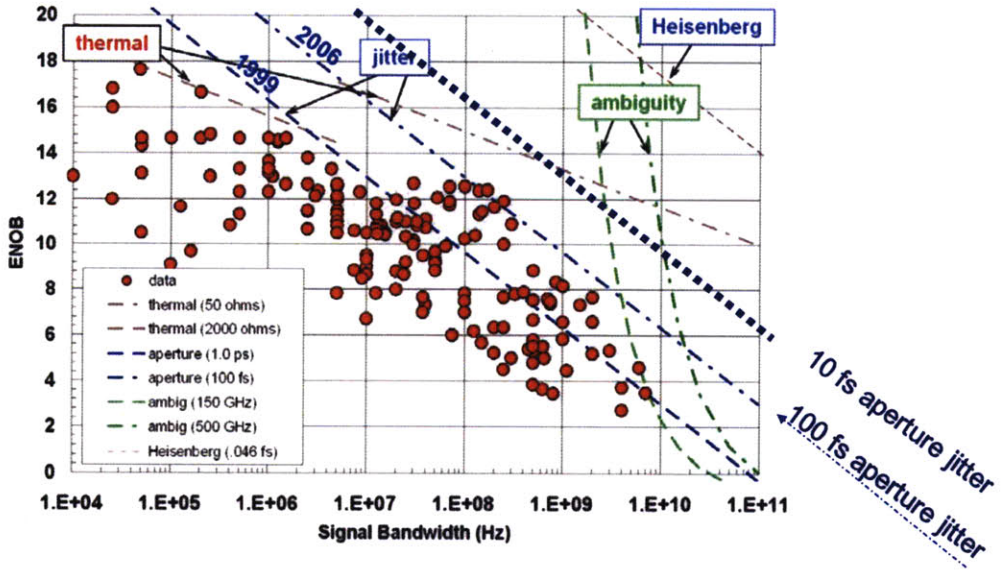

Figure 2.2: Electronic ADC performance limits [ref. 65]

Figure 2.2 shows the state-of-the-art performance of the electronic ADCs [65]. The vertical axis is the effective number of bits (ENOB) and the horizontal axis is the bandwidth of the analog input signal. Dashed lines demonstrate the performance limits of the ADCs over the years. As an example, for a ENOB of 8, electronic ADCs can only support the analog input signal bandwidth of 2.5 GHz in 2007.

Photonic ADCs utilizing time-stretched femtosecond pulses have proven to have potential to out-perform electronic ADCs [66-68]. Significant progress has been achieved recently in the area of photonic ADCs. Two approaches are favored by researchers among various methods.

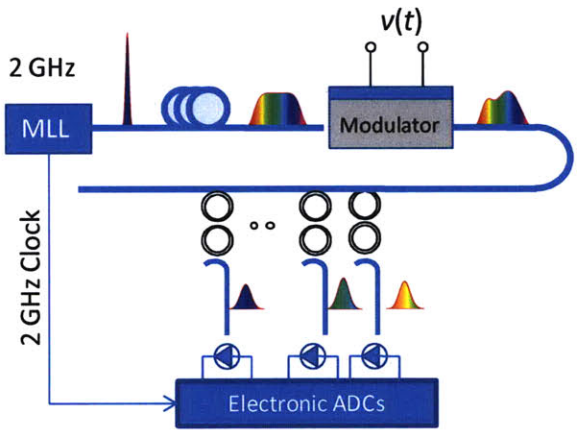

Figure 2.3: Photonic ADC Scheme proposed by MIT [Ref. 67]

Figure 2.3 shows the schematic diagram of one of the preferred approaches. A mode-locked laser source producing a 2 GHz pulse train with 100 femtosecond pulse duration serves as the source of the system. The 2 GHz pulse train propagates through a dispersive element that chirps the pulses before the pulse train reaches the intensity modulator. The analog signal to be digitalized is applied to the modulator as the modulation signal. When the chirped pulses propagate through the modulator, the analog signal is mapped onto the envelope of the chirped pulses in the time domain as well as in the wavelength domain, making it possible to carry out sampling in the wavelength domain via wavelength filter banks. In addition to serving as the source, the 2 GHz mode-locked femtosecond laser also serves as the clock source for the electronic ADCs as the last step of digitization.

Another popular approach is demonstrated in Figure 2.4. It employs a similar approach as the first example utilizing the mode-locked laser and the dispersive element before the intensity modulator. However, instead of sampling in the wavelength domain after the modulator, it exploits the time-stretching scheme where the pulses are chirped further so that effectively the system slows the analog signal down prior to its being digitized. In theory, if the WDM separates the optical signal into M divisions, a stretch factor of M can be implemented in this stage to increase the effective input bandwidth of the analog signal by a factor of M.

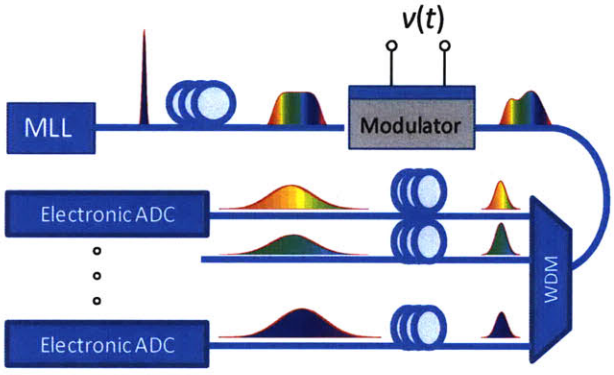

Figure 2.4: Photonic ADC proposed by UCLA [Ref. 68]

Even though photonic ADCs provide significant advantage over electronic ADCs especially in wide-band operations, researchers still face several challenges including the system complexity in the optical domain, low cost, and the fundamental limitation set by the electronic ADCs as the last stage of the system.

Mode-locked lasers play an important role in photonic ADC systems since they serve as the optical source of the system as well as the clock signal generator. Naturally the repetition rates of the mode-locked laser sources in these systems directly dictate the systems' sampling rates. Furthermore, low noise operation is critical for ADCs and timing jitter is an always-decreasing parameter required by these systems.

2.4. Stringent Requirements

The requirements for the laser sources are always based on their application needs. Judging from the needs of the applications discussed in section 2.2 and section 2.3, in addition to other applications including frequency metrology, terahertz generation and detection, and remote optical frequency standards distribution, fiber laser sources with the following characteristics are highly desired:

- Operation wavelength is centered at 1550 nm
- Repetition rate is in the multi-gigahertz range
- Pulse duration is around 100~200 femtoseconds
- Low timing jitter preferably below 10 fs in [1kHz, 10 MHz]

Note that all of the above requirements need to be satisfied at the same time.

In the following sections 2.4.1 and 2.4.3, a detailed discussion will be given to further understand the reasons behind these four requirements.

In section 2.5 we will discuss the technical considerations of how to approach this challenging task.

2.4.1. Operating Wavelength

During the last two decades, telecommunication has been one of the major industries that enabled worldwide growth of the economy. One of the by-products from these rapid technology developments in the telecommunication industry is the abundance of commercially available optical components operating in the telecommunication wavelength. Thanks to the well developed technologies behind these components during the telecommunications boom, standard

undersea components usually have low noise performance, wideband operation, with lifetime well over 20 years, and are inexpensive and commercially available. This is the fundamental reason for researchers to consider building their applications in the 1550 nm wavelength range if their systems are flexible on the center wavelength selection.

2.4.2. High Repetition Rates and Femtosecond Pulse Duration

Figure 2.5 and Figure 2.6 show a time domain and frequency domain representation of a mode-locked pulse train. Aside from pulse energy, operating center wavelength, pulse duration, and pulse spectral width, are two more parameters of interest that influence the feasibility to go towards higher repetition rates. T_R denotes the pulsation period while its inverse, f_R, denotes pulse repetition rate. As we observe from Figure 2.5 and Figure 2.6, pulse trains with higher repetition rates demonstrate denser pulse spacing in the time domain, and a higher separation between the comb lines in the frequency domain.

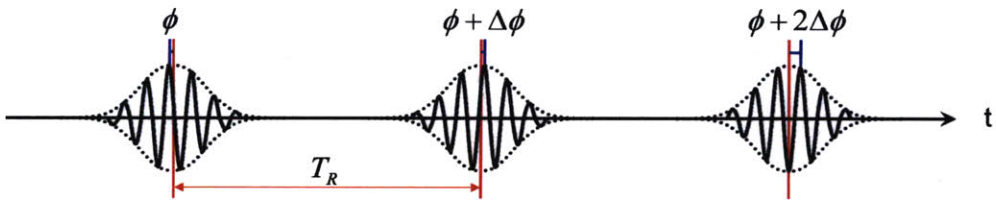

Figure 2.5: Time domain representation of a mode-locked pulse train

In most of the cases, the overall mode-locked spectral width in frequency domain is limited by the gain bandwidth; the average power of the pulse train is limited by the pump power available. Thus wider comb line spacing results in higher optical power per comb line. This is very valuable for frequency metrology since a higher optical power per comb line enables higher

signal to noise when beating one of the comb lines against a spectral line of the device/material under test.

As mentioned in section 2.2, applications such as optical arbitrary waveform generation are drivers towards higher repetition rates. In these applications, each of the optical comb lines needs to be separated in the frequency domain by a de-multiplexer so that the phase and amplitude modulations can be carried out on each of the separated comb lines. It is very critical to eliminate the crosstalk during this process, which means that wider comb line spacing will make it easier to separate them. To date, the state-of-the-art de-multiplexer can only operate in the 10 GHz range, thus it is ideal for the comb line spacing to reach 10 GHz of separation, i.e. the repetition rate of the mode-locked lasers to reach 10 GHz.

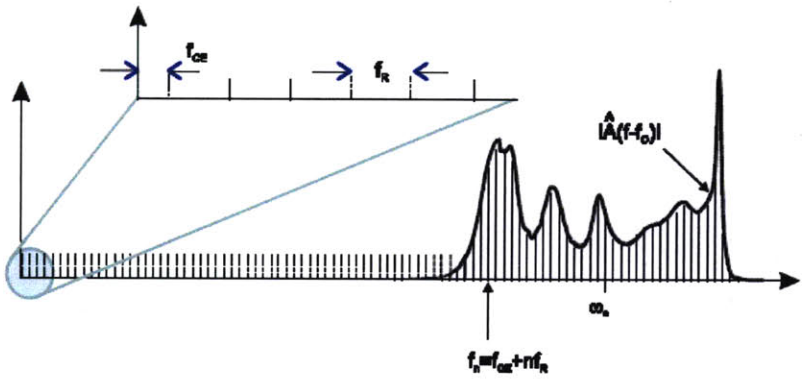

Figure 2.6: Frequency domain depiction of a mode-locked pulse train

Other applications utilize the short pulse properties of the mode-locked pulse train in combination with electronic detection. In certain cases, the application requires to have a high average power, short pulse duration, as well as low nonlinear effects, i.e. it requires higher repetition rates to keep the pulse energy low, for example in timing and frequency stabilization systems [69]. The cross-correlation operation within the timing link requires that the pulse duration to be as short as possible while the electronic detection after the cross-correlation

requires a high average optical power for high signal to noise ratio. The only solution to this problem is to scale up the repetition rate of the laser source.

2.4.3. Low Timing Jitter

Low noise performance is utterly important to all the applications above. Frequency metrology applications reply on the precise frequency comb line position for accurate measurement results. OAWG applications require low timing jitter pulse trains to produce shot per shot real time configurable optical waveforms. Timing and frequency distribution applications require often sub-10 femtosecond timing jitter performance from the locked optical links, hence low noise sources are key to successful system implementation.

2.5. Possible Approaches and Thesis Organization

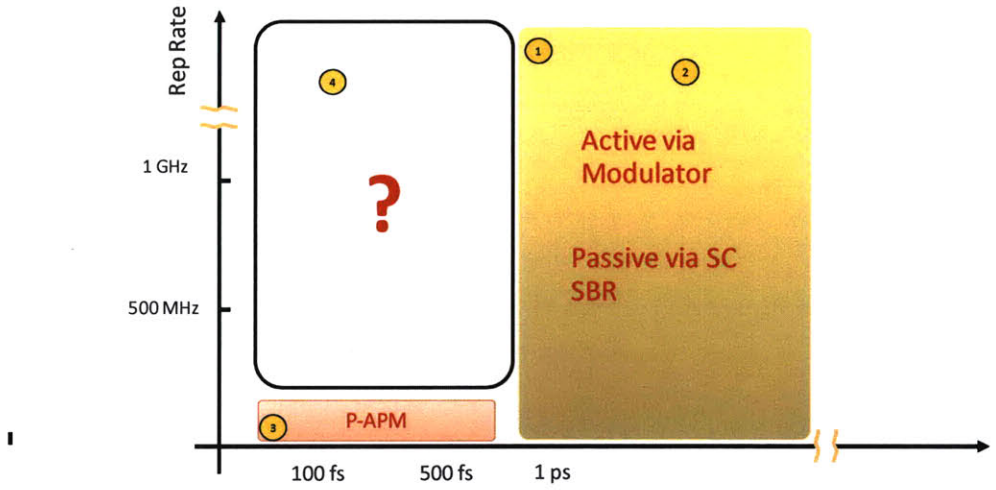

Figure 2.7: Roadmap for high repetition rate fiber lasers at 1550 nm

Scaling up the repetition rates to the multi-gigahertz range is a challenging task in traditional fiber lasers. Prior to the research accomplished in this thesis, the highest repetition rate achieved in fundamentally mode-locked femtosecond fiber lasers to our best knowledge was around 80 MHz [70]. Lack of demanding applications to push to higher repetition rates was one reason, but most critically, the technology barrier set by the gain fiber fabrication techniques, commercially feasible pump powers, as well as the lack of novel cavity designs and mode-locking techniques has hindered progress in scaling up the repetition rates.

Figure 2.7 shows the roadmap of the current achievement in terms of repetition rates and pulse durations. Data point (1) (2) (3) and (4) represent several examples of typical laser sources at 1550 nm. Where (1) represents a 154 GHz actively mode-locked fiber laser with a pulse duration of 800 fs [71]. (2) represents a 77 GHz ErYb glass laser with 3 ps pulse duration[72], (3) represents a typical P-APM fiber laser with 100 fs pulse duration and a repetition rate of 80

MHz [70]. (4) represents a Cr^{4+}:YAG laser mode-locked via Kerr lens mode-locking with 4 GHz repetition rate and a pulse duration of 80 fs [73].

2.5.1. Repetition Rate Multiplication

One approach is repetition rate multiplication; however, there are limitations to this approach.

Repetition rate multiplication can help to a degree in our approaches, especially external repetition rate multiplication techniques. As discussed in Chapter 1 as well as in the following sections, passive mode-locking is the preferred path due to its low noise, compact size, and short pulse duration. Intra-cavity repetition rate multiplication is extremely difficult especially in P-APM and NOLM lasers.

In addition, repetition rate multiplication techniques, especially external cavity repetition rate multiplication, exploits the filtering action in frequency domain as discussed in Chapter 5. A high multiplier means a large reduction in average optical power. If the multiplier is too large, there will not be enough optical power to seed an amplifier for the downstream applications.

Furthermore, the repetition multiplication, especially by external multiplication, may add considerable intensity noise to the pulse train even though it is minimal in the initial source [74]. Although the timing jitter is not degraded in this process, the frequency jitter induced intensity fluctuations may contribute to the intensity noise of the multiplied pulse trains as we will see in Chapter 5.

As a result, it is always desirable to start with a high as possible fu fundamental repetition rate laser.

2.5.2. Improving Fundamental Repetition Rates

Due to the low noise performance as well as the femtosecond pulse duration requirements, several traditional approaches for higher repetition rates do not apply in this case. These approaches include the use of multimode pump diodes as well as cladding pumped gain fibers, since optical power couples between different transverse modes during propagation of the pump light in the fiber, and results in large power fluctuations hence strong intensity noise. Active mode-locking schemes are also not appropriate due to their picosecond pulse durations as well as sub-par noise performance.

The recently reported GHz-Cr^{4+}:YAG laser [73] presents a possible solution, however the low gain and problems in material reproducibility make this type of laser difficult to use. Fiber lasers with a NOLM as mode-locker are also not favored due to their self-starting issues.

The only options are to either scale up the repetition rates of the P-APM laser or to shorten the pulse duration in SBR mode-locked lasers. Both approaches will be discussed in Chapter 4 and Chapter 5, respectively.

Chapter 6 will discuss the fundamental limitations of scaling up the repetition rates.

Chapter 3.

High Fundamental Repetition Rate Ytterbium Fiber Lasers

3.1. Motivation

Compared to ytterbium doped fibers, erbium doped fibers have much lower power conversion efficiencies per unit length. This means that the length of the ytterbium gain fiber can be much shorter. Before the availability of Direct Nano-particle Deposition (DND) technology [75], the optimum length of the most effective erbium gain fiber (OFS Lot# 1128) was around 1 meter. In addition, this erbium gain fiber has a normal dispersion of 75 ps^2/km, so certain length of SMF28 fiber is required to compensate for this dispersion. Furthermore, 980/1550 nm WDM and fiber collimators may also be required in the fiber cavity to couple the pump power into the gain medium and for free space output. All these components put a constraint on the length of the fiber laser cavity. As a result, the shortest fiber cavity length was around 4 meters, corresponding to a repetition rate lower than 100 MHz.

Obviously, this limit was set by the erbium doping concentration and power conversion efficiency. The repetition rate of erbium doped fiber lasers couldn't be improved, unless novel doping technologies emerged.

One immediate approach to achieve high repetition rate, femtosecond mode-locked sources at 1550 nm is to explore the possibilities of wavelength up-conversion to 1550 nm from a high repetition rate, femtosecond mode-locked laser source at a lower wavelength.

Ytterbium doped fibers are well developed and can be much more highly doped than erbium fibers. At the time of this research, the highest doping concentration of the ytterbium fiber is around 23,000 ppm, making the optimum gain fiber length of only 20 cm. In addition, free space grating pairs can be used in the ytterbium laser to compensate the dispersion, this further decrease the length of the laser cavity. Mode-locked ytterbium fiber lasers via P-APM routinely generate sub-100 fs pulses at 1030 nm, making them perfect candidates for improving the repetition rate and wavelengths shifting to 1550 nm with additional amplification.

Due to the fact that the shift is a soliton process in Soliton Self Frequency Shift (SSFS), the spectral phase is clean. The SSFS setup is simple and cost effective since no other pump is required, compared to what is in optical parametric amplification setup.

In this research project, the possibilities for scaling up the repetition rate of ytterbium fiber lasers and eventually wavelength shifting the femtosecond pulses from the YDFL at 1030 nm to 1550 nm, is also considered. In addition, the timing jitter and intensity noise performance of the pulses undergoing SSFS is studied, which is critical for certain applications.

3.2. Fundamentally Mode-locked 200 MHz Ytterbium Fiber Laser

3.2.1. Introduction

Rapid progress has been made with Yb-fiber lasers operating at 1 μm in the past two years. A new mode-locking regime exploiting self-similar pulse propagation has been demonstrated [3] and these lasers now routinely generate sub-100 fs pulses with over 5 nJ of energy at repetition rates of 30-50 MHz [76]. To our knowledge, only the lower limit to the repetition rate arising from residual birefringence has been studied. Thus, it seems natural to explore the upper limit to the repetition rate.

In this case, a high repetition rate (>~ 150 MHz) is desirable to attain sufficiently large comb line spacing. Higher repetition rates can be achieved with harmonically mode-locked lasers as well. However, active harmonic mode-locking leads to picosecond pulses and passive harmonic mode-locking is not stable enough for these applications. At the time of this research, the repetition rates of fundamentally mode-locked fiber lasers with pulse durations of 100 fs or less have barely reached 100 MHz at 1 μm[78], and 130 MHz (with an Er/Yb-codoped glass waveguide amplifier) at 1.55 μm [79]. Repetition rates up to 300 MHz have been reported from Er-fiber lasers, however the pulse duration were limited to nearly 500 fs [80].

3.2.2. Design Considerations

In this section, we report systematically scaling the fundamental repetition rate of an Yb-fiber laser up to 200 MHz, while preserving sub-100-fs pulse duration. We choose Yb-fiber as the gain medium since it offers the highest gain per length among readily available fibers. Increasing the repetition rate of fiber lasers encounters two distinct challenges: (i) in practice, the cavity

length is ultimately limited by the physical size of the components constituting the laser cavity, (ii) more fundamentally, there is a threshold power for initiating passive mode-locking.

The commonly used techniques for passive mode-locking of fiber lasers relies on intensity dependent phase shifts accumulated by the pulse as it traverses through the fiber. Nonlinear polarization evolution (NPE) [81] is the most commonly used technique due to its large modulation depth (~50%) and essentially instantaneous response. If a polarizing beamsplitter is used, the rejected light is extracted out of the cavity and acts as a useful output port. Other techniques include the nonlinear optical loop mirror [82] and its variants, which also have been demonstrated to generate high-energy, short pulses [83]. However, these techniques require longer fiber lengths, rendering them unsuitable for high repetition rate operation. Decreasing the cavity roundtrip time causes less energy to be stored in the cavity, limiting the peak power of the pulse, and for given power, a shorter fiber section results in smaller nonlinear phase shift to be accumulated. Therefore, with all other parameters unchanged, to first order, the pump power threshold for mode-locking increases quadratically with the repetition rate, unlike the linear dependence for a laser mode-locked by a saturable Bragg reflector.

3.2.3. Experimental Setup

The cavity setup shown in Figure 3.1 is similar to the laser described in Ref. [78] with one important difference: the gain fiber is located at the beginning of the fiber section with respect to the direction of pulse propagation as in Ref. [84], in order to maximize the nonlinear effects. The lead fiber of the input collimator was kept as short (12 cm) as allowed for comfortable splicing to the Yb fiber. The highly-doped (23,000 ppm) Yb fiber (core diameter 6 μm, NA 0.16) is only 22 cm long. The calculated group-velocity dispersion (GVD) coefficient is 23 fs^2/mm. Pump light is delivered through a 980 nm/1030 nm wavelength de-multiplexing (WDM) fiber coupler with Lucent-980 fiber (mode field diameter ~5 μm, NA 0.16) with a GVD coefficient of 27 fs^2/mm [84]. The pump source is a fiber-coupled telecom-grade diode laser at 981 nm, which delivers a maximum power of 400 mW. The remaining fibers are that of the fiber collimators, standard

single-mode fiber (SMF) for 1 μm wavelength with a calculated GVD of 24 fs^2/mm. A ring cavity was chosen for higher repetition rate. A bulk isolator (with an estimated dispersion of +3000 fs^2) imposes unidirectional operation. A pair of diffraction gratings (600 lines/mm, incidence angle of 45 degree) provides anomalous dispersion of adjustable magnitude. The gratings are of low quality with 50% total transmittance. Mode-locking is initiated and stabilized by NPE.

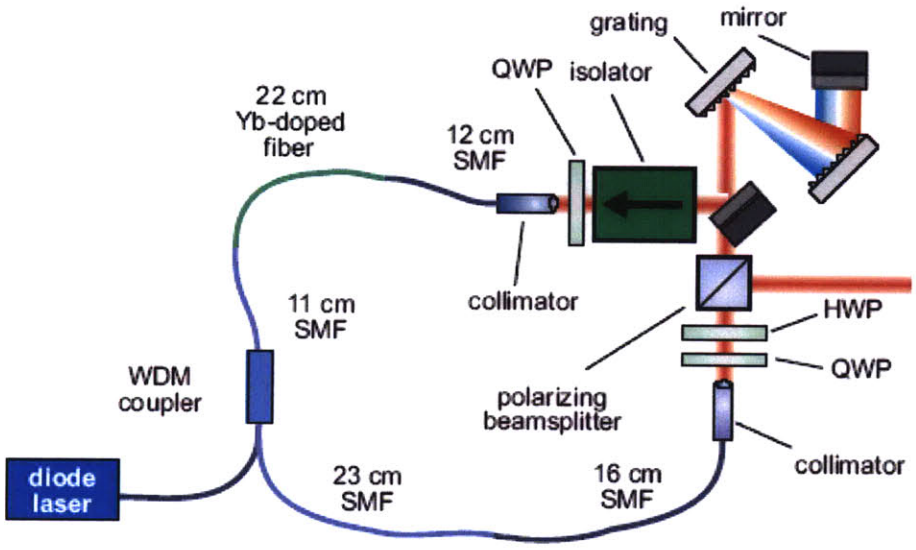

Figure 3.1: Experimental setup. Abbreviations: SMF single mode fiber, HWP half-wave retarder, QWP quarter-wave retarder, PSB, polarizing splitter beam-cube, WDM wavelength de-multiplexing coupler.

3.2.4. Experimental Results

The repetition rate of the cavity was increased in discrete steps, starting from 100 MHz, by shortening the undoped fibers. The grating spacing was adjusted for the desired cavity dispersion. The free-space section was 50 cm-long.

At a repetition rate of 162 MHz, the total fiber length is 90 cm. Mode-locking is easily obtained by adjusting the wave-retarders for the NPE. Once set, mode-locking is self-starting, and requires no further adjustment. The net cavity GVD was first set to net anomalous (negative) and systematically reduced to zero and changed to normal (positive) GVD. At each GVD setting, the laser was mode-locked similarly. This way, we observed the main features of the various pulse evolutions previously observed in fiber lasers: soliton-like pulses at negative GVD, dispersion-managed solitons around zero GVD [32] and some indications of self-similar pulses at positive GVD [3].

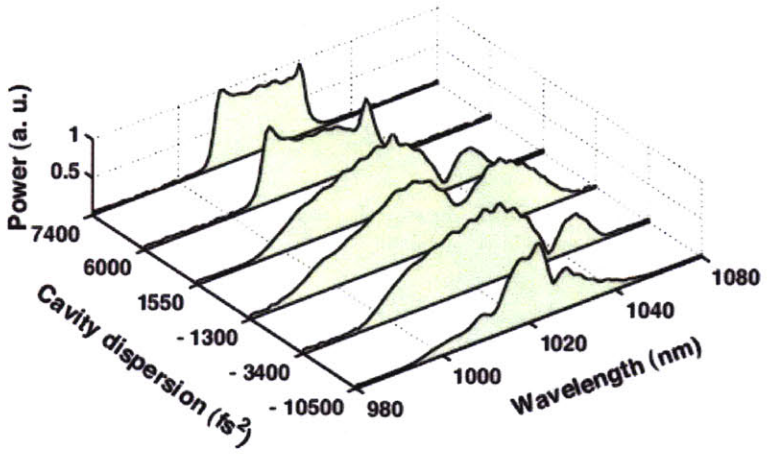

Figure 3.2: Evolution of the pulse spectrum as the cavity dispersion is changed from −10500fs2 to +7400 fs2.

The effect of increasing the repetition rate has consequences reaching beyond that of a higher mode-locking power threshold: the shorter fiber segment corresponds to a smaller swing in the dispersion map created by the positive GVD fibers and the negative GVD from the gratings. At sufficiently short lengths, the pulse would cease to stretch and compress and would simply experience the average GVD. At a repetition rate of 162 MHz, this effect is not severe yet and the typical transformation of the spectral shape reported in Ref. [78] is observed experimentally as the dispersion is adjusted from −10500 fs2 to +7400 fs^2 (Figure 3.2). Due to

uncertainties in the GVD coefficients and the fiber lengths, we estimate that the absolute values of net GVD has an error of ± 1500 fs^2. However, relative changes to the net GVD are known precisely since the GVD of the gratings is well known. The pulse duration after external de-chirping ranges from 70 fs to 135 fs. The corresponding characteristic dispersive length in the fiber segment ranges from 6.4 cm to 23.0 cm, which suggests an intra-cavity breathing ratio of ~4, given the fiber length of 90 cm. This value is in contrast to the high-energy fiber lasers that were operated at 30-40 MHz repetition rate, commonly attaining intra-cavity breathing ratios of 10-30 [3, 76].

We describe the performance of the laser at 162 MHz with a view toward applications. In accordance with previous results, we attain the shortest pulses at small net negative GVD. At a net GVD of -1300 fs^2, the pulses rejected at the NPE port are de-chirped to yield an intensity autocorrelation width of 96 fs, from which we infer a pulse width of 70 fs, assuming a Gaussian pulse shape (Figure 3.3). The output pulse energy is 150 pJ, limited by the pump power. Measuring the power of a portion of the intra-cavity beam, which is reflected off the first grating, enables us to accurately determine the pulse energy in the fiber segment to be 0.65 nJ. Although multiple pulsing is not a serious concern at this energy level, long-range autocorrelation measurements and the RF spectra were checked to rule out this possibility. The RF spectrum shows that the pulse contrast is at least 60 dB (at the measurement bandwidth of 10 Hz) (Figure 3.4).

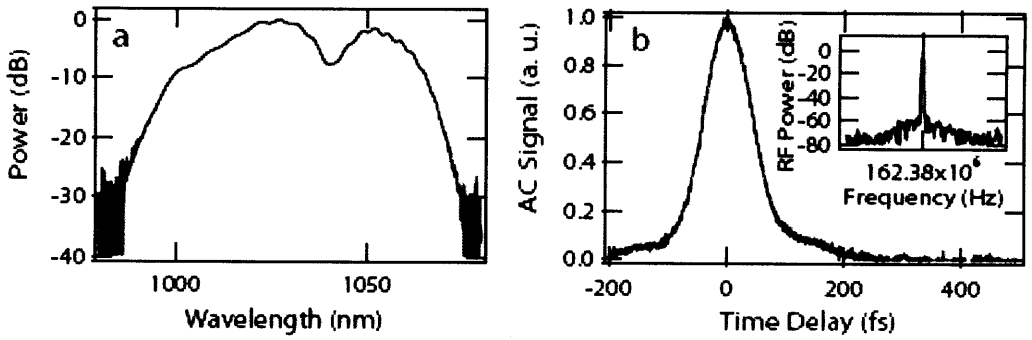

Figure 3.3: (a) Optical spectrum at cavity dispersion of −1300 fs2 at 162 MHz repetition rate. (b) Intensity autocorrelation of the pulses after external de-chirping. Inset: RF spectrum of the pulses.

Even though mode-locked operation is possible at large positive GVD (Figure 3.3), there are differences from previous results reported for similar Yb fiber lasers at lower repetition rates due to the weaker dispersion map. It was not possible to operate this laser exhibiting self-similar pulse evolution with all of its characteristic features [3]. Operation at +6000 fs^2 and +7400 fs^2 has little intra-cavity breathing and the spectral shape is different from that of similariton lasers. For the latter case, the amount of dispersion necessary to de-chirp the pulses is twice that provided by the grating pair inside the cavity. From the measured autocorrelation and the known magnitudes of dispersion from the gratings, we determine that the pulse always maintains a large positive chirp within cavity, varying from ~ 3.5 times the transform-limit at the beginning of the fiber section to ~ 7 times at the end of the fiber section. Even though these pulses exhibit the monotonic stretching of positively chirped pulses in the fiber segment as in self-similar propagation, the pulse breathing is much weaker and the pulse shape does not appear to be parabolic. This deviation is not surprising, considering that the self-similar mode of operation necessitates significant reshaping of the pulse during each roundtrip [85]. We expect that it would be possible to attain true self-similar operation at higher repetition rates with the use of specialty fibers with a higher dispersion coefficient to ensure sufficient pulse breathing and a tighter mode confinement (alternatively, higher pump power) for stronger nonlinear effects.

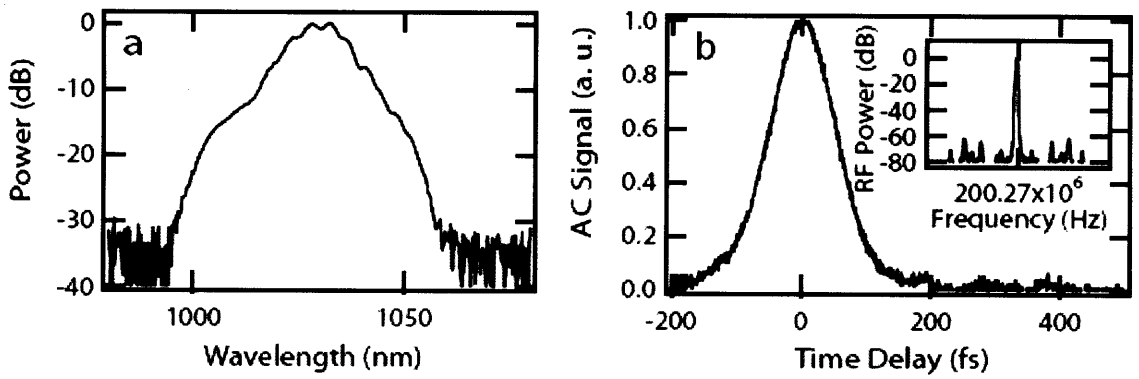

Figure 3.4: (a) Optical spectrum at cavity dispersion of -8400 fs^2 at 200 MHz repetition rate. (b) Intensity autocorrelation of the pulses after external dechirping. Inset: rf spectrum of the pulses.

It was possible to increase the repetition rate up to 200 MHz by reducing the total fiber length to 66 cm, which is finally limited by the physical size of the cavity elements. At this repetition rate, mode-locking could be obtained only when the net GVD of the cavity is anomalous. Attempts at mode-locking for GVD smaller than -3000 fs^2 have failed. Mode-locking at large negative GVD is not more difficult than at 162 MHz, so we attribute failure of mode-locking at zero and positive GVD partially to insufficient strength of the dispersion map [86], or simply to the self-starting mechanism being too weak. At net GVD of -8400 fs^2, where mode-locking is obtained easily, the pulse energy is 145 pJ (average power of 29 mW). The optical spectrum, autocorrelation, and RF spectrum are shown in Figure 3.4. The inferred pulse duration is 85 fs (assuming a Gaussian pulse shape). The mode-locked train and the RF spectrum indicate clean mode-locking. Since the physical size of the cavity restricts us to ~200 MHz, we conclude that insufficient nonlinearity is not the immediate limitation to repetition rate in femtosecond fiber lasers mode-locked by NPE. We estimate that the repetition rate can be increased to 250-300 MHz by shrinking the free-space region and minimizing the undoped fiber length with a careful engineering effort.

3.2.5. Summary

In conclusion, we have demonstrated sub-100 fs pulse generation from a fiber laser with repetition rates up to 200 MHz. This laser is a reliable and inexpensive tool constructed entirely from commercially available components. Along with previous results for low repetition rates, it is now established that passively mode-locked Yb fiber lasers producing ~ 100-fs pulses can be operated with repetition rates anywhere between 20 and 200 MHz. With external amplification, this laser can serve as an ideal seed source for super-continuum generation for applications that benefit from higher repetition rates, such as frequency metrology, micromachining, and bio-medical imaging.

3.3. Wavelength Up-conversion from Ytterbium Fiber Lasers

The SSFS in optical fibers is a well-known phenomenon and applications such as widely tunable sources have been demonstrated in the past [87, 88]. In this section, we present one of the longest SSFS at the time of the experiment, connecting the wavelengths of 1.03 μm and 1.55 μm where powerful rare earth doped fiber amplifiers are available. This experiment opens up opportunities for applications such as seeding of parametric amplifiers or the pursuit of carrier-envelope phase independent clockworks, since the difference frequency between 1.04 μm and 1.5 μm is at 3.39 μm, where a transportable frequency standard exists [89]. Frequency metrology applications are critically dependent on the coherence properties of the frequency-shifted pulse. We also characterized the timing jitter of the shifted pulse train with respect to the input pulse energy. The increased timing jitter is traced back to the laser intensity noise.

3.3.1. Experimental Setup

Numerical simulations guided us to use NL-3.0-975 photonic crystal fiber (PCF) from Crystal-Fibre with a nonlinear coefficient γ= 25 W-1Km-1 and $\beta 2$= -8 ps^2/km at 1.03 μm and -33 ps^2/km at 1.55 μm. The experimental setup is shown in Figure 3.5. Pulses at 1.03 μm with energy of 0.24 nJ are generated from an ytterbium doped fiber laser with a repetition rate of 33 MHz. An ytterbium-doped fiber amplifier followed by a grating pair compressor produces nearly transform-limited pulses with 78 fs duration and 3.8 nJ of energy. These pulses are coupled into a 1.5 m-long PCF via an objective lens. The pulse energy in the PCF is 1.5 nJ. The output from the PCF is connected to an erbium doped fiber amplifier (EDFA), which boosts the energy of the frequency-shifted pulse at 1.55 μm to 1.2 nJ. The pulse width of the shifted pulse at 1.55 μm is measured to be 714 fs without dispersion compensation.

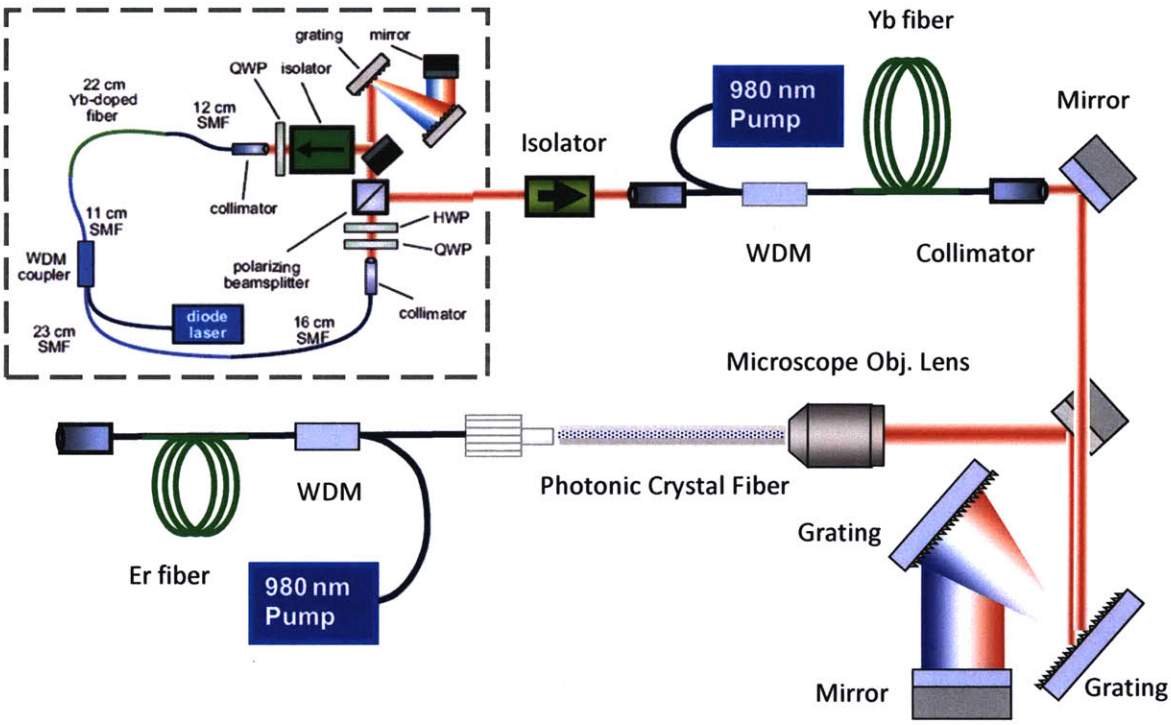

Figure 3.5: Experiment setup to generate 1.55 μm pulses from a 1.03 μm source.

Normalized pulse spectra before and after the frequency shift are shown in Figure 3.6. We are able to control the amount of frequency shift across the entire spectral range by adjusting the launched pulse energy into the PCF, while the spectrum of the red-shifted pulse keeps a soliton-like shape. Even longer self-frequency shifts are possible with a longer PCF and/or higher pulse energy.

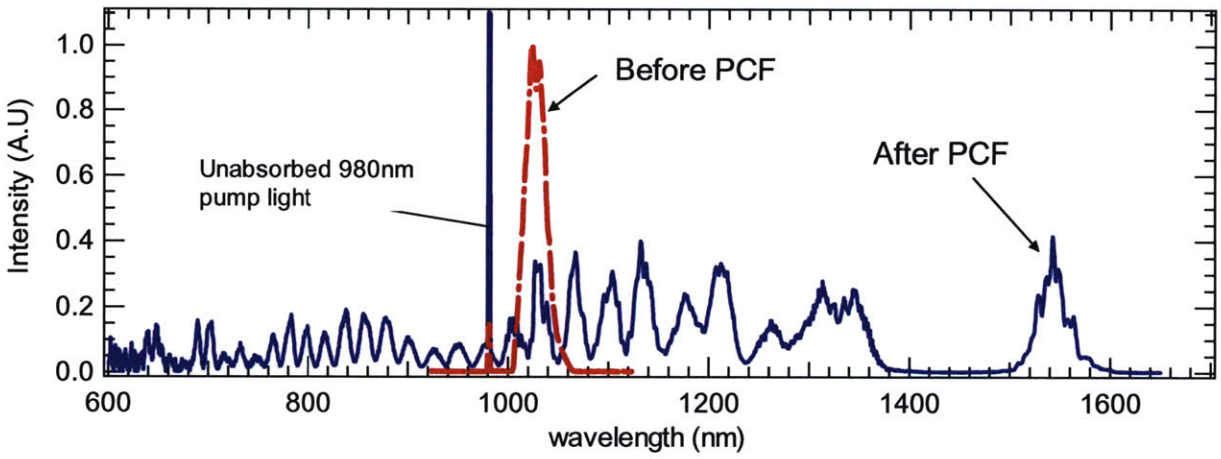

Figure 3.6: Normalized pulse spectrum measured by an optical spectrum analyzer before (dashed line) and after the PCF (solid line).

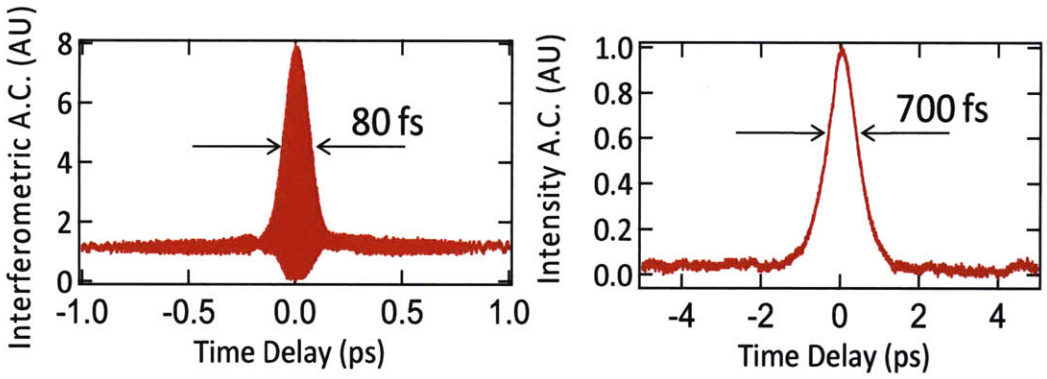

Figure 3.7: Auto-correlation measurements before the PCF at 1030 nm yields a calculated pulse duration of 80 fs. Autocorrelation measurements after the PCF and EDFA yields a pulse duration of 700 fs.

As shown in Figure 3.7 the pulse entering the PCF is close to its transform limit with a pulse duration and spectral width of 78 fs and 23.6 nm, yielding a time bandwidth product of 0.52. Pulse duration after the EDFA is 714 fs negatively chirped due to the excess SMF28 fiber in the EDFA.

3.3.2. Timing Jitter Theory in SSFS Process

A simplified model for the timing jitter between the Raman shifted pulse and the original pulse entering the PCF can be derived from the well-known formula for frequency shift of a first order soliton undergoing SSFS [90]. Before going into the details of the theory, we would like to list the definitions of all the variables involved and they are listed in Table 3-1.

	Definition	Unit
S_{RIN}	Normalized power spectral density of the relative intensity noise (RIN) of the laser	1/Hz
S_t	Spectral density of the timing jitter between the Raman shifted pulse and the original pulse.	S^2/Hz
β_2	GVD of the fiber	ps^2/m
T_R	Raman response time	ps
z	Incremental fiber length	m
E_0	Pulse energy	pJ
γ	Nonlinear coefficient of the fiber	$W^{-1}m^{-1}$
L	Total fiber length	m

Table 3-1: Definitions of variables in timing jitter in the SSFS process

According to reference [90], the amount of frequency shift during a SSFS process expressed in terms of angular frequency can be written as eq. (3.3.1), where β_2 is the GVD of the fiber, T_R is the Raman response time, z is the incremental fiber length, E_0 is the pulse energy, and γ is the nonlinear coefficient of the fiber. (3.3.1),

$$\omega_R(z) = -\frac{1}{30}\frac{\gamma^4 E_0^4}{|\beta_2^3|}T_R z, \tag{3.3.1}$$

Since we are trying to calculate the timing jitter introduced by and only by the SSFS process, it would be fair to compare the SSFS shifted pulse against a reference pulse that

undergoes the exact same fiber without SSFS effects. We assume pulse A is the pulse that is undergoing the SSFS process while it is transmitted along the fiber, while pulse B is the base-line reference pulse that is transmitted through the exact same fiber but magically without SSFS effect mathematically. Our task is to write the arriving timing difference between pulse A and B, and relate this term to the noise drivers in the SSFS process.

The arriving time difference between pulse A and pulse B can be calculated in the following way: Denote β_{2e} as the effective second order dispersion coefficient of the fiber. This parameter accounts for the change of the second order dispersion as a function of wavelengths, since the center wavelength of the SSFS shifted pulse A is changing constantly while it is transmitted through the fiber. Remember that the amount of the angular frequency shift $\omega_R(z)$ is apparently a function of the propagation distance z along the fiber. The center wavelength of the reference pulse B is denoted as ω_0 and stays the same while the pulse B is transmitted through the fiber.

At any propagation distance z, the angular frequency difference between the SSFS shifted pulse and the reference pulse can be expressed as $[(\omega_R(z)+\omega_0)-\omega_0]$, which equals to $\omega_R(z)$. The angular frequency difference $\omega_R(z)$ multiplied by the effective second order dispersion β_{2e} yields the effective group velocity difference. The effective group velocity difference integrated over the incremental distance z yields the arrival timing difference as expressed in equation (3.3.2).

$$t(L)=\int_0^L \beta_{2e}[(\omega_R(z)+\omega_0)-\omega_0]dz=\int_0^L \beta_{2e}\omega_R(z)dz \tag{3.3.2}$$

Note that β_{2e} and effective γ are the properties of the fiber, hence can be regarded as constants, even though it may not be easy to calculate these two parameters. With these parameters as constants, the above integral yields:

$$t(L)=\frac{L}{2}\beta_{2e}\omega_R(L) \tag{3.3.3}$$

Taking the derivative on both sides yields:

$$\Delta t(L) = \frac{L}{2}\beta_{2e}\Delta\omega_R(L) = \frac{L}{2}\beta_{2e}4\omega_R\left(\frac{\Delta E}{E_0}\right) = 4t(L)\left(\frac{\Delta E}{E_0}\right) \tag{3.3.4}$$

The intensity noise of the laser is a major contributor to the timing jitter of the SSFS shifted pulse train. In addition, the timing jitter is also linearly proportional to the fiber parameters β_{2e} and the amount of the total angular frequency shift.

Computing the power spectral density of both sides of equation (3.3.4) yields the noise spectral density relationship between the timing jitter of the SSFS shifted pulse train and the intensity noise of the pulse train itself:

$$S_t(f) = 16t^2(L)S_{RIN}(f) \tag{3.3.5}$$

3.3.3. Timing Jitter Experimental Verification

We verified our timing jitter modeling experimentally. The shifted component is spectrally filtered and photo detected to generate harmonics of the repetition rate. Figure 3.8 shows that the measured timing jitter spectrum obtained by electronically mixing the harmonics at 1.3 GHz of the frequency-shifted component and the direct output of the Yb amplifier.

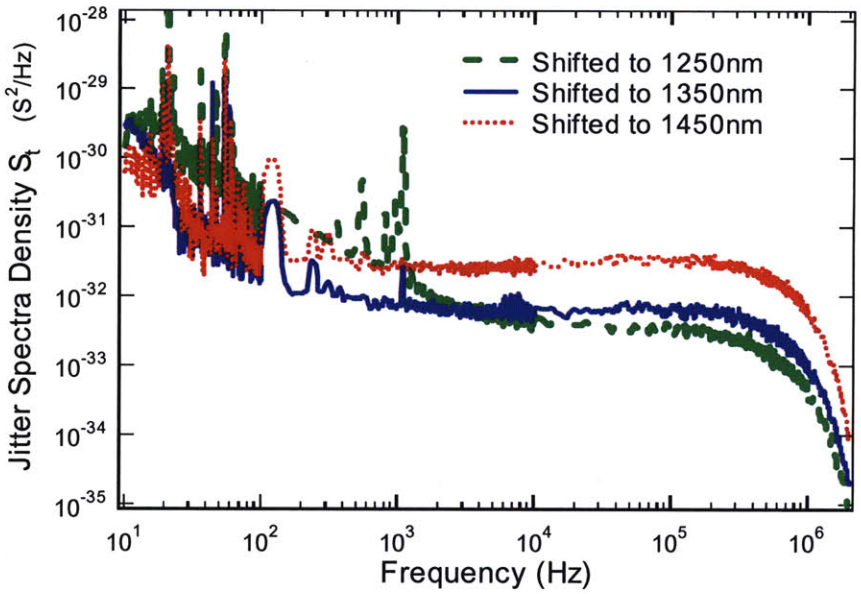

Figure 3.8: Measured timing jitter spectral density.

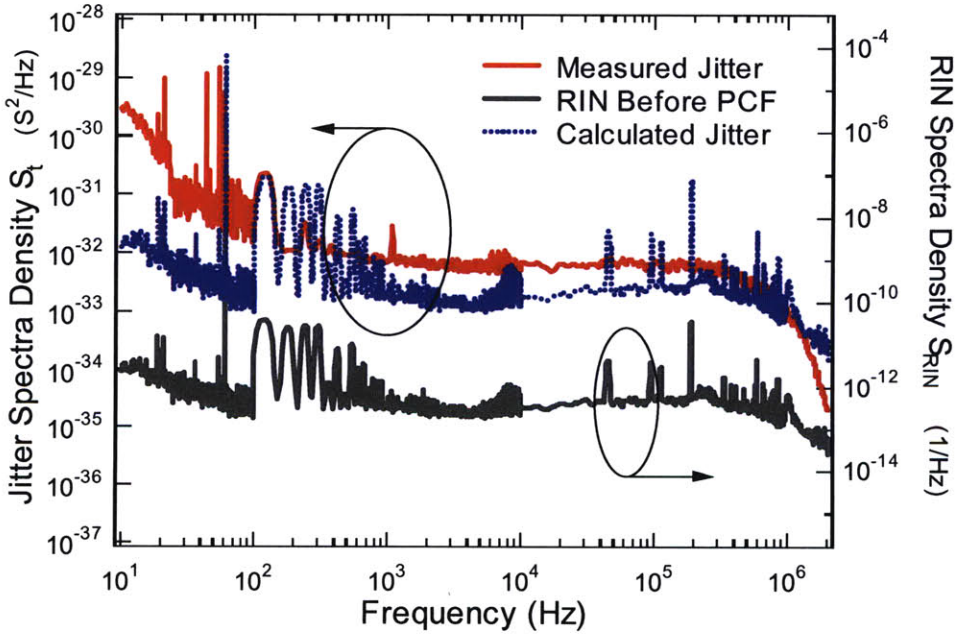

Figure 3.9: Calculated timing jitter spectral density at 1350nm with an integrated timing jitter of 57 fs, compared to measured timing jitter spectral density at 1350nm, with an integrated value of 60fs.

The timing jitter calculated using Eq. (3.3.5) is in good agreement with the measured jitter as shown in Figure 3.9. The measured timing jitter integrated from 10 Hz to 10 MHz are 47 fs, 60 fs, and 140 fs for the pulses shifted to 1250 nm, 1350 nm, and 1450 nm respectively, where the majority of the noise contributions arise from 1 kHz to 1 MHz frequency range. This large timing jitter is clearly an obstacle for the intended frequency metrology applications. However, it should be possible to suppress the RIN by using a noise eater.

3.3.4. Discussions

We have achieved SSFS over 520 nm, from 1.03 μm to 1.55 μm, connecting the two wavelength ranges, where powerful fiber amplifiers are available. The timing jitter added by the SSFS process was studied theoretically and experimentally. We expect this source to find applications in seeding of parametric amplifiers and assuming successful use of noise suppression techniques, as clock works for frequency metrology systems.

Not surprisingly, the timing jitter is highly dependent on the intensity noise of the incoming pulse train, since the SSFS is a nonlinear effect where the peak power of the pulse decides the amount of the frequency shift, in turn the arrival timing. This can be an obstacle for using this approach in noise sensitive applications.

Chapter 4.

High Fundamental Repetition Rates Erbium Fiber Lasers

4.1. Motivation

In previous sections, we have demonstrated high repetition rate, femtosecond fiber lasers using Ytterbium as gain media. We have also learned that SSFS pulse trains from 1.03 μm to 1.55 μm is not practical for low noise applications. It is necessary to explore the possibilities of improving the repetition rates directly at 1.55 μm despite of the lower gain per unit length achievable from erbium fiber gain media, so that the wonderful advantages of operating at erbium wavelength can be taken. Among the advantages detailed in previous sections, the abundant commercially available telecomm-grade components as well as the strong technology foundation in this area built by a decades of intense efforts are the main attractions to researchers. In this section, both PAPM and SBR mode-locking mechanisms are demonstrated.

4.2. Polarization Additive Pulse Mode-locked Lasers

4.2.1. Introduction

Prior to the thesis experiments, the NPR required for polarization additive-pulse mode-locking (P-APM) typically has limited the fundamental repetition rates of erbium doped fiber lasers (EDFLs) to typically below 100 MHz, with the highest repetition rate of 108 MHz reported [91]. Because active mode-locking does not produce pulses significantly shorter than 1 ps, femtosecond EDFLs with higher repetition rates (>100 MHz) are usually achieved using short cavities with semiconductor saturable absorbers[92] or harmonic mode-locking. The latter approach could perhaps achieve low jitter operation with an intra-cavity Fabry-Perot etalon for supermode suppression; but this has only been demonstrated with picosecond semiconductor lasers [70]. Furthermore, stabilization of the etalon to the laser cavity repetition rate adds significant complexity to the laser system and reduces its robustness.

Low timing jitter, low relative intensity noise (RIN), and high repetition rate femtosecond EDFLs are desirable for many applications, such as femtosecond laser frequency comb generation for frequency metrology and arbitrary optical waveform generation, timing and frequency distribution via optical fiber links, and high speed optical sampling. The highest fundamental repetition rate from a femtosecond EDFLs mode-locked solely via P-APM prior to this work was less than 80 MHz [93].

4.2.2. Design Considerations

Here we present a systematic scaling of the fundamental repetition rate of a P-APM soliton EDFL [93] to 194 MHz with a pulse duration of 167 fs. This laser has very low timing jitter and superior RIN performance compared to stretched-pulsed EDFLs with lower repetition rates. To the best of our knowledge, this is the highest fundamental repetition rate and shortest pulse

duration obtained from a P-APM soliton EDFL and the lowest RIN reported from a fiber laser at the time of the research.

Increasing the repetition rate of fiber lasers encounters two distinct challenges: (i) in practice, the cavity length is ultimately limited by the physical size of the components constituting the laser cavity, (ii) more fundamentally, there is a threshold power for initiating passive mode-locking.

The commonly used techniques for passive mode-locking of fiber lasers rely on intensity dependent phase shifts accumulated by the pulse as it traverses through the fiber. Nonlinear polarization evolution (NPE) [81] is the one of the most commonly used method due to its large modulation depth (~50%) and essentially instantaneous response. If a polarizing beamsplitter is used, the rejected light is extracted out of the cavity and acts as a useful output port. Other techniques include the nonlinear optical loop mirror [82] and its variants, which also have been demonstrated to generate high-energy, short pulses [83]. However, these techniques require longer fiber lengths, rendering them unsuitable for high repetition rate operation. Decreasing the cavity roundtrip time causes less energy to be stored in the cavity, limiting the peak power of the pulse, and for given pump power, a shorter fiber section results in smaller nonlinear phase shift to be accumulated.

$$\gamma \times L \times P_0 \;=\; \gamma \times \frac{v_g}{f_R} \times \frac{P_{ave}}{\tau \times f_R} \;\propto\; \frac{1}{f_R^{\,2}} \tag{4.2.1}$$

This relationship can be expressed as in equation (4.2.1), where γ is the effective nonlinear coefficient of the fiber cavity, L is the total length of the cavity, P_0 is the peak power of the pulse train, v_g is the group velocity of the pulse train, f_R is the repetition rate of the laser, τ is the pulse duration, P_{ave} is the average power of the pulse train. It is clear that the total nonlinearity of the cavity is inversely proportional to the repetition rates of the laser. With the limited pump power and gain fiber doping concentration, risk of not having enough nonlinearity to start and maintain PAPM mode-locking is apparent while the repetition rate is being scaled up.

4.2.3. Experiment

The experimental setup is shown in Figure 4.1. A 50 cm long highly-doped gain fiber with cumulative anomalous group velocity dispersion (GVD) of D_2 = -10,000 fs^2 is located after the polarization beam splitter to maximize the NPR in the subsequent single-mode fiber (SMF). The erbium doped fiber is counter-pumped through a 980 nm/1550 nm wavelength division multiplexing (WDM) coupler by two polarization-multiplexed 500 mW diodes.

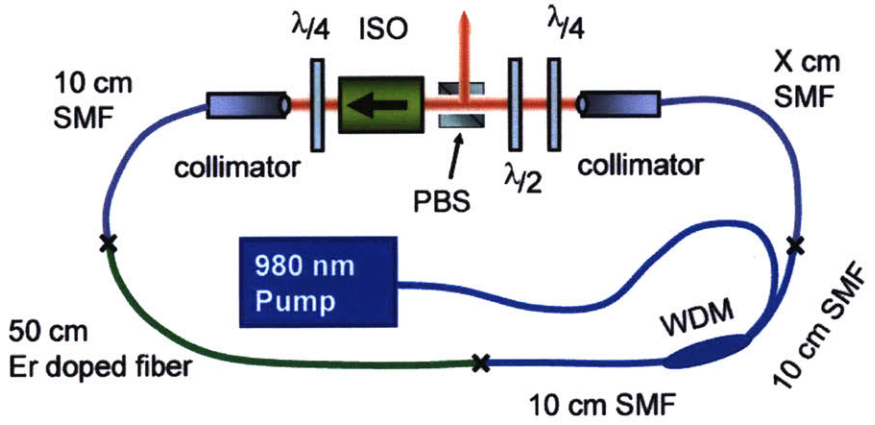

Figure 4.1: Experiment Setup. (ISO: isolator; PBS: Polarization Beam Splitter; SMF: Single-Mode Fiber)

All other fiber in the cavity is SMF with a cumulative GVD of D_2 = -20,000 fs^2. The free space section is 10 cm long. The WDM coupler leads and one collimator lead are each 10 cm in length; the length of the other collimator lead (X), initially 170 cm long, was cut back gradually to 10 cm to scale the repetition rate from 74 MHz to 194 MHz. Half-wave and quarter-wave plates are used for polarization adjustment. Mode-locking is initiated and stabilized by P-APM.

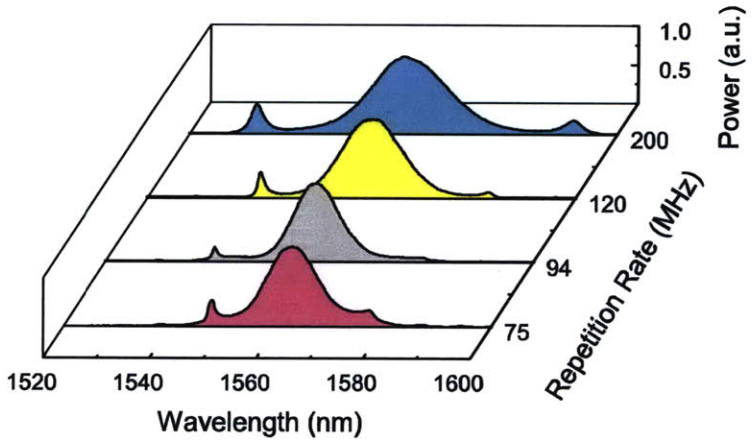

Figure 4.2: Normalized pulse spectrum evolution as repetition rate increases.

At 194 MHz, mode-locking is self-starting at a pump power of 700 mW. Single-pulsed mode-locked operation is maintained with the pump power as low as 450 mW, resulting in an output power of 30 mW and an estimated intra-cavity power of 60 mW. Figure 4.2 shows the laser output spectra for different fiber lengths with repetition rates ranging from 75 MHz to 194 MHz. The pulse duration directly from the laser reaches 167 fs at a repetition rate of 194 MHz as shown in the interferometric autocorrelation trace in Figure 4.3.

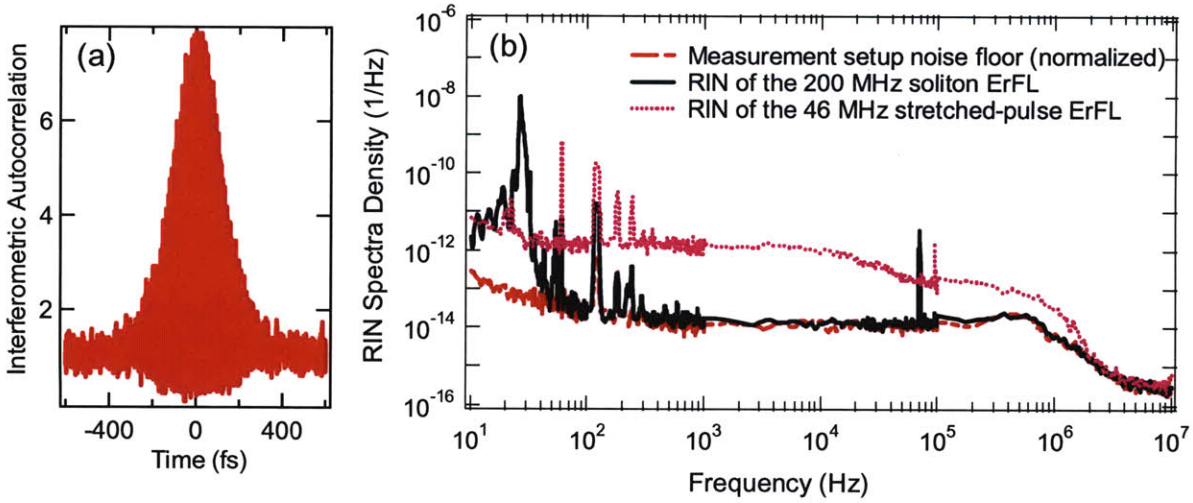

Figure 4.3:(a) Interferometric autocorrelation measurement. (b) RIN measurement of the 46 MHz stretched-pulse EDFL and the 194 MHz soliton EDFL.

Because the nonlinear coefficient of the gain fiber is similar to that of SMF, and its anomalous dispersion is only half that of SMF, soliton formation causes the pulse spectrum to broaden and the pulse duration to shorten as the cavity is shortened. The resonant sidebands due to periodic perturbations by the cavity are characteristic of soliton-like pulse formation [33] and their positions agree with the dispersion measurements and assumed intra-cavity power levels. As expected from soliton theory, the separation of the resonant sidebands increases as the cavity is shortened while the soliton phase shift is approximately constant, which further tolerates the wider mode-locked spectrum. The two combined effects, shortening of the pulse duration while reducing the pulse energy, keep the soliton nonlinear phase shift constant per roundtrip and enable the generation of the shortest pulse durations from a P-APM soliton EDFL. Due to the short cavity length, the mode-locking is very robust against environmental disturbances compared to lower repetition rate P- APM fiber lasers.

4.2.4. Noise Characterization

The RIN of the laser was measured and compared to the RIN of its 980 nm pump laser and that of a stretched-pulse EDFL, as shown in Figure 4.3. Care was taken to ensure that the same electronic measurement setup and configuration was used for all three measurements. The optical power was attenuated by a neutral density filter to an average optical power level of 0.5 mW on the photo-detector to avoid intensity saturation of the photo-diode. The photo-detector is an unbiased, 50 Ω terminated EOTech ET3020 large area InGaAs detector. The electrical output from the photo-detector was first amplified by a battery-operated low noise pre-amplifier, and then by a battery-operated Stanford Research System SRS560 amplifier. An Agilent 89410A vector signal analyzer was used to measure the power spectral density of the output of the second stage amplifier. The noise floor of the Agilent 89410A vector signal analyzer is about 9 nV/sqrt(Hz) and the noise floor of the pre-amplifier is around 17 nV/sqrt(Hz) over the frequency range of 10 kHz to 1 MHz. The cascaded electronic amplifiers have a total amplification of 100 and an effective corner frequency of the low-pass filtering of 1 MHz.

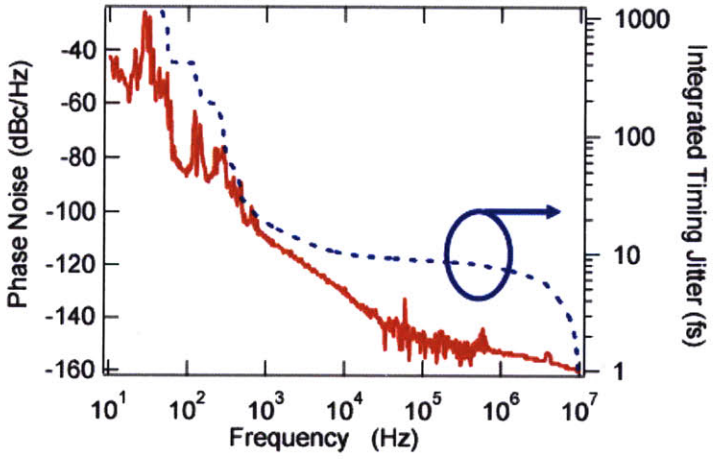

Figure 4.4: Phase noise measurement measured at 1.35 GHz harmonic, and the incrementally integrated timing jitter starting from 10 MHz down to 10 Hz.

The reference stretched-pulse EDFL is operated at a repetition rate of 46 MHz, located on a similar optical table, and pumped by a 980 nm pump diode of the same model as that used in the 194 MHz soliton EDFL. The measured RIN of the stretched-pulse EDFL was 0.03% integrated from 1 kHz to 1 MHz. This agrees with the measurements of other similar stretched-pulse EDFLs and validates the accuracy of the described RIN measurements. The measured 980 nm laser diode is the pump diode of the 194 MHz soliton laser. The frequency resolved RIN spectra of the 980 nm pump diode exhibits the typical white noise characteristics of semiconductor diodes. This white noise would extend to the relaxation oscillation frequency of the laser diode, were it not for the low-pass filtering from the electronic amplifiers.

Compared to the stretched-pulse EDFL, the 194 MHz soliton EDFL has excellent RIN performance. Above 100 Hz, the noise power of the soliton EDFL is below the noise floor of the measurement setup, and is at least two orders of magnitude lower, which gives an upper bound of the integrated RIN of 0.003% from 1 kHz to 1 MHz. The large noise peak at 30 Hz, found in the RIN spectrum of the 194 MHz soliton laser and its pump diode, is due to the cooling fan on the pump diode controller chassis, which was rotating at approximately 15 rps. Inside the motor, the slip rings disconnect and change their polarities twice every rotation, inducing a 30 Hz electro-magnetic field that couples into the pump diode current. A similar spike at 22 Hz is also visible in the RIN measurement of the 46 MHz stretched-pulse EDFL, which is pumped by a different diode on a different diode controller chassis.

The improved noise performance of the soliton laser can be traced back to the higher repetition rate and the soliton-like pulse formation. Soliton formation leads to strong inverse saturable absorption in the energy dynamics of the laser. Specifically, soliton pulses with higher energy will have a shorter duration, a wider spectrum, and thus will experience more loss from gain filtering. This mechanism leads to a shorter pulse energy relaxation time. Together with the higher repetition rate, which is known to reduce laser intensity fluctuations[89], this mechanism substantially reduces the laser intensity fluctuations. The stretched-pulse and similariton lasers, which were invented to circumvent the soliton energy limitations imposed by nonlinearity, do not benefit from this energy stabilization mechanism. The observed factor of >10 decrease in the

soliton laser RIN can be partially attributed to a factor of 4 increase in repetition rate, leaving a factor of >2.5, which is due to this energy stabilization effect.

The timing jitter was also measured for the 194 MHz soliton EDFL. Figure 4.4 shows the phase noise of the 7th harmonic (1.358 GHz) of the laser measured with an HP5052a signal source analyzer. The timing jitter progressively integrated starting from 10 MHz down to 1 Hz is also shown. The timing jitter integrated from 1 kHz to 10 MHz is 18 fs.

Both the RIN and the timing jitter measurements indicate that the 194 MHz soliton EDFL has superior noise performance above 1 kHz, making it a promising candidate for ultra-low jitter and intensity noise applications. The timing jitter below 1 kHz can be removed by controlling the length of the free-space section via a piezo-electric actuator, and locking to a microwave frequency standard with greater long-term stability. The intensity noise below 1 kHz can also be reduced further by direct feedback onto the pump diodes. However, these approaches cannot compensate for noise above ~10 kHz due to component bandwidth limitations. Thus, a femtosecond fiber laser source with ultra-low noise behavior above the single kHz range opens up opportunities to produce femtosecond fiber laser sources with extremely low noise performance approaching the quantum limit. The quantum-limited timing jitter for the 194 MHz soliton laser in the frequency interval [1 kHz, 10 MHz] is estimated to be 5 fs.

4.2.5. Summary

We have demonstrated extremely low timing jitter and intensity noise, 167 fs pulse generation directly from a P-APM soliton EDFL with a fundamental repetition rate of 194 MHz. This laser exhibits superior noise performance and has the lowest RIN and one of the lowest RMS timing jitters reported to date from fiber lasers. External cavity repetition rate multiplication may also be used to further extend the range of applications for this laser in optical sampling, femtosecond timing distribution and optical arbitrary wave form generation.

4.3. Saturable Bragg Reflector Mode-locked Lasers

4.3.1. Introduction

With the constraints of achieving femtosecond pulse duration and low timing jitter, passive mode-locking is the only path to reach multi-gigahertz fundamental repetition rate. Record high repetition rates of a few hundred MHz have been reported in previous section using polarization additive pulse mode-locking (P-APM).

However, as demonstrated in the previous section, the repetition rates of the P-APM mode-locked lasers are limited by the total nonlinearity achievable in the fiber section. The fiber section has to be long enough for adequate nonlinear polarization rotation action to initiate and maintain mode-locking. With the currently available pump power and doping concentrations of the erbium gain fibers, it is very challenging to further improve the repetition rates of the P-AMP mode-locked lasers.

Passively mode-locked fiber lasers using saturable Bragg reflectors (SBRs) with up to 2 GHz repetition rate, with setups very similar to the one presented here, have been reported, however, those attempts failed to produce femtosecond pulses [94], which is of key importance for low jitter and for frequency metrology applications.

4.3.2. Design Considerations

Here, we demonstrate, for the first time, a fundamentally mode-locked femtosecond EDFL with a repetition rate of 3.2 GHz and a timing jitter of 48 fs [1kHz-10MHz]. This result exceeds previous attempts to increase the repetition rate of fiber lasers by about tenfold, and sets a clear pathway to achieving low timing jitter, mode-locked femtosecond sources at 1550 nm with up to ten GHz of repetition rate.

Since the cavity length of a multi-gigahertz repetition rate laser is only several centimeters, the P-APM mechanism is too weak; mode-locking by a SBR is however possible. SBR mode-locking only results in femtosecond pulses when soliton pulse shaping [95], governed by Eq. (4.3.1), can be employed. The average power and, therefore, pulse energy is limited by the available pump power and doping concentration of the gain fiber. In order to generate the shortest pulse duration τ with limited pulse energy W, the cavity dispersion D needs to be minimized and the cavity nonlinearity γ needs to be maximized. Note that D needs to be kept negative for soliton formation.

$$\frac{P_{ave}}{R} = W = \frac{4|D|}{\delta \cdot \tau} = \frac{4|D_{Fiber} + D_{SBR}|}{\delta \cdot \tau} \tag{4.3.1}$$

Fortunately, unlike traditional fiber lasers, dispersion of the fiber section no longer dominates the total cavity dispersion for multi-gigahertz lasers. Other components such as the SBR play important roles for dispersion compensation. It is also critical to keep the finesse of the laser cavity high to increase pulse energy.

4.3.3. Experiment

The experimental setup is shown in Figure 4.5. Guided by simulation based on the above considerations, we choose a 3 cm-long highly doped erbium-ytterbium fiber (NP Photonics) with a group-velocity dispersion (GVD) of -60 fs2/mm and a nonlinear coefficient of ~3 W-1km-1 as the gain medium. One end of the gain fiber is butt-coupled to an SBR, and the other to a 2% dielectric output coupler. We carefully choose the SBR so that the dispersion of the SBR is slightly positive with 1000 fs^2 to compensate about half of the negative dispersion from the gain fiber. The SBR also has a 6% modulation depth, a 2 ps recovery time, and a saturation fluence of 25 μJ/cm2. Pump light is provided by two polarization combined 500 mW 980-nm-laser diodes, free-space coupled via an aspherical lens into the gain fiber through the output coupler. The output signal is separated from the pump light by a dichroic mirror.

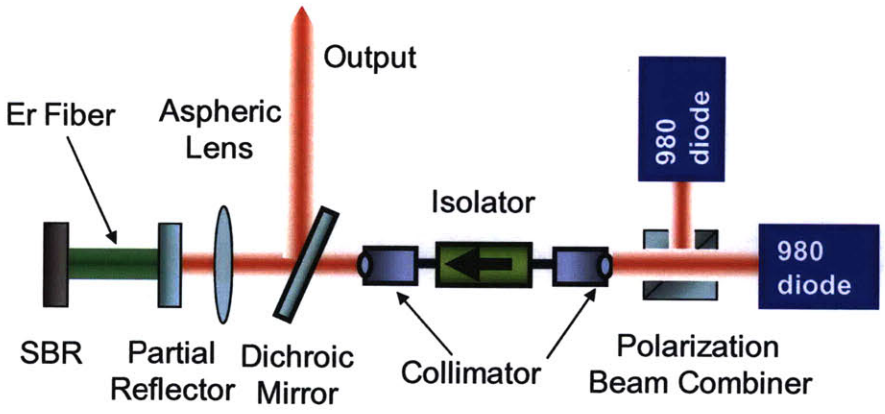

Figure 4.5: : Experimental setup.

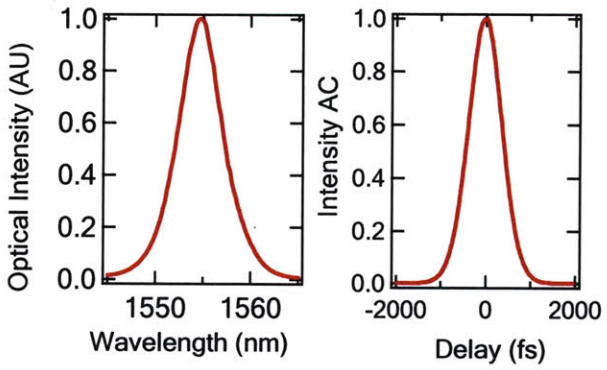

Figure 4.6: Optical spectrum and intensity autocorrelation measurement

The setup is simple, compact, and self-starting. This laser can be made reliable in a turn-key configuration. When the laser is pumped with ~700 mW of 980 nm pump power the mode-locked optical spectrum is 5.3 nm wide shown in Figure 4.6. Figure 4.6 also shows the intensity autocorrelation of the pulse train after amplification by an erbium-doped fiber amplifier resulting in a pulse duration of 600 fs, which was limited by dispersion compensation of the amplifier. The average output power from the laser cavity is 2 mW and was used to seed a subsequent erbium doped fiber amplifier for applications demanding higher average power. The intra-cavity average

power is calculated to be 100 mW yielding a pulse energy of 33 pJ. These numbers agree relatively well with soliton theory and our simulations.

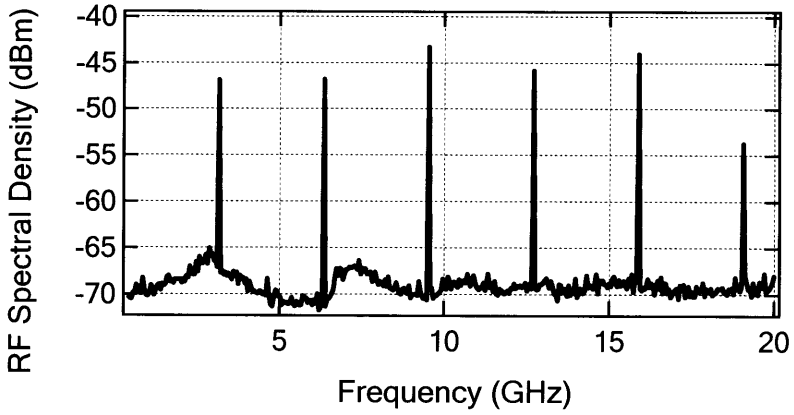

Figure 4.7: RF spectrum, span=20 GHz

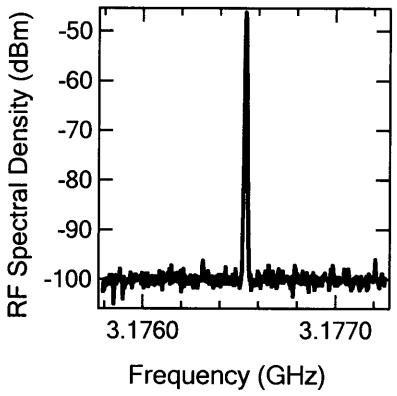

Figure 4.8: RF spectrum, span =2 MHz, RBW=3kHz,

Figure 4.7 shows the measured RF signal using a 10 GHz photodetector. Figure 4.8 shows one of the RF comb lines with a 3 kHz resolution bandwidth indicating clean mode-locked operation with a noise suppression better than 55 dB. Since the timing jitter is the critical characteristic for many applications, measurements of the timing jitter were carried out using an HP5052a signal source analyzer. Figure 4.9 shows the single sideband phase noise measurement

and the timing jitter progressively integrated from 10 MHz down to 1 kHz. The timing jitter integrated from 1 kHz to 100 MHz is 48 fs.

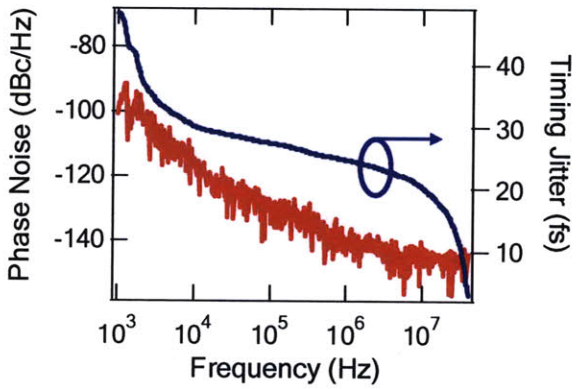

Figure 4.9: Phase noise measurement, and integrated timing jitter starting from 10 MHz down to 1 kHz.

4.3.4. Summary

We have demonstrated the first compact, multi-gigahertz, fundamentally mode-locked EDFL producing femtosecond-duration pulses. The output pulse train exhibits a low timing jitter of 48 fs [1kHz-10MHz] as necessary for a range of applications from frequency metrology, arbitrary optical waveform generation, high speed sampling and calibration of astrophysical spectrographs. Under the limitations set by the available pump power from single mode pump diodes, the laser design sets a clear pathway to achieve even shorter pulses and higher fundamental repetition rates beyond 10 GHz.

The saturable absorber is damaged after several hours of operation due to the thermal load on the SBR. The 980 nm pump light that leaked through the gain fiber is the main contribution to the thermal damage of the 3 GHz fiber laser.

Chapter 5.

External Repetition Rate Multiplication

5.1. Motivation

As discussed in previous chapters, it is a challenging task to scale up the fundamental repetition rate of EDFLs. Specialty components such as highly doped gain fibers are not commercially available to date. As stated in Chapter 4, the cavity of the high repetition rate fiber laser needs to be carefully designed so that the dispersion and nonlinearity can support short pulse operation. Even though the repetition rates of the SBR mode-locked soliton lasers can be improved to a much greater degree than the P-APM mode-locked lasers, as discussed in Chapter 4, there is also a limit to this approach, which will be discussed in Chapter 6 in detail. In certain applications, researchers may need lasers with repetition rates beyond the reach of the approaches depicted in Chapter 3 and Chapter 4.

This leads to an alternative but yet effective way of generating high repetition rates, low noise, femtosecond, 1550 nm laser sources: repetition rate multiplication via Fabry-Perot (FP) cavity.

5.2. External Fabry-Perot Cavity

5.2.1. Design Considerations

Actively mode-locked lasers with intra cavity Fabry-Perot (FP) filters or passively mode locked lasers using saturable absorbers can produce pulse trains with repetition rates well over 1 GHz [91, 92, 96], but subsequent pulse compression is needed to reach pulse durations in the range of 100 fs.

To date, pulse generation from fiber based sources at 1550 nm with pulse durations in the 100 fs range have only been achieved by P-APM in EDFLs [32]. Due to the relatively high pulse energy required to achieve P-APM, fundamental repetition rates below 100 MHz are typical. It is difficult to incorporate intra cavity FP filters into P-APM lasers due to the sensitivity to back reflections in this type of lasers. Furthermore, at GHz repetition rates, the typical pulse energy achievable in fiber lasers and the reduced fiber length would not generate enough nonlinearity for P-APM mechanism, without powerful single-mode pump diodes providing several watts of output power. However, as demonstrated in Chapter 4, the development in scaling up the fundamental repetition rate to 200 MHz has opened up opportunities to multiply the repetition rate externally with FP filters to GHz rates with acceptable power penalty.

Another design consideration is the quality of the FP cavity that is used to multiply the repetition rate. It includes the finesse as well as the thermal and mechanical stability of the FP cavity. Super invar [97] has been used in precision mechanical apparatus due to its excellent thermal stability. Of course an ideal solution would be to construct the entire FP cavity using a single piece of super invar material. However, in the laboratory environment, a well concealed structure may lead to lack of access to the optical path for alignment as well as diagnosis. In addition, components such as Brewster plate may need to be inserted inside the FP cavity if the Hänsch-Couillaud locking mechanism is used to lock the cavity to the laser.

An alternative but very practical solution is to construct the FP cavity using the super invar as the frame of the FP cavity and standard mirror mounts to hold the cavity mirrors. Standard mirror mounts are equipped with sufficient adjustment options for the cavity fine tuning and super invar provides the stability needed.

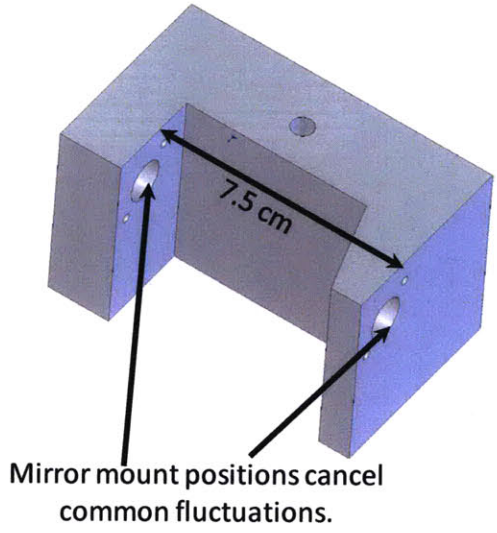

Figure 5.1: Super invar FP cavity design

At the multi gigahertz range, the cavity length is as close as several center meters. The thickness of standard commercial mirror holders is almost in the same range of the cavity length. If the structure is not carefully designed, the thermal expansion of the mirror holders dominates the thermal expansion of the cavity and defeats the purpose of using the super invar structure. A differential design can circumvent this problem. As shown in Figure 5.1, the super invar structure makes up the frame of the FP cavity, but the mirror holders are mounted on the same side of the two super invar walls. This way, the mirror holders expand and contract in the same direction due to temperature variations and mutually cancel out the changes.

5.2.2. Experiment

Here, we demonstrate the generation of low timing jitter, 150 fs pulse trains from fiber lasers with repetition rates of 2 GHz for the first time, by locking a 200 MHz fundamentally mode-locked EDFL to an external dispersion compensated F-P cavity. Detailed system characterizations including timing jitter and relative intensity noise are also reported.

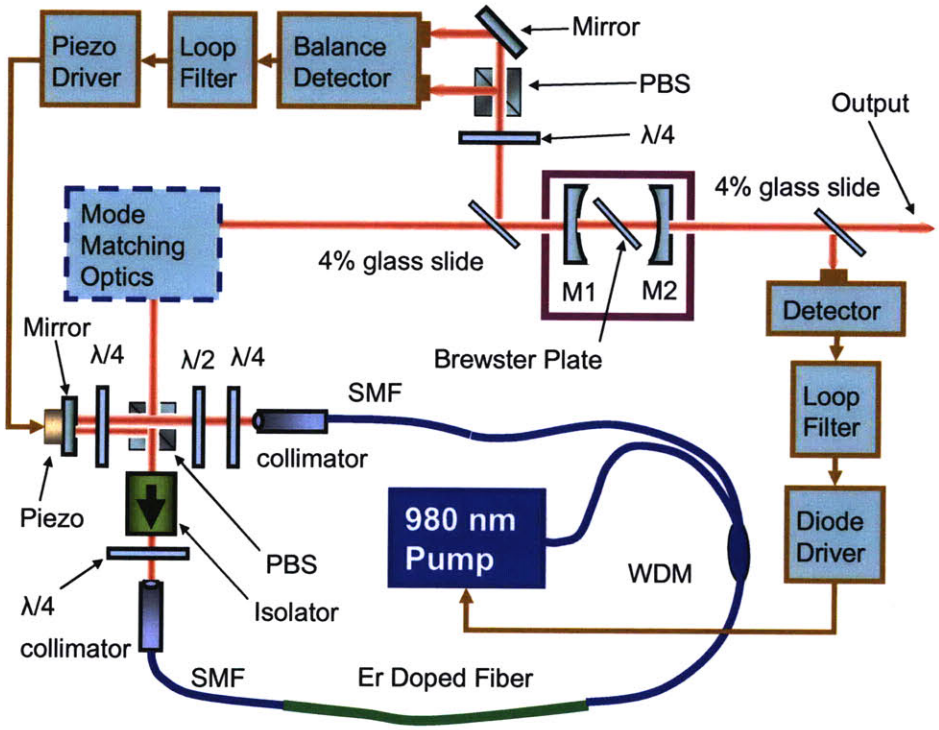

Figure 5.2: Experimental setup. (λ/4: quarter waveplate; λ/2: half waveplate; SMF: single mode fiber; M1-M2 FP mirrors; PBS: polarizing beam splitter.

The experimental setup is shown in Figure 5.2. A fundamentally passively mode-locked EDFL similar to [98], but in a sigma cavity configuration was constructed as the seed laser to generate 130 fs pulses at a repetition rate of 200 MHz. The output of the laser is coupled and mode-matched into a free space FP cavity. The Hänsch-Couillaud locking scheme [99] is used to

lock the mode comb of the laser to the transmission maxima of the external FP cavity by controlling the piezo-mounted mirror on the sigma arm of the EDFL cavity. A second feedback loop is used to control the driving current to the 980 nm pump diode, to stabilize the laser output power. The locking bandwidths for the two feedback loops are 20 kHz and 10 kHz respectively.

Two sets of partial reflectors were used in the FP cavity to generate a high finesse cavity (F=2000) and a low finesse cavity (F=200). The finesse numbers quoted are derived from the measured fundamental mode suppression in the RF spectra, since the main contributor to the intracavity loss in the case of high finesse cavities is the surface quality of the Brewster's plate, which is difficult to characterize separately. All of the partial reflectors used in the F-P cavities are dispersion flattened around 1550 nm, so that the FP resonances are uniformly spaced in the wavelength range of the EDFL. The average power is 45 mW, 2 mW, and 1 mW at the output of the EDFL, the output of the FP cavity with low finesse and with high finesses, respectively. In additional to the 90% loss due to spectral filtering from the 200 MHz to 2 GHz, the loss mechanisms also include Hänsch–Couillaud locking and free space to fiber coupling. A dispersion compensated erbium-doped fiber amplifier (EDFA) with a gain of 19 dB is added at the output of the FP cavity for autocorrelation measurement and subsequent applications.

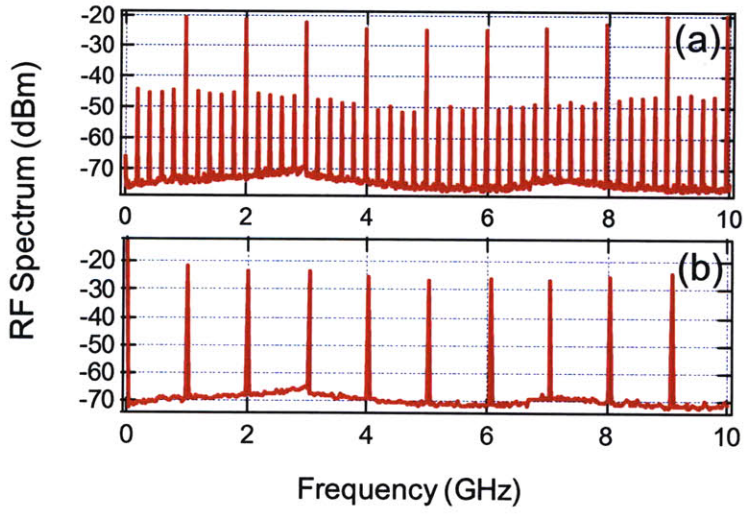

Figure 5.3: Measured RF spectra of the 1 GHz pulse trains from the external FP cavities, detected with a 10 GHz photodetector. (a) F=150, (b) F=2000

Figure 5.3 shows the RF spectra of the repetition rate multiplied pulse trains at 1 GHz for the cases of low and high finesse FP cavities. The low finesse cavity suppresses the 200 MHz fundamental spurs by 24 dB in the RF domain, corresponding to 32 dB in the optical domain; the high finesse cavity suppresses the 200 MHz fundamental spurs by 50 dB in the RF domain, corresponding to 56 dB in the optical domain. These numbers are consistent with the expected cavity losses due to mirror reflectivities and the intracavity Brewster plate.

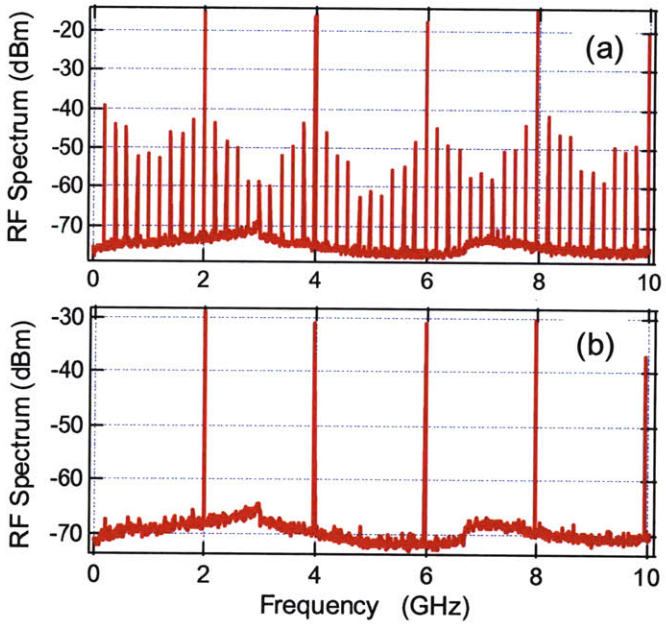

Figure 5.4: Measured RF spectra of the 2 GHz pulse trains from the external FP cavities, detected with a 10 GHz photodetector. (a) F=200, (b) F=2000

Figure 5.4 shows the RF spectra of the repetition rate multiplied pulse trains at 2 GHz for the cases of low and high finesse FP cavities. The low finesse cavity suppresses the 200 MHz fundamental spurs by 24 dB in the RF domain, corresponding to 30 dB in the optical domain; the high finesse cavity suppresses the 200 MHz fundamental spurs by 40 dB in the RF domain, corresponding to 46 dB in the optical domain. These numbers are consistent with the expected

cavity losses due to mirror reflectivities and the intracavity Brewster plate. A brief summary of the measured and calculated suppression values are listed in Table 5-1.

	1GHz	1GHz	2GHz
Finesse	150	2000	2000
Mirror Reflectivity	98%	99.85%	99.85%
Measured RF suppression	24 dB	50 dB	40 dB
Measured optical suppression	32 dB	56 dB	46dB
Calculated optical suppression	35 dB	58 dB	49 dB

Table 5-1: Measured RF beat tone suppression at 200 MHz and the calculated optical comb line suppression at 200 MHz.

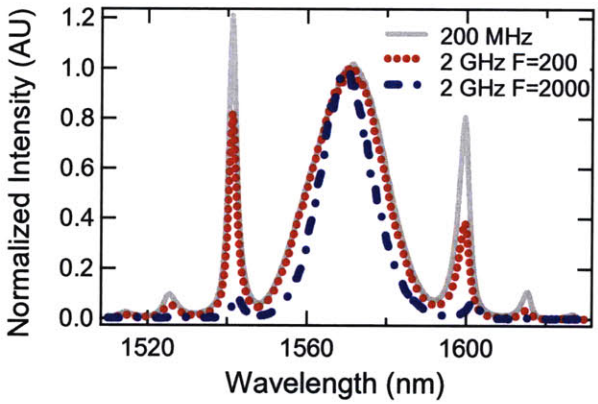

Figure 5.5: Optical spectra of the pulse trains before (dashed) and after (solid) the FP cavity.

The optical spectra of the pulse train before and after the external 2-GHz FP cavities are shown in Figure 5.5 for the cases of a low finesse and high finesse cavity. The 3 dB spectral bandwidth of the 200-MHz pulse train is 22.5 nm, and the 3 dB spectral bandwidths of the repetition rate multiplied pulse trains are 22.5 nm (F=200) and 17 nm (F=2000), respectively.

Since the FP-cavity mirrors are dispersion flattened, the residual cavity dispersion limiting the spectral width of the transmitted pulses is currently due to the 150 μm thick fused silica Brewster plate inside of the FP cavity. In addition, the uncontrolled fceo shift of the seed laser also contributes to the spectral narrowing of the transmitted pulse train [100].

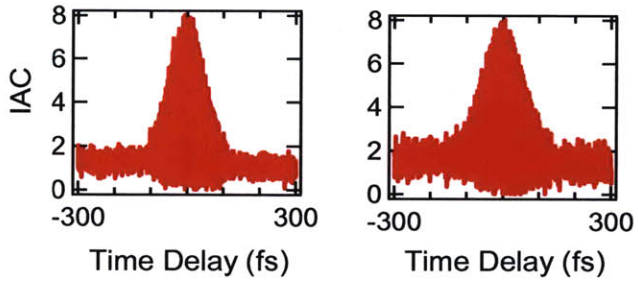

Figure 5.6: (a) Interferometric autocorrelation of the pulse train directly from the 200 MHz seed laser. (b) Interferometric autocorrelation of the amplified pulse train at the output of the 2 GHz cavity with F=200.

In order to verify short pulse characteristics of the repetition rate multiplied pulse train, interferometric autocorrelation traces (IAC) before and after the FP cavities were also taken. Figure 5.6 shows the IAC of the pulse train directly from the seed laser, with a pulse duration of 130 fs; Figure 5.6 also shows the IAC of the 2 GHz pulse train in the case of a low finesse FP cavity, with a pulse duration of 150 fs. Since the spectral width of the 2-GHz pulse train is the same as that of the seed laser as shown in Figure 5.3.4, the additional pulse broadening is mainly due to the bandwidth narrowing during the post amplification process to measure the IAC. Compared to the 200 MHz pulse train, 10 times the average optical power is required for a 2-GHz pulse train to generate an IAC trace with the same quality.

5.2.3. Noise Characteristics

The timing jitter of the high repetition rate pulse trains is of critical importance for many applications.

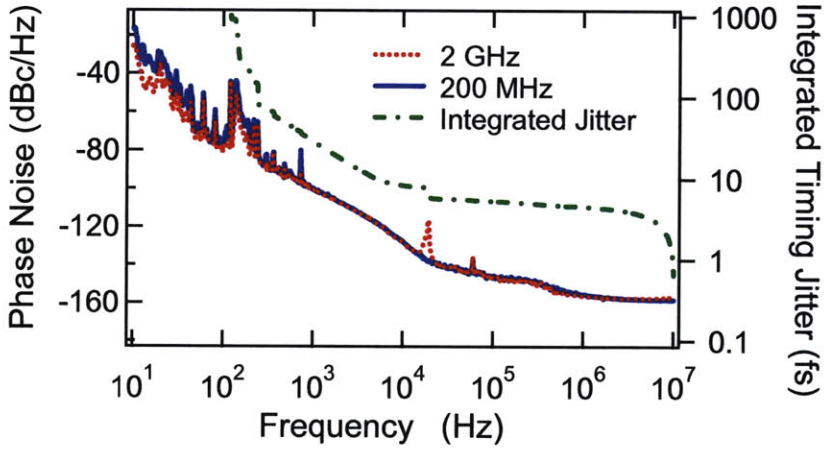

Figure 5.7: Measured phase noise of the 2 GHz (harmonic) of the seed laser (solid) and the 2GHz fundamental output from the FP-cavity (dashed), and integrated timing jitter starting from 10 MHz down to 10 Hz (dash-dotted).

Figure 5.7 shows both the phase noise of the seed pulse train at its 10th harmonic (2 GHz) and of the 2-GHz pulse train at its fundamental, measured with an HP5052a signal source analyzer. The 2-GHz pulse trains exhibit the same phase noise as the 200-MHz seed pulse train. The timing jitter progressively integrated starting from 10 MHz down to 1 Hz is also shown. The timing jitter integrated from 1 kHz to 10 MHz is 27 fs for both cases.

Another important characteristic of lasers is its relative intensity noise (RIN). Figure 5.8 shows the RIN characterization of the pulse train directly from seed laser in (1) and the 2-GHz pulse trains after the cavity with finesse F=200 and F=2000 in (2) and (3), respectively. The integrated RIN for the different cases are listed in table 1. Comparing curves (1) (2) and (3), the degradation of the RIN after repetition rate multiplication is well correlated with the finesse of the cavity and the frequency dependence of the RIN is similar for all cases. The degradation is 20

dB and 30 dB when the pulse train is filtered by the FP cavity with finesse of 200 and 2000, respectively.

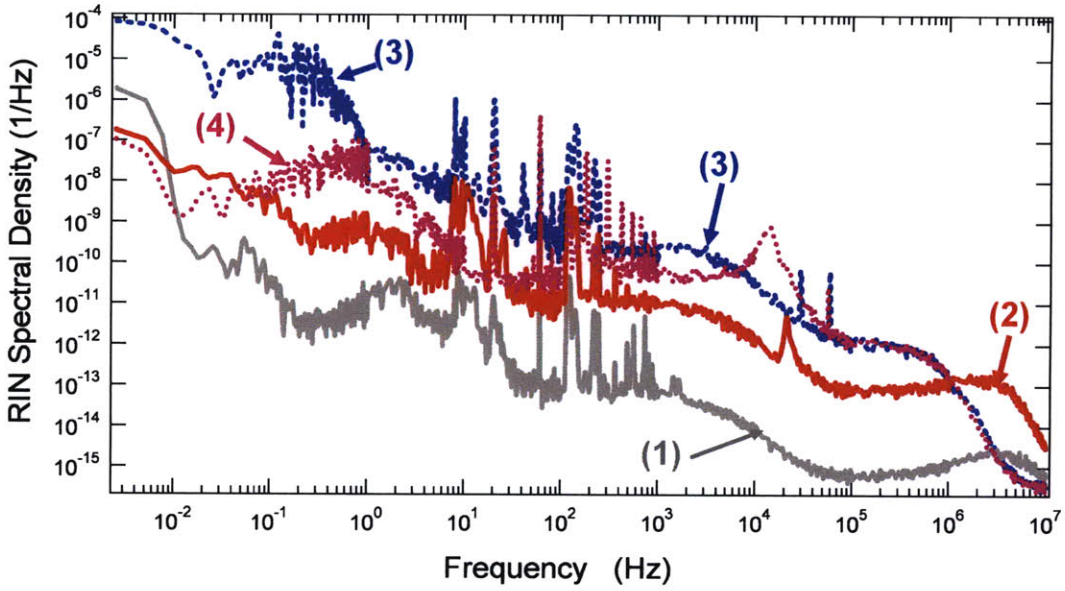

Figure 5.8: : RIN measurements: (1) directly from the 200-MHz seed laser; (2) after the 2-GHz cavity with F=200, without fceo stabilization; (3) after the 2-GHz cavity with F=2000, without feedback; (4) after the 2-GHz cavity with F=2000, with feedback.

	[10^{-2} Hz -1 kHz]	[1 kHz -10 MHz]	[10^{-2} Hz -10 MHz]
(1) 200 MHz seed laser	0.003%	0.012%	0.0124%
(2) F=200 no f_{ceo} stabilization	0.04%	0.08%	0.09%
(3) F=2000 no f_{ceo} stabilization	0.31%	0.14%	0.34%
(4) F=2000 with f_{ceo} stabilization	0.14%	0.23%	0.27%

Table 5-2: Integrated RIN measurement results for various cases.

This can be understood as a frequency jitter to intensity noise conversion. As the finesse of the cavity increases, the transmission window of the FP filter becomes narrower and, therefore, the transmitted optical power is more sensitive to frequency jitter of the seed laser with respect to

the cavity resonances. As shown in Table 5-2, due to the very low RIN of the seed laser, the RIN of the repetition rate multiplied pulse trains is still sufficiently low for various applications. The second feedback loop takes the intensity fluctuations of the pulse train after the external cavity and feeds the error signal back to the driving current to the 980 nm pump diode of the seed laser, hence stabilizes the fceo of the seed laser with respect to the FP filter resonances and thereby reduces the output RIN. Trace (d) of Fig. 5.2.7 shows the RIN of the 2-GHz pulse train after the cavity with F=2000 when the fceo is stabilized, which clearly demonstrates the reduction of the enhanced RIN due to the repetition rate multiplication. Due to the limited bandwidth of the measurement equipment, RIN and timing jitter performance around the frequency of 200 MHz could not be characterized, which could be a point of interest due to the loading and unloading of the pulse trains inside of the FP cavities.

5.2.4. Summary

In conclusion, 150 fs pulse trains with a repetition rate of 2 GHz and a timing jitter of 27 fs [1 kHz -10 MHz] are demonstrated for the first time from a compact fiber laser system. This approach provides an effective low timing jitter solution to the applications that require laser sources with the repetition rates beyond the reach by fundamentally mode-locked lasers.

Chapter 6.

Fundamental Limitations

Based on the previous chapters, it is apparent that passively and fundamentally soliton mode-locked lasers in combination with SBRs are the ultimate laser structure to achieve repetition rates in the high GHz regime with a fully integrated approach. In addition, the simplicity of the design makes it a promising candidate en route to a photonic integrated waveguide approach.

In this chapter, we will discuss and predict in detail the fundamental limitations in scaling up the repetition rates in this type of laser. We use specifically erbium doped fiber lasers as an example, but the formulation of the theory is generally applicable.

The organization of this chapter is as follows: first, we identify in detail the key properties of the erbium amplification system as well as the soliton formation to set the theoretical background of the analysis; second, we explore various limiting factors, such as the pump power, doping concentration, and limitations of dispersion engineering; last we aggregate all the limiting factors and derive the practical limits of the repetition rates in this type of lasers.

6.1. Theoretical Background

Various laser cavity designs were implemented in achieving high repetition rate low jitter femtosecond lasers, all of them fall into the following basic building blocks shown in Figure 6.1 . These building blocks include a single piece of gain fiber, an SBR which initiates and maintains mode-locking, and a dichroic partial reflector which couples the pump light in and signal light out of the cavity.

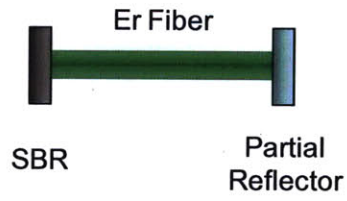

Figure 6.1: fundamental building blocks of soliton high repetition rate lasers

The pulse dynamics of this type of laser is soliton formation as described in equation 6.1.1, where W is the pulse energy, D is the total dispersion of the cavity, δ is the total nonlinearity of the cavity, τ is the pulse duration.

$$W = \frac{4|D|}{\delta \cdot \tau} \tag{6.1.1}$$

Substitution into equation 6.1.1 at both sides expression for the related pulse parameters one arrives at equation 6.1.2, where the average power P_{ave} is related to pump power, doping concentration, gain fiber length, and intra-cavity loss; R represents the repetition rate of the laser; γ is the nonlinear coefficient of the gain fiber. L is the length of the cavity which is the length of the gain fiber. D can be further expanded into 6.1.3 where β_2 is the dispersion coefficient of the gain fiber, D_{SBR} and D_{PR} are the dispersion contributed from the discrete components SBR and the partial reflector, defined as $D = \frac{1}{2}\frac{\partial^2 \phi}{\partial \omega^2}|_{\omega_0}$.

$$\frac{P_{ave}}{R} = \frac{4|D|}{2 \cdot \gamma \cdot L \cdot \tau} \tag{6.1.2}$$

$$D = -\beta_2 \cdot L + D_{SBR} + D_{PR} \tag{6.1.3}$$

$$R^2 = \frac{P_{ave} \cdot \gamma \cdot c \cdot \tau}{4 \cdot n \cdot |D|} \tag{6.1.4}$$

Using relationship $L = \frac{c}{2nR}$, we can re-write the repetition rate R as a function of all other parameters, which yields equation 6.1.4, where c is the speed of light and n is the refractive index of the fiber. Note that P_{ave} is also a function of L, hence a function of R if the pump power and doping concentration are fixed, we will expand this term in the next section. Equation 6.1.4 is the simple governing equation for the limitation of the practically achievable repetition rates.

There are several insights: the nonlinear coefficient γ will stay approximately same with different fiber structures and host. τ is desired to be around 100 femtosecond in our study. With nonlinear coefficient and pulse duration staying approximately the same, we can clearly see that the average power P_{ave} and total dispersion D contribute to the repetition rate of the laser. In the next several sections, we will discuss in detail the contribution from each of these two terms.

6.2. Average Power

Several factors influence the amount of average power available from the laser cavity. These include available low noise pump power, doping concentration, as well as the specific laser dynamics, the intra-cavity loss, gain length, and output coupling.

State-of-the-art high gain erbium fibers exhibit doping concentrations (n_{er}) in the range of 4 wt % -8 wt % [101] corresponding to 3.75-7.5x10^{20} ions/cm^3. Various reasons make researchers prefer 980 nm pumps versus 1480 nm pumps, including the much higher available power from single mode semiconductor chips emitting at 980 nm wavelength, cost difference of these two types of diodes, and the better noise figure [102, 103] of 980 nm diodes. The state-of-the-art semiconductor diode pump at 980 nm offers as high as 750 mW of pump power delivered in single mode fibers, whereas tens of watts of power can be delivered in multimode fibers. Of course, multimode fiber delivery systems are not of our interest since the mode beating between the transverse modes may introduce large amount of intensity noise which would hamper low noise applications.

By using a polarization beam combiner and pumping the laser from both ends, in theory one can put four times the power of a single mode 980 nm diode into the gain medium (4x750 mW= 3 W). The idea of resonant pumping has been entertained and proposed to further increase the pump light absorption. Resonant pumping recycles the left-over pump light from a single pass pumping and in theory eliminates the waste in pump power, even though it may make the system more complicated to implement. This scheme enables the total absorption of the entire 3W of pump power. Taking account the 80% practical limit of the coupling ratio as well as the loss introduced by the necessary optical components in the pump beam such as the isolator (10% loss) and dichroic mirror, 2100 mW of pump power is expected to be absorbed by the gain fiber.

Since most of the SBRs are reflectors instead of transmitters, the laser cannot be pumped from both ends. The above estimation reduces to its half at 1050 mW maximum absorbed pump power.

6.3. Laser Dynamics

In this section, we discuss in detail and derive the analytical expressions of the average power as a function of known parameters such as pump power, doping concentration, total cavity dispersion, and cavity loss.

Symbols	Definition	Typical Value	Unit
c	Speed of the light	3×10^8	m/s
n	Refractive index	1.5	Unitless
γ	Nonlinear coefficient	3×10^{-3}	$W^{-1}m^{-1}$
τ	Pulse duration	100	fs
ΔD	Minimum achievable dispersion coefficient	TBD in next section	fs^2
α	Total cavity loss	20%	Unitless
P_p	Pump power	1	Watt
n_{er}	Erbium doping concentration	1.3×10^{20}	$Ions/cm^3$
A_{sig}	Effective area of the signal light	$\pi 4^2=16\pi$	μm^2
A_{pump}	Effective area of the pump light	$\pi 3.5^2=13\pi$	μm^2
Γ	Overlap factor	0.5	Unitless
h	Planck constant	6.626×10^{-34}	Js
f_s	Photon frequency at 1550 nm	193	THz
f_p	Photon frequency at 980 nm	306	THz
g_0	Small signal gain coefficient	Variable	Unitless
σ_p	Absorption cross section at 980 nm	2.5×10^{-25}	m^2
σ_s	Emission cross section at 1550 nm	3×10^{-25}	m^2
τ_{nm}	Er ion lifetime between energy state n and m	Variable	ms
ϕ_p	Photon flux at pump frequency	Variable	$s^{-1}m^{-2}$
ϕ_s	Photon flux at signal frequency	Variable	$s^{-1}m^{-2}$
L	Cavity length	Variable	m
R	Repetition rate	Variable	GHz

Table 6-1: Table of constants in erbium doped fiber laser systems

The definitions, symbols, and typical values of the parameters related to this discussion are listed in Table 6-1. The analysis is in two steps: we first treat the gain fiber as the single pass

amplifier and extract the saturation intensity of the gain media; we then use the laser dynamics to relate the intra-cavity average power to the saturation intensity.

The erbium gain medium at 980/1550 nm can be simplified as a standard three level system depicted in Figure 6.2, with a ground state denoted by state 1, an intermediate state as state 3 (into which energy is pumped), and the state 2. Since state 2 often has a long lifetime, it is sometimes referred to as the meta-stable level. State 2 is the upper level of the amplifying transition and state 1 is the lower level. The populations of the levels are labeled N1, N2 and N3. This three level system is intended to represent that part of the energy level structure of Er^{3+} that is relevant to the amplification process. We will consider here the problem simple one-dimensional fiber geometry. That is, we assume constant pump and signal intensities as well as erbium ion distribution in the transverse dimensions over the effective cross-sectional area of the fiber.

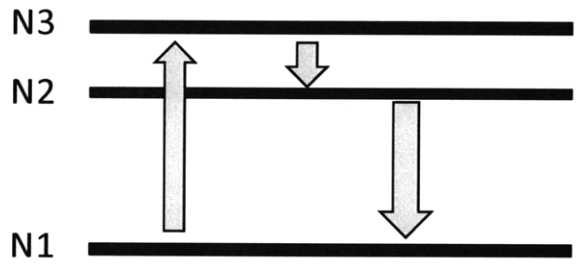

Figure 6.2: Three level model of Erbium.

The incident light intensity flux, in number of photons per unit time per unit area, at the frequency corresponding to the 1 to 3 transition is denoted by ϕ_p corresponding to the pump field. The incident flux at the frequency corresponding to the 1 to 2 transition is denoted by ϕ_s corresponding to the signal field. Standard rate equations of this three level system can be written as 6.3.1 to 6.3.3.

$$\frac{dN_3}{dt} = -\frac{N_3}{\tau_{32}} + (N_1 - N_3)\phi_p\sigma_p \tag{6.3.1}$$

$$\frac{dN_2}{dt} = -\frac{N_2}{\tau_{21}} + \frac{N_3}{\tau_{32}} - (N_2 - N_1)\phi_s\sigma_s \tag{6.3.2}$$

$$\frac{dN_1}{dt} = \frac{N_2}{\tau_{21}} - (N_1 - N_3)\phi_p\sigma_p + (N_2 - N_1)\phi_s\sigma_s \tag{6.3.3}$$

In steady state, the time derivatives are zero, and the total populations N is given by

$$N_1 + N_2 + N_3 = N \tag{6.3.4}$$

The subsequent derivations are very well known and can be found in several text books. The most well-known ones are [104, 105]; this thesis follows the notations and derivations from reference [104]. For detailed analysis of the derivation process, readers are referred to [104, 105].

According to [104], from equation 6.3.1-6.3.4, one can arrive at equation 6.3.5-6.3.7, where several assumptions have been used during the derivation: the decay time of τ_{32} is assumed to be very fast, around 1 μs in the erbium system, hence the population at level 3 is close to zero. The pump power is assumed to be well above the pump threshold. The threshold pump intensity is expressed in equation 6.3.5, which is to the first order not a function of the erbium doping concentration, only of the pump absorption cross section and the decay time. If we carry out the calculation using the known parameters listed in Table 6-1, I_{th} is in the range of 0.5 mW, note that this corresponds to rendering transparent only an infinitesimally short length of the erbium-doped fiber [104]. We also assume the pump power is the same along the entire length of the fiber for the ease of derivation.

$$I_{th} = \frac{hf_p}{2\sigma_p\tau_{21}} \tag{6.3.5}$$

$$g_0 = \sigma_s n_{er}\eta \tag{6.3.6}$$

$$I_{sat} = \frac{hf_s}{2\sigma_s \tau_{21}}(1 + \phi_p \sigma_p \tau_{21} \Gamma) \tag{6.3.7}$$

Equation 6.3.6 shows the small-signal gain g_0 of the gain fiber where σ_s is the signal transition cross section, n_{er} is the erbium doping concentration, η is the factor which estimates the deficiency of the doping concentration including quenching and clustering effect that reduces the effective doping concentration. Equation 6.3.7 shows the saturation intensity of the gain fiber, where ϕ_p is the pump photon flux, σ_p is the pump absorption cross section, τ_{21} is the upper state life time, σ_s is the signal absorption cross section, and Γ_p indicates the geometric overlaps between mode size of the Gaussian beam inside the fiber and the doped fiber core.

$$\phi_p = \frac{P_{pump}}{hf_p A_{pump}} \tag{6.3.8}$$

$$P_{sat} = A_{sig} I_{sat} \tag{6.3.9}$$

The pump photon flux ϕ_p in equation 6.3.7 can be expressed in equation 6.3.8, where P_{pump} is the pump power in watts and A_{pump} is the pump light effective area in the fiber. Combining 6.3.7-6.3.9, the saturation power of the gain medium can be expressed in 6.3.10.

$$P_{sat} = \frac{A_{sig} hf_s}{2\sigma_s \tau_{21}}(1 + \frac{P_{pump} \sigma_p \tau_{21} \Gamma}{hf_p A_{pump}}) \tag{6.3.10}$$

$$P_{sat} = \frac{A_{sig} f_s \sigma_p P_{pump} \Gamma}{2A_{pump} f_p \sigma_s} \tag{6.3.11}$$

Generally in a well inverted system, the term $\frac{P_{pump}\sigma_p\tau_{21}\Gamma}{hf_pA_{pump}}$ in equation 6.3.10 is much larger than unity. Using the typical value listed in Table 6-1, $\frac{P_{pump}\sigma_p\tau_{21}\Gamma}{hf_pA_{pump}}$ is equal to 130.774. So equation 6.3.10 can be rewritten as equation 6.3.11.

Using the well-known laser dynamics relationship between the saturation power and the intra-cavity average power shown in equation 6.3.12, one can reach at equation 6.3.13 which is the governing equation of the average power for given fiber doping concentration, pump power, cavity loss, and the laser dynamics.

$$P_{ave} = P_{sat}(\frac{g_0 L}{\alpha} - 1) \tag{6.3.12}$$

$$P_{ave} = \frac{A_{sig} f_s \sigma_p P_{pump} \Gamma}{2A_{pump} f_p \sigma_s}(\frac{\sigma_s n_{er} \eta L}{\alpha} - 1) \tag{6.3.13}$$

We will verify this equation by comparison with experimental results next. Using the values from the 3 GHz fundamentally mode-locked laser presented in chapter 4, where L =3 cm, absorbed pump power is 600 mW, doping concentration is 0.6 x 10^{20} ions/cm^3, intra-cavity loss α is estimated to be 20%, η is estimated to be 0.8, Γ is estimated to be 0.5, core diameter is 7.1 μm, and rest of the parameters are from the table 6.3.1, the average intra-cavity power is calculated to be 110 mW, which agrees well with the experimentally observed value of 100 mW [106].

Another example of a 2 GHz laser where L =5 cm, absorbed pump power is 600mW, doping concentration is 1.2 x 10^{20} ions/cm^3, intra-cavity loss α is estimated to be 25%, η is estimated to be 0.8, Γ is estimated to be 0.5, core diameter is 6.0 μm, and rest of the parameters are from the table 6.3.1, the average power is calculated to be 220 mW which also agrees well with the experimental value of 230 mW.

6.4. Dispersion Engineering

Dispersion engineering is of utmost importance in this type of laser design in achieving high repetition rates. According to equation 6.1.4, the ideal dispersion value should be very close to zero and yet anomalous to keep the soliton formation. This poses a challenge to dispersion engineering.

$$\Delta D = \Delta\beta \cdot L + \Delta D_{SBR} + \Delta D_{PR} \tag{6.4.1}$$

In reality, there are fabrication errors of the fiber introduced in the manufacturing process. Standard fiber drawing processes generates around 5% of error in fiber core diameter. Depending on the dispersion value and region of the dispersion in cylindrical waveguide dispersion calculation, this approximately corresponds to 5% of the dispersion error of the fiber.

Similarly, there are also errors introduced in the mirror design and fabrications. Typical dispersion uncertainties from mirror fabrication processes are about >10% when the target dispersion is above 100 fs^2. Even though the amount of error can drastically decrease if the target dispersion value is close to zero, the absolute fabrication error is still above several fs^2.

These dispersion uncertainties limit the absolute total dispersion generated reproducibly in a laser cavity. Combining the above estimated dispersion errors shown in equation 6.4.1, a total dispersion error of 5-10 fs^2 maybe reasonable. However, since the dispersion has to be anomalous to take advantage of soliton formation, designers may also want to target the total dispersion at a value slightly higher than zero to avoid going over board to normal dispersion due to fabrication uncertainties. So generally an absolute dispersion value of 10-15 fs^2 becomes the ultimate limit for dispersion engineering for this type of laser cavity.

Another valuable point is that when the dispersion engineering is in its perfect form, the total dispersion of the cavity is not a function of the cavity length anymore, since engineers can

first measure the dispersion of the gain fiber, and then design the dichroic coating of the SBR to totally compensate the dispersion of the gain fiber, thus the total dispersion of the cavity is only limited by the coating fabrication uncertainties.

6.5. Aggregated Analysis

In this section we derive the key equation that relates the repetition rate R to all other independent parameters. Care needs to be taken in the derivation, since the parameter R relates the average power to the pulse energy, and the cavity length L is related to the repetition rate R by $L = \frac{c}{2nR}$ as well as the total nonlinearity δ of the cavity. We will eliminate these dependent parameters and arrive at an aggregated equation of R as a function of all independent parameters, in order to find insights to the fundamental limitation of scaling up the repetition rate.

Starting from equation 6.3.13 and equation 6.1.4, one can arrive at equation 6.5.1, using the relationship $L = \frac{c}{2nR}$. Note that we cannot further simplify what is in the parentheses since the term $\frac{\sigma_s n_{er} \eta c}{2\alpha n R}$ is not significantly larger than unity.

$$R^2 = \frac{A_{sig} f_s \sigma_p P_{pump} \Gamma \gamma c \tau}{8 \cdot n \cdot |D| A_{pump} f_p \sigma_s} \left(\frac{\sigma_s n_{er} \eta c}{2\alpha n R} - 1 \right) \tag{6.5.1}$$

Rearranging equation 6.5.1, and using the new symbol "a" and "b" to represent 2 sets of independent parameter combos, we arrive at 6.5.2.

$$R^2 = a\left(\frac{b}{R} - 1 \right) \tag{6.5.2}$$

Where

$$a = \frac{A_{sig} f_s \sigma_p P_{pump} \Gamma \gamma c \tau}{8 \cdot n \cdot |D| A_{pump} f_p \sigma_s};$$

$$b = \frac{\sigma_s n_{er} \eta c}{2\alpha n};$$

Equation 6.5.2 is a standard cubic equation which has two complex solutions and one real solution. Apparently the complex solutions cannot be used for a real quantity of laser repetition rate, we write the real solution in equation 6.5.3.

$$R = \frac{-(2/3)^{1/3} \cdot a^{2/3}}{(9b + \sqrt{3(4a + 27b^2)})^{1/3}} + \frac{a^{1/3}(9b + \sqrt{3(4a + 27b^2)})^{1/3}}{2^{1/3} \cdot 3^{2/3}} \tag{6.5.3}$$

This is the final governing equation that connects the physically measurable independent parameters to the repetition rates of the laser. These physically measurable parameters include doping concentration, laser pump power, cavity loss, gain length, net dispersion, and the fiber geometric properties.

We verify this equation by comparison with the experimental results from Chapter 4. With a total dispersion of -1800 fs^2, to achieve 500 fs pulse duration (note not 100 fs yet), using an NP Photonics gain fiber with doping concentricity of 2wt % corresponding to 1.25 x 10^{26} ions/m^3, intra-cavity loss is 30%, and rest of the parameters following the same typical values in Table 6-1, the relationship of the highest repetition rate versus pump power is shown in figure 6.5.1. Note, that the pulse duration is set at 500 fs in this calculation to correlate to our current laboratory experiment. As shown in Figure 6.3, the data marker shows at a pump power of 700 mW, the repetition rate should be 3.2 GHz which correlates well with our experiment result shown in chapter 4.

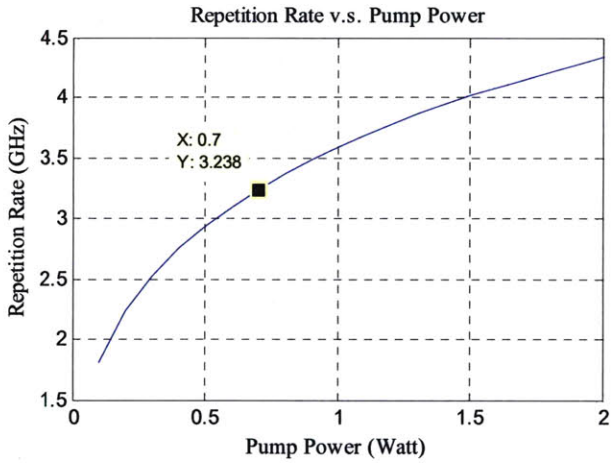

Figure 6.3: Repetition Rate vs. Pump power Scenario #1: 500 fs pulse, 2wt% doping concentration, 30% loss, 1800 fs2 total dispersion

Let's look into this scenario more. If one wants to create a 100 femtosecond pulse from the same setup, assume all other independent parameters unchanged, the amount of the pump power needed to reach the same repetition rate is close to 4 watt as shown in Figure 6.4. Thermal damage is a major concern at this power level, significant efforts in thermal engineering and thermal management may be required to implement systems like this.

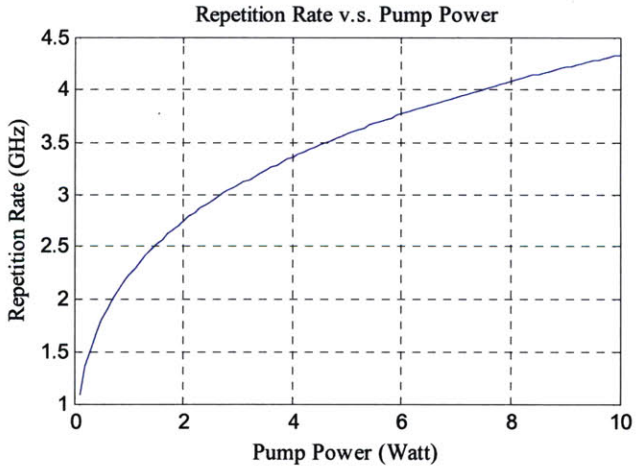

Figure 6.4: Repetition Rate vs. Pump power Scenario #2: 100 fs pulse, 2wt% doping concentration, 30% loss, 1800 fs2 total dispersion

In the next several sections, we will look into several scenarios where one of the parameters is clamped or limited, and explore the repetition rate behavior as a function of other parameters. This will give us more insights of how to carry out the future efforts as well as understanding the fundamental limitations. We will summarize all the results in section 6.5.5 and present the results of the repetition rate limitation with the currently available technology.

Note that, in these analyses, thermal damage threshold is not considered. Well implemented thermal engineering is assumed.

6.5.1. Doping Concentration Limited

In this sub-section, we will study the scenario of several commonly available doping concentrations. Currently the highest gain per unit length achievable is from NP Photonics' 4% doped erbium doped fibers [107], even though it is not the highest doping concentration reported [101] due to quenching and clustering effects at higher doping concentration. We will look at the behavior of the repetition rate R as the function of the pump power as well as the total cavity dispersion under two different doping concentrations: 2wt% and 4wt%.

Figure 6.5 shows a scenario where the doping concentration is 2wt% corresponding to 1.25 x 10^{26} ions/m^3. The repetition rates increase as the total dispersion of the cavity decreases and the pump power increase. This is very apparent from the soliton theory, where if the dispersion decreases faster than the nonlinearity of the cavity, the soliton pulse energy becomes smaller, hence the cavity can support higher repetition rates.

Figure 6.6 shows another scenario where the doping concentration is 4wt% corresponding to 3.5 x 10^{36} ions/m^3 and all other parameters are the same as in above scenario. Almost three times higher repetition rate can be achieved with this type of fiber.

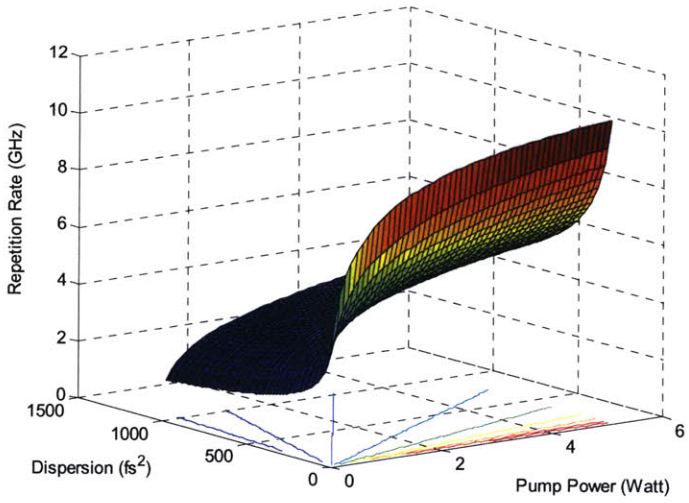

Figure 6.5: Repetition Rate as a function of pump power [0.1 W – 5 W] and total dispersion [15 fs2 -1015 fs2], 2wt% doping concentration, 25% intra-cavity loss, 100 fs pulse duration.

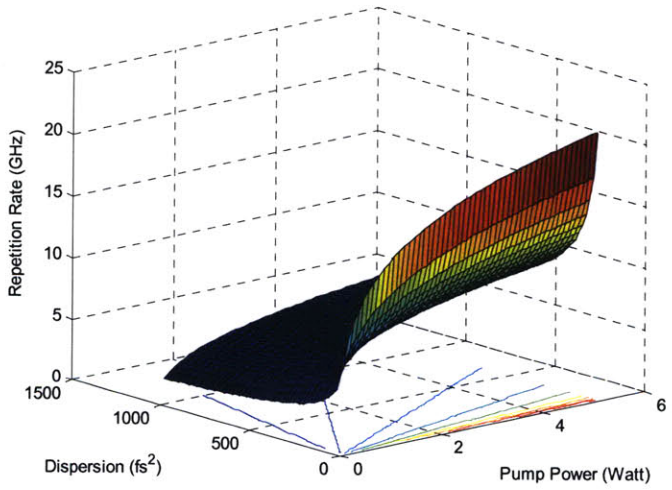

Figure 6.6: Repetition Rate as a function of pump power [0.1 W -5 W] and total dispersion [15 fs2 -1015 fs2], 4wt% doping concentration, 25% intra-cavity loss, 100 fs pulse duration.

6.5.2. Dispersion Limited

In this section, we will study the scenario where the total intra-cavity dispersion is limited by the fabrication uncertainty to -15 fs^2 or -30 fs^2. As for the plotting range of doping concentrations, even though the state-of-the-art doping concentration is around 8wt% corresponding to 7 $x10^{26}$ $ions/m^3$ [101], this doping concentration did not offer the highest gain per unit length [107] due to quenching and clustering effects. However, for simplicity reason, we assume the quenching and clustering effects eventually can be circumvented in the future. We plot the range of the doping concentration from 0.5 $x10^{26}$ $ions/m^3$ to 10.5 $x10^{26}$ $ions/m^3$.

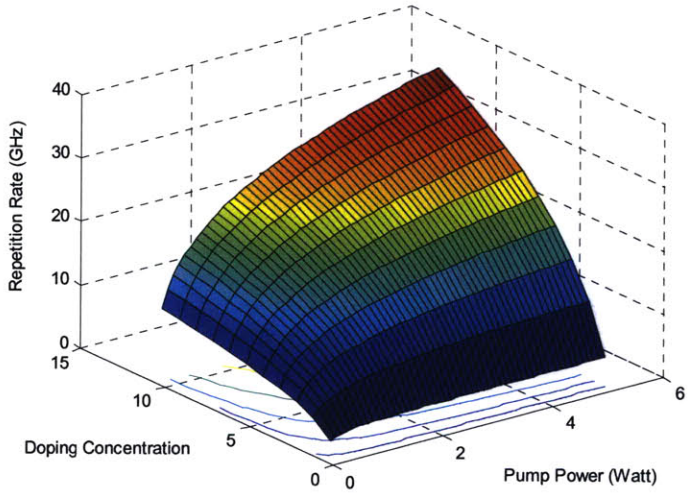

Figure 6.7: Repetition Rate as a function of pump power [0.1 W -5 W] and doping concentration [0.5 – 10.5] in the unit of 1026 ions/m3, 25% intra-cavity loss, 100 fs pulse duration, total dispersion is 15 fs.

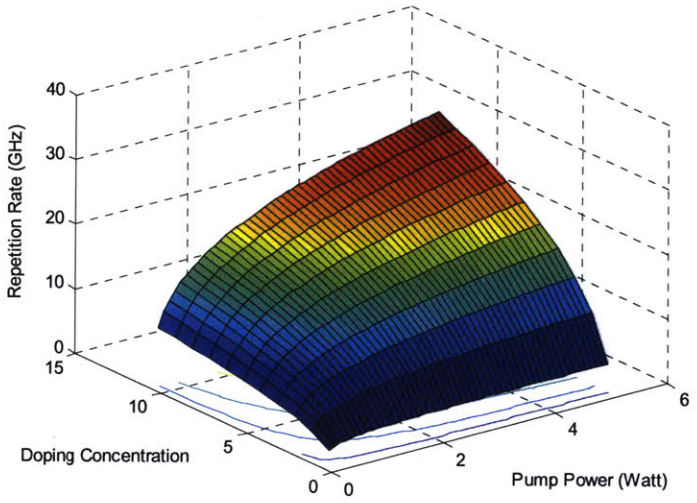

Figure 6.8: Repetition Rate as a function of pump power [0.1 W -5 W] and doping concentration [0.5 – 10.5] in the unit of 1026 ions/m3, 25% intra-cavity loss, 100 fs pulse duration, total dispersion is 30 fs.

We look at the behavior of the repetition rate R as the function of the pump power as well as the doping concentration under the total dispersion limitation of 15 fs^2. Figure 6.7 and Figure 6.8 show the comparison of the behavior of the repetition rate of the laser as the function of the doping concentration and pump power, when a total cavity dispersion of 15 fs^2 and 30 fs^2 has been used A small increase in repetition rate is expected from the decrease of total cavity dispersion.

6.5.3. Intra-cavity Loss Limited

We assumed a 25% loss in the previous sections. This is a reasonable assumption in the current experimental setups, especially in the 3 GHz fundamentally mode-locked laser where the SBR is

in physical contact with the fiber ferrule and there is not mechanisms to fine tune the alignment. An alternative way of implementation is shown in Figure 6.9, where the entire laser structure is held inside of a cylinder structure. The SBR and the partial reflector are hold by very soft springs on the back. The gain fiber is hold inside of the fiber ferrule. All components can be slide fairly easily inside of the cylinder. There are two set screws that secure the positions of all the components once it is aligned. This setup enables the self-alignment between the SBR and partial reflector surface against the fiber ferrule. Since the diameter of the fiber ferrule is small compared to the surface area of the SBR and partial reflector, and the end-surface of the ferrule is flat and perpendicular to the body of the ferrule, the large SBR and the partial reflector surface area generates enough torque for them to self-align with the end-surface of the ferrule while being pushed by soft springs. This setup is ideal for the laboratory environment but not for the commercial/industrial configuration, since the soft spring may pick up mechanical vibrations from the environment and shift, hence the entire setup is not intended for industrial applications.

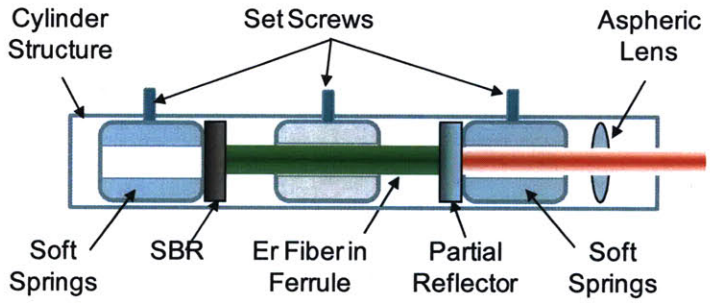

Figure 6.9: Improved experimental setup for self-aligned cavity

For commercial and industrial systems, the assembly can be achieved using the structure in Figure 6.10. In this configuration, the gain fiber is installed in the fiber ferrule and the SBR is epoxied on one end. A dichroic partial reflective coating can be deployed on the other end of the fiber ferrule to act as an output coupler. The fiber ferrule is connected to another fiber connector end via fiber connecting mechanism. This type of connection typically only introduces 0.1-0.2 dB of loss corresponding to 2-4 % of loss, making it ideal for low loss cavity operation. The 980

nm pump light will be coupled into the system via a 980/1550 nm WDM. The output of the pulse will also be coupled out of the system via this WDM. The entire system is compact, easy to manufacture, and sturdy, making it an ideal integrated product for commercial use.

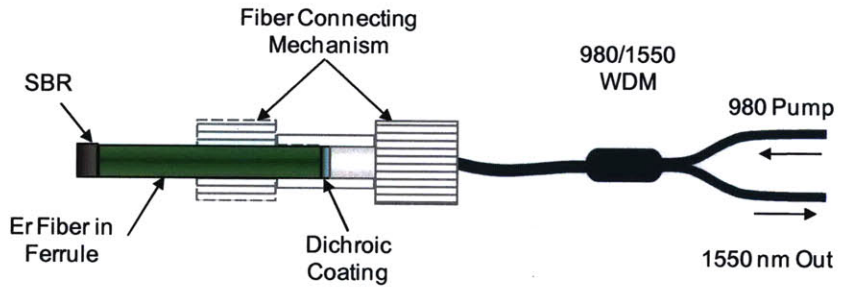

Figure 6.10: Configurations for commercial units

With above improvements of the cavity design, it is possible to make the intra-cavity loss much smaller than 20%-30%. For example at Figure 6.10, the configuration potentially may only introduce 2% from the fiber connection in addition to another several percent of the linear loss from the SBR. This can be achieved by making the linear loss of the SBR very low and incorporating resonant layers in the SBR.

Equipped with these loss numbers, we will explore the scenario of repetition rate scaling where the cavity loss is limited. Figure 6.11 and Figure 6.12 show the comparison of repetition rate behavior as a function of the pump power and total cavity dispersion when the intra-cavity loss is 12.5% and 25% respectively. As we can observe, the intra-cavity power loss plays a major factor here increasing the repetition rate of the laser as much as three times when the intra-cavity loss is reduced from 25% to 12.5%.

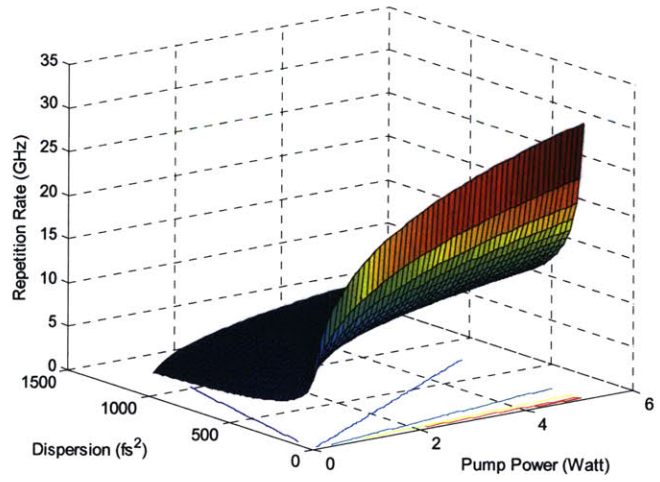

Figure 6.11: Repetition Rate as a function of pump power [0.1 W-5 W] and total cavity dispersion [15 fs^2 -1015 fs^2], 12.5% intra-cavity loss, 100 fs pulse duration.

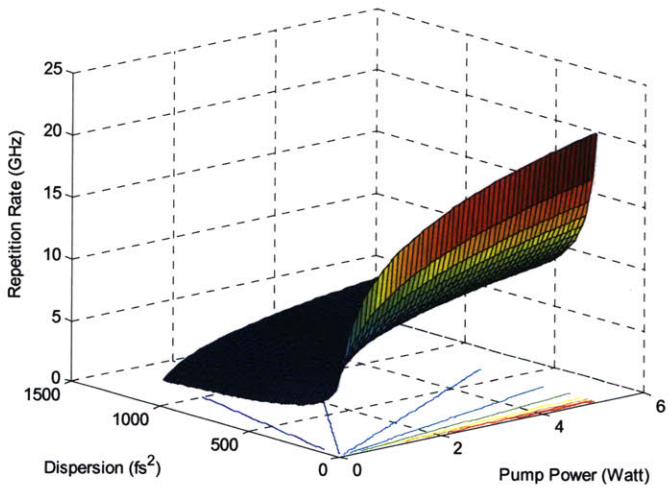

Figure 6.12: Repetition Rate as a function of pump power [0.1 W-5 W] and total cavity dispersion [15 fs2 -1015 fs2], 25% intra-cavity loss, 100 fs pulse duration.

6.5.4. Pump Power Limited

In this section, we will discuss the repetition rate behavior with the pump power as the limiting factor. As introduced in section 6.2.3, the pump power is a major limitation for scaling up the repetition rate of this type of laser. As discussed in section 6.2, currently it is only feasible to couple 1.05 Watt of 980 nm pump power to the gain fiber if the two single mode pump diodes are combined with a polarization beam combiner and the laser is pumped from one side only.

Figure 6.13 and Figure 6.14 show the comparison of the repetition rate behavior as a function of the total cavity dispersion and the doping concentration of the gain fiber, when the pump power is at 1.05 W and 2.10 W. Intra-cavity loss is assumed to be 25%, pulse duration is 100 fs. An increase of the repetition rate is apparent when the pump power is scaled up.

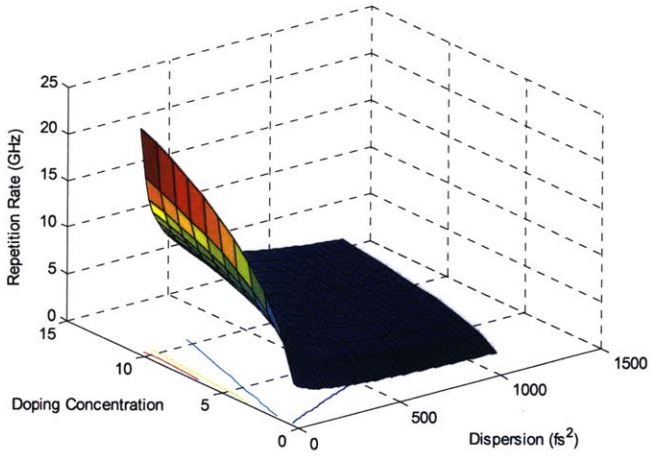

Figure 6.13: Repetition Rate as a function of dispersion [15 fs^2 -1015 fs^2] and doping concentration [0.5 – 10.5] in the unit of 10^{26} ions/m^3, 25% intra-cavity loss, 100 fs pulse duration, pump power is limited at 1.05 Watt.

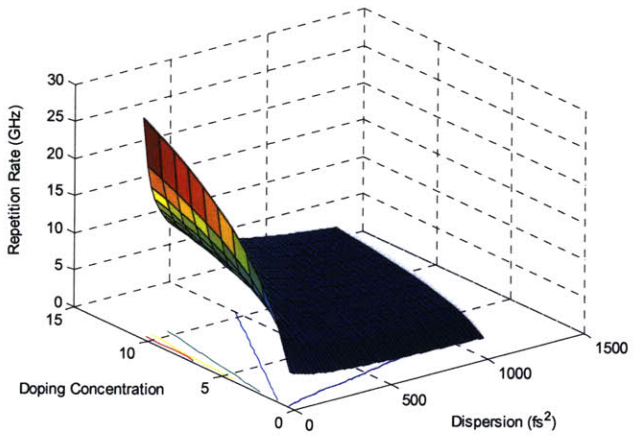

Figure 6.14: Repetition Rate as a function of dispersion [15 fs2 -1015 fs2] and doping concentration [0.5 – 10.5] in the unit of 1026 ions/m3, 25% intra-cavity loss, 100 fs pulse duration, pump power is limited at 2.10 Watt.

6.5.5. Achievable Repetition Rate with Current Technology

Using the governing equation 6.5.3, we can estimate the upper limit of the repetition rates achievable with current state-of-the-art technologies as far as available pump power, dispersion compensation scheme, cavity loss improvement, and doping concentration.

Currently, we are using two single mode 980 nm diodes combined with polarization beam combiner, which gives us pump power of 1.05 Watt, since the SBRs cannot be transparent at 980 nm and a bi-directional pumping scheme cannot be implemented. Ideally, the dispersion of the gain fiber can be measured and the SBR and/or partial reflector coating can be designed to compensate the fiber dispersion, so that the total cavity dispersion is close to zero. As discussed in section 6.4, this total dispersion is limited by the fabrication uncertainty of ~15 fs^2. Currently the highest gain fiber without running into severe quenching problem has a doping concentration

of 4 wt% corresponding to 3.5 x 10^{26} ions/m^3. We also assume that care can be taken to improve the loss of the cavity to 10%. Rest of the parameters can be found in Table 6.1.

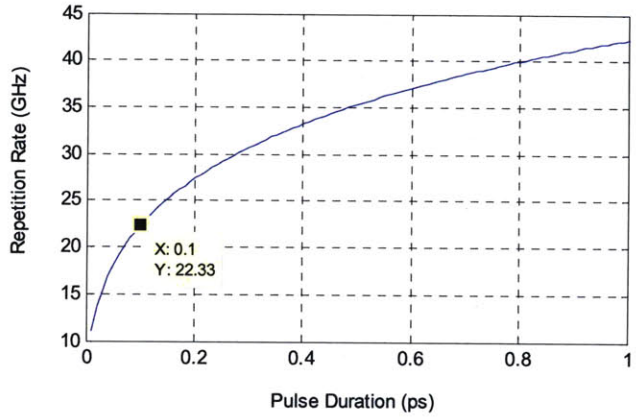

Figure 6.15: Repetition Rate as a function of pulse duration [0.1 ps – 1 ps] dispersion is 15 fs^2 and doping concentration is 3.5 x 10^{26} ions/m^3, 10% intra-cavity loss, pump power is limited at 1.05 Watt.

With these limitations, Figure 6.15 shows the repetition rate as the function of the pulse duration. We can clearly see that if a pulse duration of 100 fs is desired, 22 GHz is the maximum repetition rate we can achieve using the current fiber technology. However, if 500 fs pulse duration is sufficient, a repetition rate of up to 35 GHz seems to be achievable.

Chapter 7.

Conclusion and Future Work

In this thesis, we have discussed and reported progress in high repetition rates achievable from femtosecond fiber lasers. This research was driven by its applications including optical arbitrary waveform generation, high speed optical sampling, frequency metrology, and timing and frequency distribution via fiber links. Low noise fiber laser sources operating at multi-gigahertz repetition rates have been developed systematically. A 200 MHz fundamentally mode-locked soliton laser and a 200 MHz fundamentally mode-locked similariton lasers were developed for the first time. Soliton formation has been recognized as the optimum route towards achieving high fundamental repetition rates from compact laser sources, with limited pump power. A 3 GHz fundamentally mode-locked femtosecond fiber laser has also been developed, the result of which verified the soliton formation theory. Techniques in external cavity repetition rate multiplication have also been discussed. A theoretical model that relates the repetition rate of the soliton laser and its other physical measurable parameters has also been developed to guide further high repetition rate laser development.

7.1. Future Work

Topics discussed in this thesis may suggest many interesting directions of research to pursue in the future. In this section a selected group of them are briefly discussed.

7.1.1. Thermal Engineering

As briefly discussed in the previous sections, the amount of heat load a SBR can withstand is generally limited by material and design of the SBR. During the course of this thesis study, significant amount of thermal damages have been observed experimentally. In general, the thermal damage is caused by three different mechanisms: optical power at 980 nm absorbed by the quantum well, optical power at 1550 nm absorbed by the quantum well, and direct heat transfer from the tip of the gain fiber to the SBR especially in the multi-GHz repetition rate fiber laser cavities.

Absorption at 980 nm: At 1550 nm operation, the Brag stack is usually made of alternating GaAs and AlGaAs layers. Both GaAs and AlGaAs do not significantly absorb optical power at 980 nm wavelengths. However, depending on the design, the SBR quantum well may absorb 980 nm pump light leaked through the erbium doped gain fiber which causes the thermal damage at the SBR. Dichroic coating with high transmission at 1550 nm and high reflection at 980 nm at the surface of the SBR not only greatly reduces the risk of thermal damage at the SBR, but also increases the effective pump power at the gain fiber by reflecting the pump light back to the cavity.

Absorption at 1550 nm: Absorption of optical power at 1550 nm is unavoidable, hence may potentially present as the limitation to the practical achievable repetition rate together with the limitation discussed in Chapter 6. In practice, both linear loss and saturated loss of the SBR contributes to the optical power absorption at 1550 nm, since the laser generally arrives at Q-switched mode-locking state prior to converting to the stable mode-locking state. At Q-switched

state, the laser is more prone to thermal damage due to the higher effective loss at the SBR. This puts a stringent requirement on the design of the SBRs to have low linear loss while maintaining the appropriate modulation depth. Additional thermal engineering can also alleviate the heat load at the SBR. The beam size at the SBR is in general around 50 μm^2, making it difficult to dissipate the heat by simply attaching the SBR to a heat sink. Thinning down the SBR wafer is critical in addition to mounting the SBR for proper heat dissipation.

Direct heat transfer: Direct heat transfer from gain fiber to SBR in general does not contribute to the SBR thermal damage directly. In most of the cases, the heat load is concentrated at a small area on the surface of the SBR where the SBR physically contracts the gain fiber. This locally concentrated heat may delaminate the coating on the SBR surface, especially if there is dichroic coating at the surface of the SBR. This delamination may lead to increase of SBR exposure to 980 nm pump light leaked through the erbium gain fiber, or alternate the reflectance of the SBR in general, resulting either further damage of the SBR or inability of mode-locking. A buffer between the gain fiber and the SBR is strongly encouraged.

7.1.2. Integrated waveguide femtosecond lasers

The topics presented in this thesis serves as a solid preliminary study for integrated waveguide approach in femtosecond mode-locked sources. Significant progress has already been reported in femtosecond waveguide lasers utilizing soliton formation [109]. Even though doping concentration in waveguide media has been a barrier preventing scaling to higher repetition rates, waveguides offers the advantages of much stronger nonlinearity and more flexible dispersion designs which potentially make it possible for GHz repetition rates operation.

7.1.3. Low noise, passively, harmonically mode-locked lasers

As discussed in chapter 6, the achievable repetition rate of the laser is relatively in cubic relationship with the pump power, dispersion, doping concentration, and cavity loss. This leads to a fundamental limit of repetition rate achievable due to the combined limitations of these parameters. An alternative approach may need to be explored to break this limit.

Researchers have been exploring approaches utilizing passively, harmonically, mode-locked lasers to generate low noise pulse trains using a intra-cavity Fabry-Perot cavity, however without significant success. In general, a Fabry-Perot structure is implemented inside of the laser cavity to sort the multiple pulses and suppress supermodes and to achieve low noise operation. However, these passively mode-locked lasers are sensitive to precise alignment of the intra-cavity Fabry-Perot resonances and lose mode-locking unless the FSR of the Fabry-Perot is a multiple of the fundamental repetition rate of the laser.

A novel structure and process is needed to solve this problem. For example, a Fabry-Perot cavity whose finesse can be adjusted via electronic control may solve this problem. The Fabry-Perot adjusted to a very low finesse (F~0) can be implemented into the cavity first. The finesse is so low that the laser can achieve passive mode-locking in soliton region. Two potential approaches can then be applied to lock the Fabry-Perot cavity to the laser from this point on.

In the first approach, the finesse of the Fabry-Perot is increased via electronic control. The soliton laser is expected to continue to operate since the Kelly sidebands may absorb the perturbations. An error signal can be extracted using either the transmission or reflection of the Fabry-Perot cavity and used to lock the Fabry-Perot to the laser. In general, this approach enables the laser to overcome mode-locking hysteresis under the weak present of the etalon effect and then lock the laser to the Fabry-Perot cavity after the laser achieved mode-locking.

In the second approach, the repetition rate of the laser is extracted from the laser output, and is used to control and adjust the FSR of the Fabry-Perot cavity under the very low finesse. Once the FSR of the Fabry-Perot cavity is adjusted and synchronized with the slow laser repetition rate fluctuation, the finesse of the Fabry-Perot cavity can be increased to suppress the supermodes and hence achieve low noise operation.

7.1.4. Commercialization

One of the major hurdles for mass commercialization of the femtosecond lasers is the cost structure of femtosecond laser sources. In general, a standard Ti: Sapphire laser costs in the range of $80-100K, and erbium doped fiber lasers typically cost in the range of $30-50K, which is prohibitive for mass consumer applications even if the technology enables them.

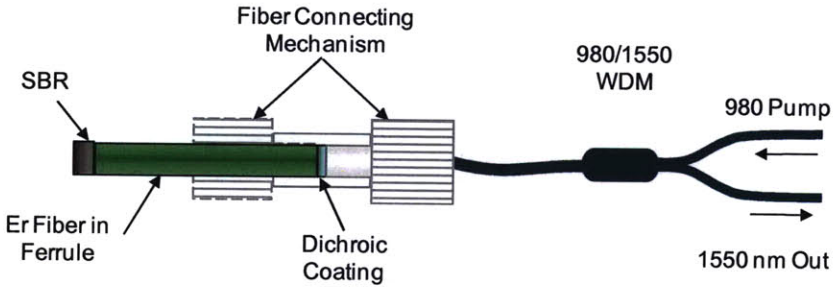

Figure 7.1:Configuration for commercial units

Topics discussed in this thesis may suggest several approaches for low cost compact femtosecond laser sources. As shown in Figure 7.1, and discussed in Chapter 6, a SBR mode-locked soliton fiber laser can be an ideal candidate for low cost mass produced products. Furthermore, waveguide lasers based on similar design principles can potentially achieve even more cost savings in mass commercialization.

Bibliography

1. Ilday, F.O., et al. *Generation of 36-femtosecond pulses from a ytterbium fiber laser.* in *Conference on Lasers and Electro-Optics (CLEO), 16-21 May 2004.* 2004. San Francisco, CA, USA: IEEE.
2. Zhou, X.Y., et al., *Generation of 28-fs pulses from a mode-locked ytterbium fiber oscillator.* Optics Express, 2008. **16**(10): p. 7055-7059.
3. Ilday, F.O., et al., *Self-similar evolution of parabolic pulses in a laser.* Physical Review Letters, 2004. **92**(21): p. -.
4. Chong, A., W.H. Renninger, and F.W. Wise, *All-normal-dispersion femtosecond fiber laser with pulse energy above 20 nJ.* Optics Letters, 2007. **32**(16): p. 2408-2410.
5. Buckley, J.R., et al., *Femtosecond fiber lasers with pulse energies above 10 nJ.* Optics Letters, 2005. **30**(14): p. 1888-1890.
6. Bartels, A. and H. Kurz, *Generation of a broadband continuum by a Ti : sapphire femtosecond oscillator with a 1-GHz repetition rate.* Optics Letters, 2002. **27**(20): p. 1839-1841.
7. Bartels, A., T. Dekorsy, and H. Kurz, *Femtosecond Ti : sapphire ring laser with a 2-GHz repetition rate and its application in time-resolved spectroscopy.* Optics Letters, 1999. **24**(14): p. 996-998.
8. Chen, L.J., et al., *Octave-spanning, dual-output 2.166 GHz Ti:sapphire laser.* Optics Express, 2008. **16**(25): p. 20699-20705.
9. Bartels, A., et al., *Spectrally resolved optical frequency comb from a self-referenced 5 GHz femtosecond laser.* Optics Letters, 2007. **32**(17): p. 2553-2555.
10. Bartels, A., D. Heinecke, and S.A. Diddams, *Passively mode-locked 10 GHz femtosecond Ti : sapphire laser.* Optics Letters, 2008. **33**(16): p. 1905-1907.
11. Hanna, D.C., et al., *Active Mode-Locking of an Yb - Er Fiber Laser.* Electronics Letters, 1989. **25**(2): p. 95-96.
12. Hofer, M., et al., *Active-Mode Locking of a Neodymium-Doped Fiber Laser Using Intracavity Pulse-Compression.* Optics Letters, 1990. **15**(24): p. 1467-1469.
13. Greer, E.J., et al., *Generation of 1.2ps, 10ghz Pulse-Train from All-Optically Modelocked, Erbium Fiber Ring Laser with Active Nonlinear Polarization Rotation.* Electronics Letters, 1994. **30**(21): p. 1764-1765.
14. Jones, D.J., H.A. Haus, and E.P. Ippen, *Subpicosecond solitons in an actively mode-locked fiber laser.* Optics Letters, 1996. **21**(22): p. 1818-1820.
15. Foursa, D., et al., *18GHz from a sigma-cavity Er-fibre laser with dispersion management and rational harmonic active mode-locking.* Electronics Letters, 1997. **33**(6): p. 486-488.
16. Longhi, S., S. Taccheo, and P. Laporta, *High-repetition-rate picosecond pulse generation at 1.5 mu m by intracavity laser frequency modulation.* Optics Letters, 1997. **22**(21): p. 1642-1644.
17. Sato, K., A. Hirano, and H. Ishii, *Chirp-compensated 40-GHz mode-locked lasers integrated with electroabsorption modulators and chirped gratings.* Ieee Journal of Selected Topics in Quantum Electronics, 1999. **5**(3): p. 590-595.
18. Kuizenga, D.J. and A.E. Siegman, eds. *FM and AM mode locking of the homogeneous laser-part I: Theory.* IEEE Journal of Quantum Electronics. Vol. 6. 1970.
19. Huggett, G.R., *Mode locking of CW lasers by regenerative RF feedback.* applied Physics Letters, 1968. **13**.

20. Duling, I.N., *ALL-FIBER RING SOLITON LASER MODE-LOCKED WITH A NONLINEAR MIRROR.* Optics Letters, 1991. **16**(8): p. 539-541.
21. Avdokhin, A.V., S.V. Popov, and J.R. Taylor, *Totally fiber integrated, figure-of-eight, femtosecond source at 1065 nm.* Optics Express, 2003. **11**(3): p. 265-269.
22. Ibarra-Escamilla, B., et al., *All-fiber passive mode-locked laser to generate ps pulses based in a symmetrical NOLM.* Laser Physics, 2009. **19**(2): p. 368-370.
23. Smith, N.J. and N.J. Doran, *PICOSECOND SOLITON TRANSMISSION USING CONCATENATED NONLINEAR-OPTICAL LOOP-MIRROR INTENSITY FILTERS.* Journal of the Optical Society of America B-Optical Physics, 1995. **12**(6): p. 1117-1125.
24. Margulis, W., K. Rottwitt, and J.R. Taylor, *HIGH-POWER FIGURE-OF-8 LASER FOR SOLITON TRANSMISSION EXPERIMENTS.* Electronics Letters, 1995. **31**(8): p. 645-647.
25. Tamura, K., et al., *Technique for obtaining high-energy ultrashort pulses from an additive-pulse mode-locked erbium-doped fiber ring laser.* Optics Letters, 1994. **19**(1): p. 46-8.
26. Haus, H.A., E.P. Ippen, and K. Tamura, *Additive-pulse modelocking in fiber lasers.* IEEE Journal of Quantum Electronics, 1994. **30**(1): p. 200-8.
27. Haus, H.A., et al., *Stretched-pulse additive pulse mode-locking in fiber ring lasers: theory and experiment.* IEEE Journal of Quantum Electronics, 1995. **31**(3): p. 591-8.
28. Ippen, E.P., *Principles of Passive-Mode Locking.* Applied Physics B-Lasers and Optics, 1994. **58**(3): p. 159-170.
29. Tamura, K., H.A. Haus, and E.P. Ippen, *Self-Starting Additive Pulse Mode-Locked Erbium Fiber Ring Laser.* Electronics Letters, 1992. **28**(24): p. 2226-2228.
30. Tamura, K., et al., *Unidirectional Ring Resonators for Self-Starting Passively Mode-Locked Lasers.* Optics Letters, 1993. **18**(3): p. 220-222.
31. Tamura, K., E.P. Ippen, and H.A. Haus, *Pulse Dynamics in Stretched-Pulse Fiber Lasers.* Applied Physics Letters, 1995. **67**(2): p. 158-160.
32. Tamura, K., et al., *77-Fs Pulse Generation from a Stretched-Pulse Mode-Locked All-Fiber Ring Laser.* Optics Letters, 1993. **18**(13): p. 1080-1082.
33. Kelly, S.M.J., *Characteristic sideband instability of periodically amplified average soliton.* Electronics Letters, 1992. **28**(8): p. 806-7.
34. Islam, M.N., et al., *Multiple Quantum Well Passive-Mode Locking of a Nacl Color Center Laser.* Applied Physics Letters, 1989. **54**(13): p. 1203-1205.
35. Kim, B.G., et al., *Nonlinear Bragg Reflector Based on Saturable Absorption.* Applied Physics Letters, 1989. **54**(12): p. 1095-1097.
36. Kopf, D., et al., *All-in-one dispersion-compensating saturable absorber mirror for compact femtosecond laser sources.* Optics Letters, 1996. **21**(7): p. 486-488.
37. Keller, U., et al., *Semiconductor saturable absorber mirrors (SESAM's) for femtosecond to nanosecond pulse generation in solid-state lasers.* Ieee Journal of Selected Topics in Quantum Electronics, 1996. **2**(3): p. 435-453.
38. Guerreiro, P.T., et al., *PbS quantum-dot doped grasses as saturable absorbers for mode locking of a Cr:forsterite laser.* Applied Physics Letters, 1997. **71**(12): p. 1595-1597.
39. Malyarevich, A.M., et al., *Glass doped with PbS quantum dots as a saturable absorber for 1-mu m neodymium lasers.* Journal of the Optical Society of America B-Optical Physics, 2002. **19**(1): p. 28-32.
40. Set, S.Y., et al., *Ultrafast fiber pulsed lasers incorporating carbon nanotubes.* Ieee Journal of Selected Topics in Quantum Electronics, 2004. **10**(1): p. 137-146.
41. Schibli, T.R., et al., *Ultrashort pulse-generation by saturable absorber mirrors based on polymer-embedded carbon nanotubes.* Optics Express, 2005. **13**(20): p. 8025-8031.
42. Harkonen, A., et al., *Dynamics of photoluminescence in GaInNAs saturable absorber mirrors.* Applied Physics a-Materials Science & Processing, 2003. **77**(7): p. 861-863.

43. Jouhti, T., et al., *1.55 mu m monolithic GaInNAs semiconductor saturable absorber.* Iee Proceedings-Optoelectronics, 2003. **150**(1): p. 77-79.
44. Okhotnikov, O.G., et al., *1.5-mu m monolithic GaInNAs semiconductor saturable-absorber mode locking of an erbium fiber laser.* Optics Letters, 2003. **28**(5): p. 364-366.
45. Liverini, V., et al., *Low-loss GaInNAs saturable absorber mode locking a 1.3-mu m solid-state laser.* Applied Physics Letters, 2004. **84**(20): p. 4002-4004.
46. Marceaux, A., et al., *High-speed 1.55 mu m Fe-doped multiple-quantum-well saturable absorber on InP.* Applied Physics Letters, 2001. **78**(26): p. 4065-4067.
47. Lecourt, J.B., et al., *Highly Fe-doped InGaAs/InP saturable absorber mode-locking of an erbium fiber laser.* Journal of Nonlinear Optical Physics & Materials, 2005. **14**(3): p. 427-437.
48. Scollo, R., et al., *Mode-Locked InP-Based Laser Diode With a Monolithic Integrated UTC Absorber for Subpicosecond Pulse Generation.* Ieee Journal of Quantum Electronics, 2009. **45**(4): p. 322-335.
49. Quinlan, F., et al., *Ultralow-jitter and amplitude-noise semiconductor-based actively mode-locked laser.* Optics Letters, 2006. **31**(19): p. 2870-2872.
50. Seong, N.H., D.Y. Kim, and S.P. Veetil, *Mode-locked fiber laser based on an attenuation-imbalanced nonlinear optical loop mirror.* Optics Communications, 2007. **280**(2): p. 438-442.
51. Zhang, Z.X., L. Zhan, and Y.X. Xia, *Multiwavelength comb generation in self-starting passively mode-locked fiber laser.* Microwave and Optical Technology Letters, 2006. **48**(7): p. 1356-1358.
52. Seong, N.H. and D.Y. Kim, *A new figure-eight fiber laser based on a dispersion-imbalanced nonlinear optical loop mirror with lumped dispersive elements.* Ieee Photonics Technology Letters, 2002. **14**(4): p. 459-461.
53. Udem, T., R. Holzwarth, and T.W. Hansch, *Optical frequency metrology.* Nature, 2002. **416**(6877): p. 233-237.
54. Li, C.H., et al., *A laser frequency comb that enables radial velocity measurements with a precision of 1 cm s(-1).* Nature, 2008. **452**(7187): p. 610-612.
55. Cundiff, S.T., *Metrology - New generation of combs.* Nature, 2007. **450**(7173): p. 1175-1176.
56. Yilmaz, T., et al., *Toward a photonic arbitrary waveform generator using a modelocked external cavity semiconductor laser.* Ieee Photonics Technology Letters, 2002. **14**(11): p. 1608-1610.
57. Weiner, A.M., J.P. Heritage, and E.M. Kirschner, *High-Resolution Femtosecond Pulse Shaping.* Journal of the Optical Society of America B-Optical Physics, 1988. **5**(8): p. 1563-1572.
58. Dugan, M.A., J.X. Tull, and W.S. Warren, *High-resolution acousto-optic shaping of unamplified and amplified femtosecond laser pulses.* Journal of the Optical Society of America B-Optical Physics, 1997. **14**(9): p. 2348-2358.
59. Chou, J., Y. Han, and B. Jalali, *Adaptive RF-photonic arbitrary waveform generator.* Ieice Transactions on Electronics, 2003. **E86c**(7): p. 1226-1229.
60. Jiang, Z., D.E. Leaird, and A.M. Weiner, *Line-by-line pulse shaping control for optical arbitrary waveform generation.* Optics Express, 2005. **13**(25): p. 10431-10439.
61. Jiang, Z., et al., *Spectral line-by-line pulse shaping.* Optics Letters, 2005. **30**(12): p. 1557-1559.
62. Wepman, J.A., *Analog-to-Digital Converters and Their Applications in Radio Receivers.* Ieee Communications Magazine, 1995. **33**(5): p. 39-45.
63. Black, W., Jr. and D. Hodges. *Time interleaved converter arrays.* in *Solid-State Circuits Conference. Digest of Technical Papers. 1980 IEEE International.* 1980.
64. Montijo, A. and K. Rush, *Accuracy in Interleaved Adc Systems.* Hewlett-Packard Journal, 1993. **44**(5): p. 38-46.
65. Walden, R.H., *Analog-to-digital converter survey and analysis.* IEEE Journal on Selected Areas in Communications, 1999. **17**(4): p. 539-50.
66. Caputi, W.J., *Stretch - Time-Transformation Technique.* Ieee Transactions on Aerospace and Electronic Systems, 1971. **Aes7**(2): p. 269-&.

67. Kartner, F.X., et al., *Electronic photonic integrated circuits for high speed, high resolution, analog to digital conversion - art. no. 612503.* Silicon Photonics, 2006. **6125**: p. 12503-12503
68. Coppinger, F., A.S. Bhushan, and B. Jalali, *Photonic time stretch and its application to analog-to-digital conversion.* Ieee Transactions on Microwave Theory and Techniques, 1999. **47**(7): p. 1309-1314.
69. Kim, J., et al., *Drift-free femtosecond timing synchronization of remote optical and microwave sources.* Nature Photonics, 2008. **2**(12): p. 733-736.
70. Fermann, M.E., et al., *Passive-Mode Locking in Erbium Fiber Lasers with Negative Group Delay.* Applied Physics Letters, 1993. **62**(9): p. 910-912.
71. Abedin, K.S., M. Hyodo, and N. Onodera, *154GHz polarisation-maintaining dispersion-managed actively modelocked fibre ring laser.* Electronics Letters, 2000. **36**(14): p. 1185-1186.
72. Zeller, S.C., et al., *Passively modelocked 77 GHz Er : Yb : glass laser.* Electronics Letters, 2007. **43**(1): p. 32-33.
73. Leburn, C.G., et al., *Femtosecond Cr4+: YAG laser with 4GHz pulse repetition rate.* Electronics Letters, 2004. **40**(13): p. 805-807.
74. Chen, J., et al., *Generation of low-timing-jitter femtosecond pulse trains with 2 GHz repetition rate via external repetition rate multiplication.* Optics Letters, 2008. **33**(9): p. 959-961.
75. Tammela, S., et al. *Direct Nanoparticle Deposition process for manufacturing very short high gain Er-doped silica glass fibers.* in *Optical Communication, 2002. ECOC 2002. 28th European Conference on.* 2002.
76. Ilday, F.O., et al., *Generation of 50-fs, 5-nJ pulses at 1.03 mu m from a wave-breaking-free fiber laser.* Optics Letters, 2003. **28**(15): p. 1365-7.
77. Ilday, F.O., et al., *Generation of 36-femtosecond pulses from a ytterbium fiber laser.* Optics Express, 2003. **11**(26).
78. Lim, H., F.O. Ilday, and F.W. Wise, *Generation of 2-nJ pulses from a femtosecond ytterbium fiber laser.* Optics Letters, 2003. **28**(8): p. 660-2.
79. Jones, D.J., et al., *116-fs soliton source based on an Er-Yb codoped waveguide amplifier.* Ieee Photonics Technology Letters, 1998. **10**(5): p. 666-668.
80. Collings, B.C., et al., *Short cavity erbium/ytterbium fiber lasers mode-locked with a saturable Bragg reflector.* Ieee Journal of Selected Topics in Quantum Electronics, 1997. **3**(4): p. 1065-1075.
81. Hofer, M., et al., *MODE-LOCKING WITH CROSS-PHASE AND SELF-PHASE MODULATION.* Optics Letters, 1991. **16**(7): p. 502-504.
82. Doran, N.J. and D. Wood, *Nonlinear-Optical Loop Mirror.* Optics Letters, 1988. **13**(1): p. 56-58.
83. Ilday, F.O. and F.W. Wise. *High-energy femtosecond stretched-pulse fiber laser with a nonlinear optical loop mirror.* in *13th International Meeting on Ultrafast Phenomena, 12-17 May 2002.* 2002. Vancouver, BC, Canada: Opt. Soc. America.
84. Deng, Y., et al., *Colliding-pulse passive harmonic mode-locking in a femtosecond Yb-doped fiber laser with a semiconductor saturable absorber.* Optics Express, 2004. **12**(16): p. 3872-3877.
85. Ilday, F.O., F.W. Wise, and F.X. Kaertner, *Possibility of self-similar pulse evolution in a Ti:sapphire laser.* Optics Express, 2004. **12**(12).
86. Berntson, A., et al., *Power dependence of dispersion-managed solitons for anomalous, zero, and normal path-average dispersion.* Optics Letters, 1998. **23**(12): p. 900-902.
87. Abedin, K.S. and F. Kubota, *10 GHz, 1 ps regeneratively modelocked fibre laser incorporating highly nonlinear and dispersive photonic crystal fibre for intracavity nonlinear pulse compression.* Electronics Letters, 2004. **40**(1): p. 58-60.
88. Lim, H., F.O. Ilday, and F.W. Wise, *Femtosecond ytterbium fiber laser with photonic crystal fiber for dispersion control.* Optics Express, 2002. **10**(25): p. 1497-1502.

89. Matos, L., et al., *Carrier-envelope phase dynamics and noise analysis in octave-spanning Ti : sapphire lasers.* Optics Express, 2006. **14**(6): p. 2497-2511.
90. Agrawal, G.P., *Nonlinear fiber optics*. 3rd ed. Optics and photonics. 2001, San Diego: Academic Press. xvi, 466.
91. Collings, B.C., K. Bergman, and W.H. Knox, *Stable multigigahertz pulse-train formation in a short-cavity passively harmonic mode-locked erbium/ytterbium fiber laser.* Optics Letters, 1998. **23**(2): p. 123-125.
92. Gee, S., et al., *Simultaneous optical comb frequency stabilization and super-mode noise suppression of harmonically mode-locked semiconductor ring laser using an intracavity etalon.* IEEE Photonics Technology Letters, 2005. **17**(1): p. 199-201.
93. Tamura, K., et al., *Soliton Fiber Ring Laser Stabilization and Tuning with a Broad Intracavity Filter.* Ieee Photonics Technology Letters, 1994. **6**(6): p. 697-699.
94. McFerran, J.J., et al., *A passively mode-locked fiber laser at 1.54 mu m with a fundamental repetition frequency reaching 2 GHz.* Optics Express, 2007. **15**(20): p. 13155-13166.
95. Kartner, F.X. and U. Keller, *Stabilization of Soliton-Like Pulses with a Slow Saturable Absorber.* Optics Letters, 1995. **20**(1): p. 16-18.
96. Abedin, K.S., N. Onodera, and M. Hyodo, *Repetition-rate multiplication in actively mode-locked fiber lasers by higher-order FM mode locking using a high-finesse Fabry-Perot filter.* Applied Physics Letters, 1998. **73**(10): p. 1311-1313.
97. Harner, L.L., *Thermally Stable Super Invar.* Journal of Metals, 1988. **40**(11): p. 114-114.
98. Chen, J., et al., *High repetition rate, low jitter, low intensity noise, fundamentally mode-locked 167 fs soliton Er-fiber laser.* Optics Letters, 2007. **32**(11): p. 1566-1568.
99. Hansch, T.W. and B. Couillaud, *Laser frequency stabilization by polarization spectroscopy of a reflecting reference cavity.* Optics Communications, 1980. **35**(3): p. 441-4.
100. McFerran, J.J., et al., *Elimination of pump-induced frequency jitter on fiber-laser frequency combs.* Optics Letters, 2006. **31**(13): p. 1997-1999.
101. Patel, F.D., et al., *A compact high-performance optical waveguide amplifier.* Ieee Photonics Technology Letters, 2004. **16**(12): p. 2607-2609.
102. Smart, R.G., J.L. Zyskind, and D.J. Digiovanni, *EXPERIMENTAL COMPARISON OF 980-NM AND 1480 NM-PUMPED SATURATED IN-LINE ERBIUM-DOPED FIBER AMPLIFIERS SUITABLE FOR LONG-HAUL SOLITON TRANSMISSION-SYSTEMS.* Ieee Photonics Technology Letters, 1993. **5**(7): p. 770-773.
103. Yamada, M., et al., *NOISE CHARACTERISTICS OF ER3+-DOPED FIBER AMPLIFIERS PUMPED BY 0.98 AND 1.48 MU-M LASER-DIODES.* Ieee Photonics Technology Letters, 1990. **2**(3): p. 205-207.
104. Becker, P.C., N.A. Olsson, and J.R. Simpson, *Erbium-doped fiber amplifiers : fundamentals and technology*. Optics and photonics. 1999, San Diego: Academic Press. xv, 460 p.
105. Desurvire, E., *Erbium-doped fiber amplifiers : principles and applications*. 1994, New York: Wiley. xxvii, 770 p.
106. Chen, J., et al., *Fundamentally Mode-locked 3 GHz Femtosecond Erbium Fiber Laser.* Ultrafast Phenomena XVI, Proceedings of the 16th International Conference, Palazzo dei Congressi Stresa, Italy, June 9--13, 2008, 2008: p. 727-729.
107. Seneschal, K., et al., *Properties and structure of high erbium doped phosphate glass for short optical fibers amplifiers.* Materials Research Bulletin, 2005. **40**(9): p. 1433-1442.
108. Byun, H., et al., *High-repetition-rate, 491 MHz, femtosecond fiber laser with low timing jitter.* Optics Letters, 2008. **33**(19): p. 2221-2223.